Universitatea
Transilvania
din Brașov

INTERDISCIPLINARY DOCTORAL SCHOOL

Faculty of Electrical Engineering and Computer Science

Julio ESPINOSA DOMINGUEZ

Advanced control of battery energy storage to mitigate frequency dependence of electric arc furnaces in weak power systems.

SUMMARY

Scientific supervisor

Prof. Dr. Eng. Ioan SERBAN

BRAȘOV, 2026

ACKNOWLEDGEMENTS

I would like to express my sincere gratitude to everyone who, in one way or another, has contributed to my professional development.

To my friends: those who have always stood by my side through every challenge, those who are no longer with us, those who passed through my life leaving a lasting mark, and those who, despite the passage of time, will always remain my friends.

To my family, who despite the physical distance, have remained close to me, offering unconditional support in every decision I have made. With special love to my parents, to my mother, whose love is with me at every moment, and to my father, who has been and will always be my guide. I also dedicate an eternal remembrance to my grandparents, who watch over and protect me from above.

My deepest gratitude goes to my supervisor, Prof. Dr. Eng. Ioan Serban, whose guidance, encouragement and unwavering support have been fundamental to the completion of this work and to the achievements attained through these years of dedication and effort.

I would like to express my sincere gratitude to Transilvania University of Brașov for this opportunity and for awarding me a full scholarship, which enabled me to develop this research.

I would also wish to express my profound appreciation to my professor, tutor, and mentor, Orlys Ernesto Torres Breffe. Through his wisdom, advice, and example, he has greatly influenced my formation as a professional and as a person. More than a professor, I consider him a father figure.

Julio Espinosa Domínguez

Table of Contents

INTRODUCTION

The development of mankind has been closely linked with the production of materials like steel, which requires a significant amount of energy to produce. The steel manufacturing process is extremely complex and begins with the selection and classification of scrap within the steelworks, followed by the smelting process and the introduction of chemical materials to produce high-alloy steels [1]. One stage of steel production is the smelting process, which takes place in steelworks using high-power electric arc furnaces (EAFs). Due to their operation characteristics, EAFs are highly demanding on power systems. EAFs cause power quality problems for the steelworks' electricity supply system, which must be mitigated to avoid impacting the nearby consumers [2], [3]. In addition to power quality issues, such as harmonic pollution, flicker, low power factor and imbalances, these high-power consumers can cause severe perturbations in the frequency of weak power systems [4], [5], such as the Cuban power system. In such cases, to avoid frequency stability problems, the power system operator may require limiting the power demand of EAFs, which can severely affect the efficiency of the steel production process [4]. It is important to note that the impact of EAFs on frequency is a major issue in the Cuban power system today, requiring different solutions compared to those used in strong grids such as the European power system [6].

One solution to frequency stability problems is the implementation of battery energy storage systems (BESS) in power systems [7], [8], [9]. The speed and effectiveness of the control systems of these devices help minimise frequency deviations, which is highly beneficial for conventional generation units that may not respond with the required speed. As the penetration rate of renewable energy sources (RES) increases, the frequency control process becomes more complex in all power systems, particularly in weak power systems [10], [11]. Therefore, the deployment of BESS is increasing significantly due to the numerous applications they have in power systems [12].

Research into the applications of BESS in EAFs has been limited mainly to improving power quality [13], [14], [15], while others such as [16], [17] have raised the possibility of using BESS to improve frequency stability in power systems. The main drawback of these applications is their reliance on BESS with high energy capacity and high C-rate values, which makes the application more expensive from a technical point of view. To address this issue, the aim of this thesis is to propose a fuzzy logic-based adaptive control for a BESS, specially designed for operation in parallel with an EAF within the Cuban power system. The primary goal is to mitigate the EAF impact on the Cuban power system, thereby reducing the frequency deviations caused by these furnaces and ensuring the continuous operation of the steelworks. In addition, the control system should be adaptable to all stages of the steelworks production process, thus improving efficiency and production levels in the industry.

Necessity and justification of the thesis

The need for this research arises from the current technical and economic constraints faced by steelworks and the power system operator in Cuba. At present, the operation of high-power furnaces at facilities such as 'Las Tunas' and 'Antillana de Acero' generates frequency fluctuations that exceed the permissible ranges (59.7–60.2 Hz), thereby jeopardising the stability of the power system.

The rationale for this work is based on the following key points:

- **Production Inefficiency:** To protect the system, steelworks are forced to operate with slow power ramps, which increases melting time, specific energy consumption and wear and tear on switching equipment.
- **Economic Impact and Power Quality:** Industries face financial penalties due to a low power factor (typically below 0.9) and the presence of harmonics. Traditional passive filters are often insufficient in the face of load variability.
- **Limitations of Conventional Solutions:** Increasing the short-circuit power at the point of common coupling (PCC) mitigates flicker but does not resolve the fundamental problem of frequency stability or dynamic reactive power compensation.

Aim and objectives

The aim of this thesis is to develop and validate a multifunctional control strategy based on BESS to mitigate the impact of electric arc furnaces on weak power systems, ensuring frequency stability, harmonic distortion compensation and power factor optimisation.

The objectives of this thesis are outlined as follows:

- Develop a control system for a BESS adapted to the specific case of the EAF integration in the Cuban power system,
- Implement an advanced fuzzy logic-based control system designed to reduce frequency influence on the EAF operation, while keeping the battery use at minimum,
- Analyse the BESS response to voltage perturbations (e.g. sags or swells) in the power system,
- Modelling of the EAF for harmonic and power factor analysis,
- Enhance the BESS functionality by providing ancillary services, such as a power factor compensation,
- Analysis of the behaviour of the BESS as an active filter in the presence of harmonics in the steelworks network,
- Evaluate and experimentally validate the control systems within the context of the Cuban power system.

CHAPTER 1 . State-of-the-art analysis of hardware and control solutions to mitigate frequency dependence of consumers in weak power systems

Climate change is a global reality. Every year, the average surface temperature of the planet increases, causing natural phenomena that, if sustained, may result in profound disruptions to societies in the near future. These facts have led the nations to seek immediate solutions to prevent a climate catastrophe. One of the measures to be taken to curb climate change is the incorporation of RES into electric power systems. This measure aims to reduce the generation of electricity from fossil fuels that contribute to pollution and global warming. The accelerated introduction of these sources has resulted in the weakening of the current networks, which have lost inertia and are more vulnerable to the transient phenomena that occur in them. The stability of the grids is essential in the process of generation and transmission of electrical energy, so solutions have been sought to ensure that the introduction of renewable energy sources does not become a cause that compromises the security of power systems. One of the solutions contributing to the massive introduction of renewable energy sources into electrical power systems is the use of energy storage systems. These systems have multiple applications and are now a viable solution to the stability problems that can occur in weak power systems [18].

Compounding this situation is the fact that the Cuban power system is isolated, with conventional generation plants that have been in operation for over 30 years and are experiencing delays in their maintenance cycles due to financial constraints. All of this poses a significant challenge for the operation and maintenance of the system, particularly in terms of stability [6].

However, the country has established strategic policies aimed at the massive integration of RES in conjunction with energy storage systems, to ensure the stability of the system. In this context and considering the current challenges facing the Cuban power system, the main objective of this chapter is to examine the frequency control methods applied in weak power systems, as well as to analyse the current status and control techniques associated with energy storage systems, to contribute to strengthening the stability of electrical networks. Considering the technological diversity that exists in storage systems, this section first focuses on an overview of their applications and then delves into the study of control strategies used in BESS, given that they are one of the most widespread technologies in weak electrical networks.

1.1. Frequency control in electrical power systems

For an electrical power system (PS) to operate properly, the frequency must be kept within a certain range. Proper frequency control is essential for maintaining power system stability and ensuring the reliable operation of frequency-dependent equipment. In order for the speed or frequency of a PS to remain constant or vary within an acceptable range, the active power equilibrium must be satisfied [19], [20]:

$$\sum P_G = \sum P_d + \sum \Delta P \tag{1.1}$$

where P_G, P_d and ΔP represent the active powers generated, demanded and their losses respectively. With the balance of the active powers a PS operates at a certain single frequency for the whole system [21].

<u>1.1.1. Load response to frequency deviations (damping)</u>

The load of a PS is composed of a wide variety of electrical devices. For resistive loads, such as incandescent lighting, electric cookers, etc., the electrical power is independent of frequency; however, for speed-dependent loads, such as fans, water pumps, etc., the electrical power varies with frequency [19], [21].

The characteristics of loads that vary with frequency are expressed by equation [21]:

$$\Delta P_G = \Delta P_d + (D \cdot \Delta f) \tag{1.2}$$

where ΔP_G is the variation in active power generated due to variation in demand, ΔP_d is the variation of active power demand that does not vary with frequency, $D \cdot \Delta f$ is the variation of load varying with frequency and $D = \frac{\Delta P_d}{\Delta f}$ is the load damping constant or variation of power demand with frequency (MW/Hz).

In equation (1.2), the term $(D \cdot \Delta f)$ always has the opposite sign to that of the load variation (ΔP_d), which is responsible for the change in frequency. As the load increases, the frequency decreases below 60 Hz and consequently the effective load variation in the system is reduced as $(D * \Delta f)$ becomes negative.

<u>1.1.2. Frequency control levels in a power system</u>

The forms or actions of frequency control shall be listed below and are summarised in Figure 1.1:

1. Primary control
2. Secondary control
3. Tertiary control

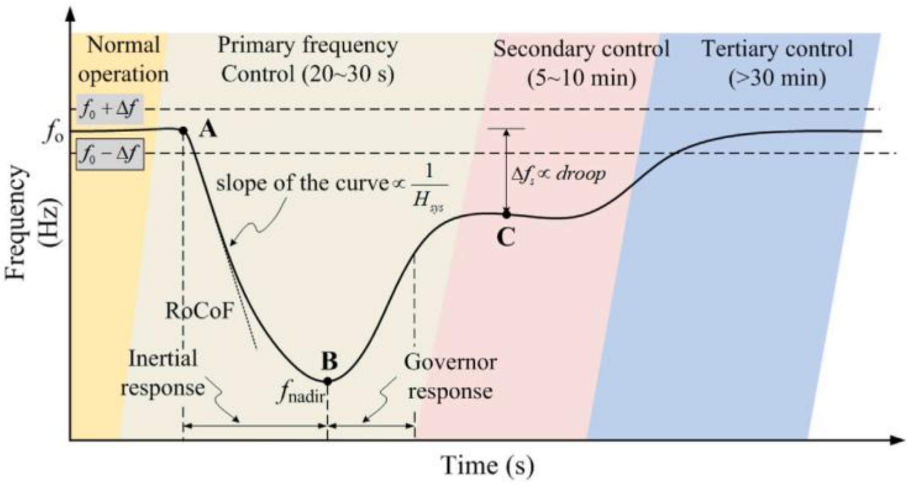

Figure 1.1. Graphical representation of time frame involved and frequency response of a system [22].

Primary control refers to the initial response of the generators, or other equipment involved, to frequency variations in the system, outside the defined dead band. These devices detect changes in frequency and respond according to a predefined droop characteristic.

Once the primary control has acted, the frequency remains with a deviation depending on the droop characteristic of the PS and the disturbance level, and further control action is required to restore the frequency within dead band. The control actions that follow the primary action are referred to as secondary control.

Secondary control aims to bring the frequency to nominal values within the dead band, but in the most economical way. Tertiary control, on the other hand, aims to rebuild this reserve by modifying the reference power of the generators in operation, by bringing generators into reserve or by adjusting schedules with other areas. In general, tertiary control is slow enough to be managed by a manual control loop [19].

In addition to the three control levels, other mechanisms are activated during significant frequency deviations or rapid rates of change. In such cases, load shedding is employed to keep the power system operational, though at the cost of disconnecting some consumers. Another mechanism is activated when frequency rises beyond certain thresholds, leading to the disconnection of generators. The first action is known as ADF, which stands for Automatic Disconnection by Frequency. The second action is known as AGD, which stands for Automatic Generation Disconnection [19], [21].

1.1.3. Strength of the power system and main issues for weak energy systems

Power systems can be considered as either strong or weak. A strong grid can withstand sudden changes under normal operating conditions, such as sudden changes in demand or the occurrence of disturbances, while maintaining voltage and frequency within acceptable margins for the power system. In contrast, a weak grid is more susceptible to such disturbances, which can cause significant fluctuations in voltage and frequency and thus affect the normal operation of the system [23], [24].

Although there are several metrics and definitions of power system strength in the literature, the IEEE1204 standard defines a weak power system based on dynamic and static performance as follows:

1. The impedance of the AC system may be high in relation to the AC supply at the connection point, i.e. the short-circuit power at the connection point may be low [25].
2. The mechanical inertia of the AC system may be insufficient in relation to the AC power supply [25].

Static power intensity is characterised by the short-circuit power level, which is low in weak electrical networks. However, the measurement only applies to the PCC from the network point of view. It is therefore useful to consider the generation connected to the PCC by using a network stiffness index such as the short-circuit ratio (SCR) [23].

$$SCR = \frac{S_{SC}}{S_n} \tag{1.3}$$

where S_n is the installed power of the generating plant and S_{SC} is the short-circuit power at the PCC.

From an SCR perspective, a grid is considered strong if it has values above 20 and weak if the SCR is below the range of 6 to 10 [23]. Although these limits are considered standard in traditional power systems, they may differ in applications that incorporate renewable generation through power inverters.

In contrast to robust and consolidated power grids, the operation of weak systems poses a significant challenge to operators due to the variety of problems that can arise. Phenomena such as resonances, voltage instability and over-voltages due to load losses are factors that can affect the performance of various controllers, especially those used in RES. In general, Table 1.1 summarises the main operational challenges faced by weak power systems according to the reference [24].

The challenges described above show that the operation of weak power systems is a complex and dynamic process, the stability of which is a constant challenge for operators. In this context, the incorporation of modern, high-capacity devices that contribute to the maintenance of network-wide stability is indispensable. Among these, energy storage systems stand out as key elements, not only facilitating system stability and expansion, but also enabling effective large-scale integration of RES.

Table 1.1. Issues faced in low-inertia and weak power systems **[24]**

Issue	Findings
Frequency Response	• Frequency is more susceptible to increased renewable generation due to lack of inertial support. • Increased sensitivity of the system to disturbance. • Increased in ROCOF and frequency deviation. • Caused load shedding or tripping generator. • Low-frequency oscillatory stability issues.
Voltage Stability	• The voltage is highly sensitive to power variations, even under low magnitude fault conditions. • A sudden increase in active or reactive power can generate significant voltage variations, leading to unstable system conditions. • Cascading over voltages caused by excessive voltage fluctuations or surges. • Voltage instabilities due to RES integration. • Higher magnitude voltage decreases. • More extensive propagation of the voltage drop. • Longer process of voltage restoration.
Cascading Failure	• It occurs because of a voltage reduction caused by a fault and is aggravated by voltage fluctuations in the converters. • Decreasing inertia in the power grid can lead to load disconnections and trigger cascading faults.
Inadequate operation of the protection system	• The increase of the ROCOF can trigger the tripping of the protection relay. • In systems with low inertia, over-current protection is

	one of the most affected, as low levels of short-circuit current may be insufficient to trip the protective relays. • Failure of the differential protection to trip due to minimal current differences. • The relationship between voltage and current is influenced by significant variations in the number of synchronous generators present during peak and off-peak periods, which can be a challenge for the correct operation of distance relays.

1.2. The need for energy storage systems in power systems

Worldwide electrical power systems are one of the essential components of modern societies. Sectors such as telecommunications, transport, industry, business, health services, education, etc. depend on electricity, so increasingly reliable and secure power systems are required. Climate change is a global concern today, and action must be taken to minimize it. For the electricity sector, climate change is a challenge because of the need to use renewable sources of electricity generation to replace traditional generation sources [26]. The integration of renewable energy sources in power systems is accelerating rapidly, with solar and wind generation being the sources with the greatest presence in electricity systems. The rate of installation of solar photovoltaic panels and wind power plants is led by countries such as the USA, India, China, Australia, Japan, and EU member states such as Germany, the UK, France, and Spain [7], [26].
As the generation of electrical energy from renewable sources increases, the nature of the power system changes, and its stability is affected. The variability of renewable sources in power generation is an unresolved problem today, in addition to the low inertial response of these sources, which can constitute a danger to the stability of electrical power systems [27].
Due to the problems presented by renewable sources within power systems, scientists and researchers have turned to the search for solutions that allow the operation of these generation sources in parallel with conventional generation sources. One of these solutions is the implementation of energy storage systems (ESS) in any part of the power system [28] . Energy storage systems must meet four main objectives: to increase the reliability of renewable energy sources; to contribute to the stability and support with ancillary services to the grid; to enable and take advantage of all the benefits of smart grids; and to contribute to the optimization of generation to meet grid demand. In order to meet these objectives, it is necessary to select the appropriate storage technology correctly, as well as to understand the technical limitations in conjunction with the choice of control strategy [29].

1.2.1. Energy storage system technologies

The importance of energy storage systems in current power systems makes the process of choosing the best technology for energy storage a challenge for today's power projects. Different energy storage technologies (see Figure 1.2) can be chosen for a particular application depending on the energy and power required, response time, duty cycles, weight, volume, and operating temperature [30].

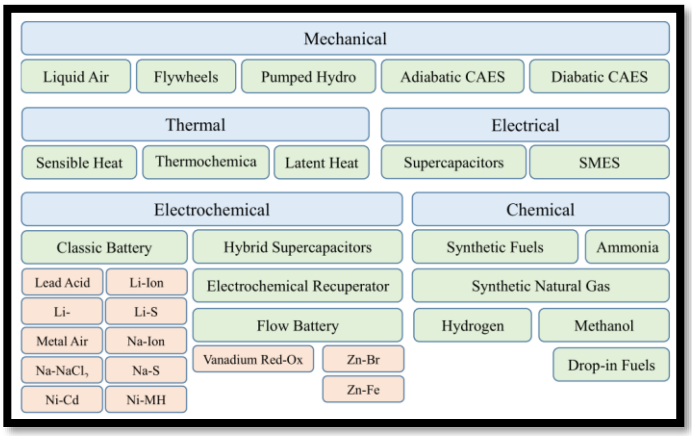

Figure 1.2. Classification of ESS technologies [7].

The classifications of the different technologies can follow various criteria, e.g., according to response times, the form of stored energy, etc. Currently, the most widely used approach is to classify ESSs according to the way energy is obtained and stored (see Figure 1.2); thus, there are mechanical, thermal, electrical, electrochemical, and chemical energy storage systems [7], [29], [30], [31], [32].

1.2.1.1. Mechanical storage systems

Mechanical ESSs convert mechanical energy into electrical energy and vice versa. At times of the day when energy consumption is lower, the system consumes electrical energy from the grid and stores it using the operating principles of potential energy, kinetic energy, pressurized gas, and forced spring. When the power system requires the stored energy, these systems perform the reversible process and deliver the required electrical energy [7], [29], [30], [31], [32].

1.2.1.2. Thermal energy storage systems (TES)

Thermal energy storage systems can store and deliver energy in the form of heat or ice, depending on the type of application. This technology is gaining momentum in the industrial and residential sectors primarily; heating and air conditioning systems are benefiting the most in buildings, small industries, and businesses [32].

1.2.1.3. Electrical energy storage systems

Electrical energy storage systems achieve energy storage directly in the form of charge and are based on electrostatic and magnetic systems (EMESS). The main technologies used in power systems are supercapacitors in conjunction with superconducting magnets, these devices store energy in the electrostatic and magnetic field respectively [7], [29], [30], [31], [32].

1.2.1.4. Electrochemical energy storage systems

Electrochemical storage systems consist of a battery that is composed of one or more cells. These cells are a series/parallel combination to obtain the required DC voltage and power [7], [29], [30], [31], [32].

1.2.1.5. Chemical energy storage systems (CES)

Chemical energy is stored in molecular compounds, and the transformation of energy is performed through the chemical bonds of some molecules. The stored chemical energy can be released through chemical reactions, where chemical bonds in materials are broken and new ones are formed [7], [29], [30], [31], [32], [33].

1.2.2. Applications of energy storage systems in electrical power systems

The applications of energy storage systems have been extended to all parts of the electrical power system. Today ESS can be applied in generation, transmission, distribution, as well as on the consumer side (Figure 1.3). This great versatility means that the use of these systems is increasing considerably every day [7].

CONVENTIONAL/BULK GENERATION SERVICES	TRANSMISSION	DISTRIBUTION	CUSTOMER SIDE	RENEWABLE GENERATION
				
• Arbitrage • Peak shaving • Load leveling • Generator bridging • Generator ramping and load following • Black start	• Frequency control • Angular stability • Voltage support • Investment deferral • Transmission support	• Capacity Support and investment deferral • Contingency grid support • Voltage control • Reactive power compensation	• End-user peak shaving • Energy cost management • Power quality • Energy back-up • Reactive power compensation	• Curtailment minimization • Capacity firming • Ancillary services support

Figure 1.3. ESS applications in power systems.

1.2.2.1. Conventional/Bulk generation services

Conventional synchronous generation aims to maintain a balance between electricity generation and consumption. Maintaining this balance is becoming increasingly complicated, as the current electricity systems demand more electricity with an adequate level of reliability and quality. The main applications of ESS in conventional generation are energy arbitrage, peak shaving, load levelling, generator bridging, generator ramping and load following and Black start.

1.2.2.2. Transmission

The security of the transmission grid is essential because the stability of the power system depends on it. For this reason, different devices are used to maintain the stability and reliability of the grid, including energy storage systems. The main applications of ESS within the transmission system are frequency control, angular stability, voltage support, transmission investment deferral and transmission support.

1.2.2.3. Distribution

Distribution networks are responsible for carrying energy to homes, small industries, and businesses. Due to their topology, these networks are very ramified and extensive and can be both above ground and underground. The main applications of ESS in distribution networks are capacity support and investment deferral, contingency grid support, voltage control and reactive power compensation.

1.2.2.4. Customer services

The energy that is generated and transmitted to the consumers in the power system must meet the required quality and reliability. The ESS can be used to improve energy management and help reduce energy costs. The main customer-facing actions that ESSs can perform are end-user peak shaving, time-of-use energy cost management, power quality, continuity of power supply and reactive power compensation.

1.2.2.5. Renewable generation services

The penetration of renewable energy sources reduces the inertia and natural damping of power systems. These phenomena, together with the high variability of the power supplied by renewable energy sources, make stability problems an issue to be solved in today's power systems. The use of ESS in conjunction with renewable energy sources helps to reduce the variability within the system and maintain balance and stability. The main applications of ESS with renewable energy sources are curtailment minimization, capacity firming and ancillary services support.

1.3. Control systems for inverters used in BESS

BESSs are systems composed of electrochemical batteries, representing one of the most prevalent technologies in contemporary power systems. The applications are innumerable, and new battery technologies are being developed every day to solve different challenges. Due to the importance of these systems, a detailed study of the control techniques is necessary, as well as the knowledge of the hardware and the main applications within the current power systems. The following sections present an updated state-of-the-art analysis, including the main topologies of the converters used in BESS, the various control strategies, the internal control loops and the controls for contingencies and transient events of the grid.

1.3.1. Power converters

One of the fundamental elements of the BESS is the power converter. This device is responsible for controlling the power flow between the battery and the grid [7], [34], [35].

The converter is bidirectional, as it controls the power flow in two directions: from the grid to the battery during the charging, or from the battery to the system during the discharging. This device must comply with the conditions imposed by the grid code and the operator's instructions, and it must also control the optimal charging level of the batteries [7], [34], [35].

Different topologies are used in these converters for BESS operation, as highlighted in Figure 1.4. These can be divided into two groups: with an output transformer connected to the power system or without a transformer (directly connected to the power system) [7], [34], [35].

The most used converters are the two-level, the three-level, and the multilevel converters. Regarding topology, the use of transformers with the converter is proving to be the preferred solution among manufacturers for higher power applications [7], [34], [35].

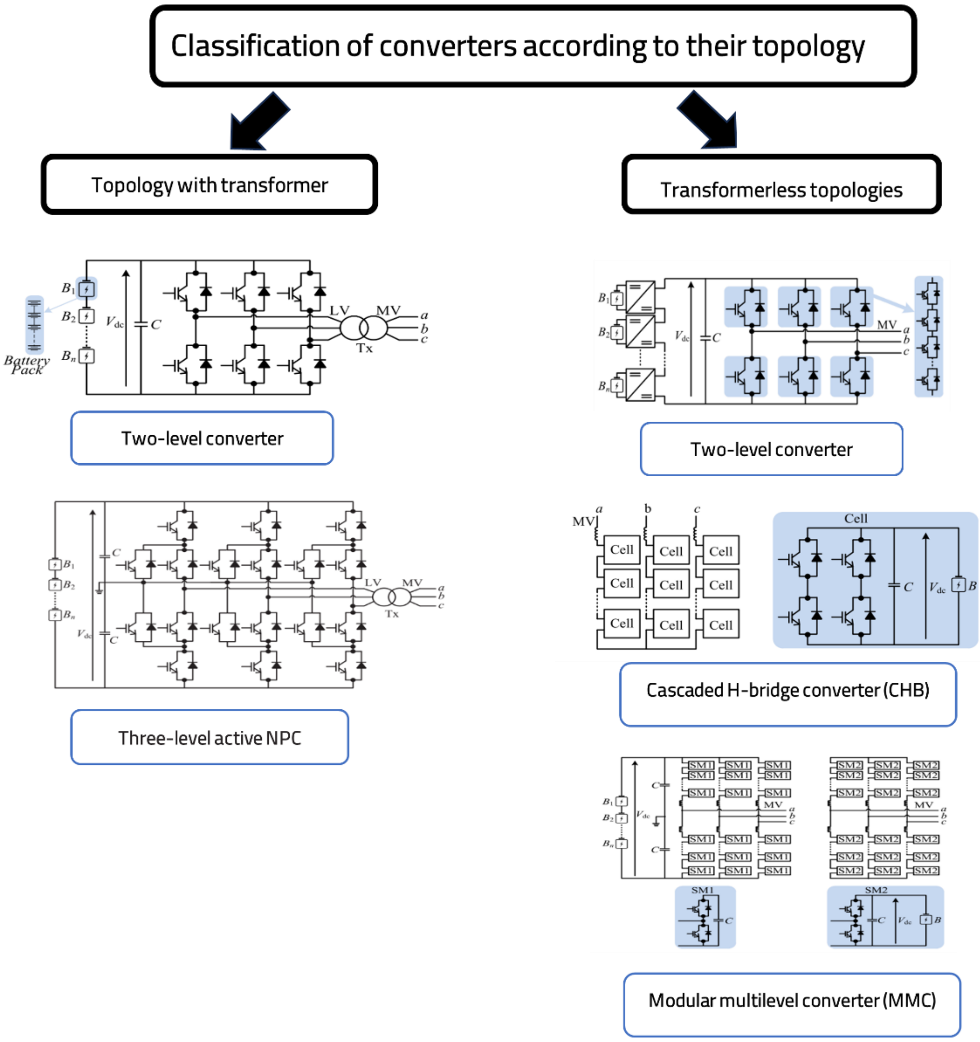

Figure 1.4. Different topologies of BESS converters [35].

1.3.2. Control of power converters

In order for the converter to supply or consume the power required by the grid, they must be controlled according to the specific requirements imposed by grid codes. In the past decade, a wide range of control solutions have been developed for BESS applications. With the growing penetration of inverter-based resources, these control strategies have evolved toward more robust and grid-oriented approaches.

The most used controllers today use two main approaches: Grid following or grid feeding (GFL) and grid forming (GFM). These control techniques differ from each other, but GFL is currently the most widely used [36], [37], [38], [39].

GFL technology depend on the existing grid, as they synchronise with the voltage and frequency set by other sources, usually synchronous machines. This makes them suitable for strong, stable electrical systems, but in weak grids they may cause instability problems in both frequency and voltage. In addition, their ability to respond to faults is limited and they often need the support of a robust grid to remain operational. In contrast, GFM technique can generate their own voltage and frequency reference, functioning similarly to a virtual synchronous machine. As a result, they provide synthetic inertia, stabilise frequency and better regulate local voltage, even in weak systems or microgrids. They also perform more robustly during disturbances and faults, helping the system to recover [36], [37], [38], [39].

1.3.2.1. Comparison of GFL and GFM technologies.

The GFL control technique operates as a grid follower and is represented as a current source connected in parallel to the grid, as shown in Figure 1.5. In general, the GFL controller is a current-controlled voltage source that must be synchronized to the grid by a phase-locked loop (PLL), and it requires a power controller that sends the reference currents to an inner current controller [36], [37], [38], [39].

In contrast, the GFM control does not necessarily require the use of the PLL for synchronization and can be represented as a voltage source with a given amplitude and frequency, as represented in Figure 1.6. In general, these controllers operate as a voltage-controlled voltage source; this behaviour allows this technology to better contribute to system stability by behaving similar to conventional synchronous generator.

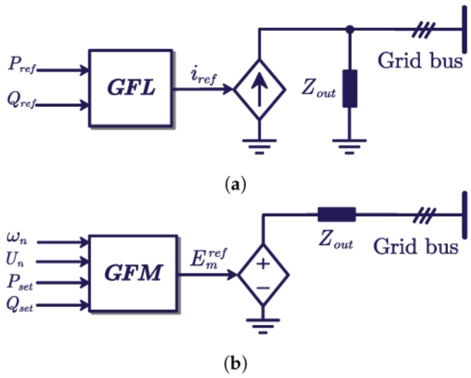

Figure 1.5. Control technologies used in renewable energy: a) Grid following. b) Grid forming [40].

Table 1.2 compares the two control technologies based on the advantages and disadvantages of each control. The basic characteristics of each technology are listed, as well as the type of network in which it is more advantageous to use it.

Table 1.2. Comparison of GFL and GFM converters [33]		
Control mode	Advantages	Disadvantages
GFL converter	1. Quick regulation	1. Lack of frequency and voltage regulation
	2. Simple control structure	2. Unable to operate in an islanded mode
	3. Stability on stiff networks where SCR>4	3. Instability on weak networks where 2<SCR<4
GFM converter	1. Stability on weak networks where 2<SCR<4	1. Instability in stiff grids where SCR>4
	2. Able to operate in an islanded mode	2. Easily susceptible to overload
	3. Provides the regulation of frequency and voltage	

1.3.2.2. GFL and GFM control structures

As explained above, the GFL and GFM technologies are different and are used according to the network characteristics. In terms of the structure of their control loops (Figure 1.6), these two technologies have different approaches, although many of their internal control loops are similar. Figure 1.6 shows the control structures of the two technologies, showing how they differ in the way they synchronize to the grid and in the way they control the power output of the inverter [7], [36], [37], [39], [41].

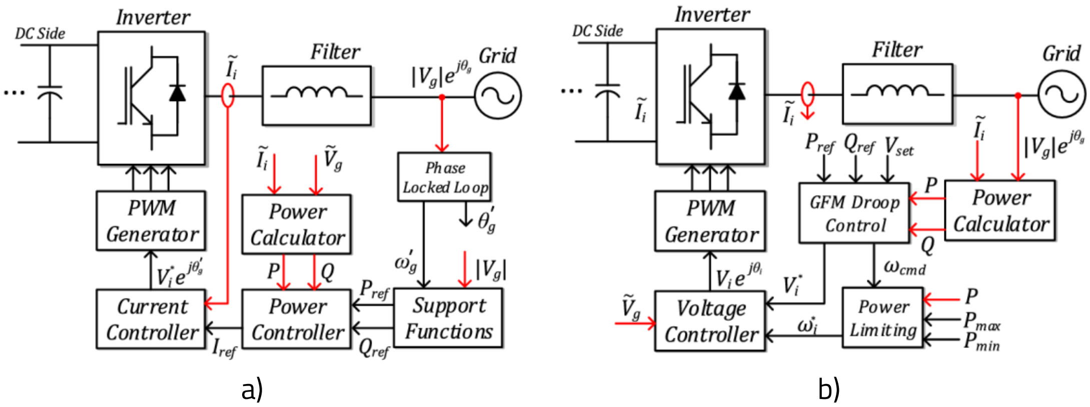

Figure 1.6. Typical block diagrams of technologies a) GFL and b) GFM [41].

1.3.3. Contingency and transient control systems

Failures and, in general, transient phenomena in power systems are unavoidable events. The randomness of the phenomena and the initial conditions before these events do not allow an accurate prediction of their occurrence. These events can be of great magnitude and pose a problem for the stability of power systems.

The above phenomena are more critical in weak networks, as the presence of transient events can jeopardise the stability of the system [23]. For this reason, grid codes (GCs) specify the operation of renewable sources during transients and frequency control during contingencies. The controls used in inverters during contingencies and transients are Voltage Fault Ride-Through (VFRT) and Frequency Control [7].

1.3.3.1. Voltage fault ride-through

The VFRT is defined in grid codes as the time required to keep the renewable resources connected during the occurrence of a voltage disturbance in the grid. The VFRT characteristic depends on the value of the voltage drop or rise with respect to time. This characteristic is slightly different for each grid code, which is country specific, as shown in Figure 1.7, and must be coordinated with the network protection devices [42].

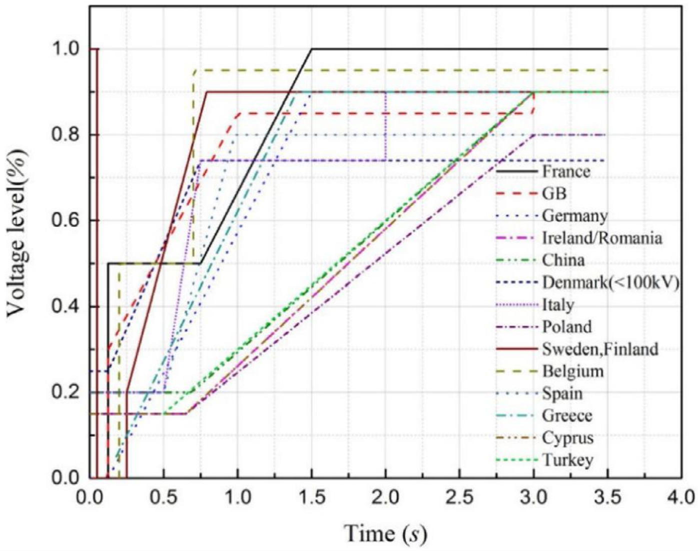

Figure 1.7. Characteristics of VFRT in different countries [42].

The VFRT curve is divided into three main regions (Figure 1.8): low voltage ride through (LVRT), zero voltage ride through (ZVRT), and high voltage ride through (HVRT). Depending on the region of the VFRT curve, the time during which the renewable source will remain connected to the grid in the event of a failure is defined [42].

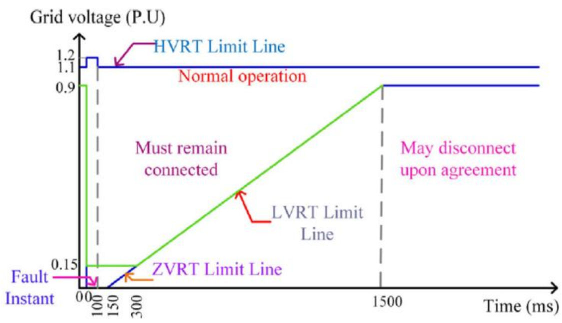

Figure 1.8. Different regions of the VFRT in the case of the German network code [42].

1.3.3.2. The Cuban grid code and VFRT requirements

Note: The material in this section is based on author's own papers published in [6] *and* [43].

In the case of the Republic of Cuba, the GC is adapted to the characteristics and particularities of its power system, which is undergoing constant updates driven by the growing development of generation from renewable sources in the nation.

When disturbances occur, it is important that RES generators remain connected for a suitable period. Moreover, this behaviour is beneficial for the stability of the system, which can be affected by significant frequency deviations due to the active power deficit. For this reason, RES must comply with the fault ride through (FRT) characteristic Figure 1.9 defined in the Cuban GC. It is of paramount importance that the generation plant remains connected in order to prevent critical situations that could compromise stability [44], [45].

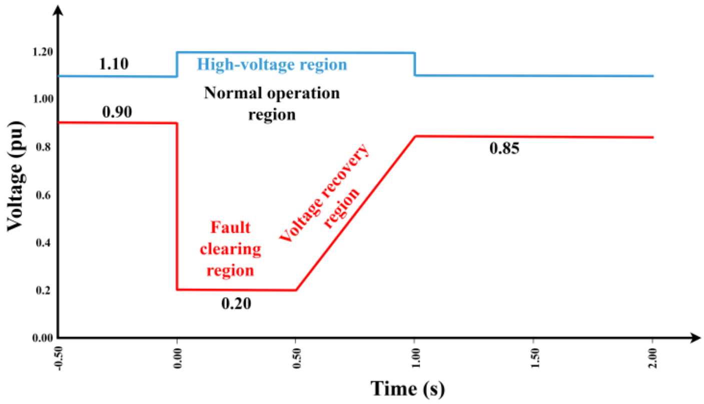

Figure 1.9. VFRT characteristic established by the Cuban grid code.

<u>Reactive current support</u>

The Cuban GC stipulates that RES must contribute to the grid stability and voltage restoration in the event of a grid fault. Consequently, inverters must possess the capability to supply or absorb reactive current. The magnitude of reactive current to be managed by the inverter is contingent upon the voltage deviation level (Figure 1.10).

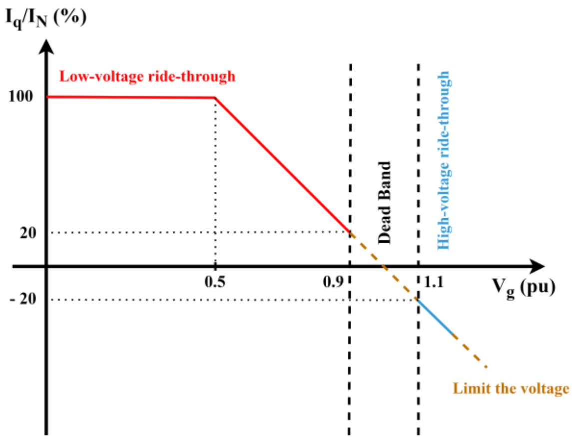

Figure 1.10. Reactive current injection requirements for the Cuban grid code.

1.3.3.3. System frequency control

The occurrence of disturbances and transients in the network can be reflected, depending on the disturbance type and level, in the behaviour of the frequency; these events can be of greater magnitude in weak systems where the inertia and frequency regulation capacity of the system is insufficient. For this reason, system operators must monitor the frequency of the power system in a detailed and continuous manner, especially in weak systems.

The growth of distributed generation, and especially the growth of renewable sources in power systems, has led to a decrease in the overall inertia of current power systems. Due to this situation, BESS is mainly used for frequency control in systems with high penetration of renewable sources [46].

BESS have several control loops for frequency control, each of which is related to the different phases of frequency control in the power system. Among the controls used for frequency control in BESS are virtual inertia control, droop control or primary control, and secondary control (Figure 1.11 – Figure 1.13).

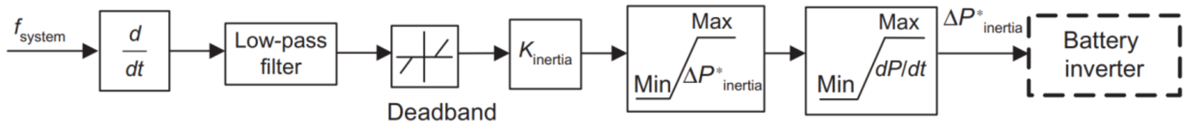

Figure 1.11. Block diagram of the BESS virtual inertia control [28].

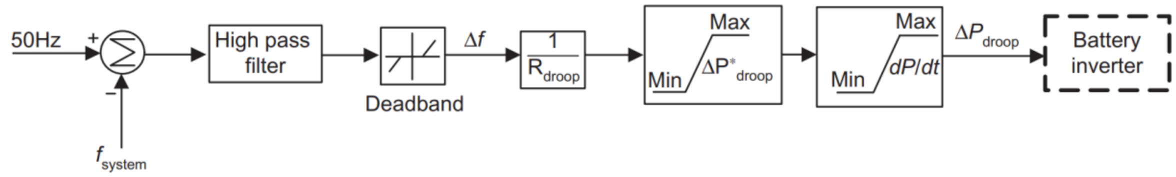

Figure 1.12. Block diagram of the primary control of a BESS [28].

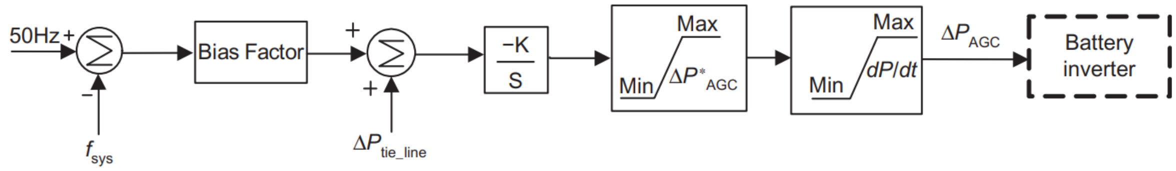

Figure 1.13. Block diagram of BESS secondary frequency control [28].

1.4. Battery storage systems projects around the world.

The integration of ESSs into power grids has become a strategic necessity, resulting from the structural transformations caused by the growing penetration of renewable generation sources, whose variable and intermittent nature poses significant challenges to the stability and reliability of the electricity system. In response to these issues, the implementation of ESS projects has experienced exponential growth worldwide, as evidenced by data reported by the United States Department of Energy [47].

Among the most notable projects are pumped storage systems and BESS. In the case of BESS, these have increased in recent years due to the modularity of batteries, as well as lower production costs (Figure 1.14). Table 1.3 shows a summary of some of the most significant projects.

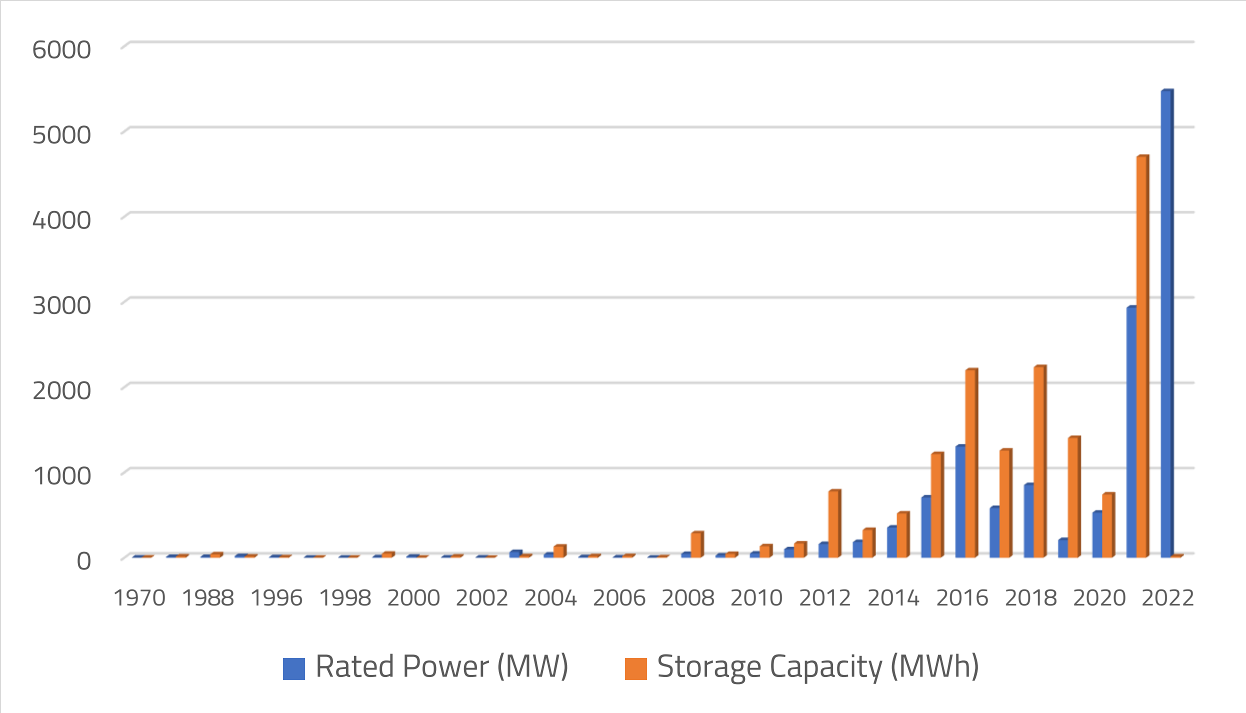

Figure 1.14. Electrochemical storage system Installations by Year [47].

Table 1.3. BESS projects worldwide		
Location	**Battery storage configuration**	**Application**
Australia	30 MW/8 MWh	Fast frequency response.
Australia	120 kW/120 kWh lithium-ion batteries & 180 kW/900 kWh vanadium redox flow batteries	Peak-shaving.
United States	8MW/2 MWh	Frequency regulation.
United States	10MW/40MWh	Spinning reserve, load levelling.
United States	100 kW/300 kWh lithium-ion batteries & 277 kW/8 kWh supercapacitors	Energy time shift, power smoothing, frequency regulation.
Germany	8.5MW/8.5MWh	Frequency control and spinning reserve.
Germany	20 MW battery-electrical heating system	Frequency regulation.
Germany	12.5 MW lithium-ion batteries & 137 MW pumped hydro storage	Energy arbitrage, frequency regulation, black start.
Puerto Rico	20MW/14MWh	Frequency control and spinning reserve.
Japan	34MW/244.8MWh	Wind power fluctuation mitigation.
Ireland	2MW/12MWh	Wind power fluctuation mitigation.
China	4 MW lithium-ion batteries & 1 MW flywheels	Power smoothing, frequency regulation.

China	5 MW/5 MWh lithium-ion batteries & 2 MW/0.4 MWh flywheels	Frequency regulation.
China	15 MW/7.5 MWh lithium-ion batteries & 5 MW supercapacitors	Frequency regulation.
China	201 MW/402 MWh lithium-ion batteries & 3 MW/187 kWh supercapacitors	Energy arbitrage, frequency regulation, black start.
Poland	1 MW/0.47 MWh lithium-ion batteries & 5 MW/26.9 MWh lead-acid batteries	Energy time shift, energy arbitrage, voltage support.
United Kingdom	50 MW/50 MWh lithium-ion batteries & 2 MW/5 MWh vanadium redox flow batteries	Energy arbitrage, frequency regulation.
India	614.4 kWh lithium-ion batteries & 480 kWh lead-acid batteries	Peak-shaving.
Italy	4 MW/8 MWh lithium-ion batteries & 43.4 MW pumped hydro storage	Energy arbitrage, frequency regulation, black start.

1.4.1. Application of a BESS in a weak system with low inertia and high penetration of renewables.

One of the most interesting projects carried out on an isolated low inertia system was the implementation of a 1 MW, 250 kWh battery to control the frequency deviation caused by a high penetration of renewable energy sources on the island of Hawaii. This project was developed in collaboration with the Hawaii Natural Energy Institute (HNEI), the University of Hawaii at Manoa, and the grid operator, Hawaii Electric Light Company (HELCO, Hilo, HI, USA) [10].

The use of a lithium-ion titanate battery allows this BESS to have a high charge and discharge rate (C-rate), enabling high battery operating speeds. The C-rate of this battery is 2.5C, calculated as the ratio of power to rated energy.

The connection between the storage system and the power system was made at the transmission level of the island. The BESS is composed of two containers (Figure 1.15); one is the power module (PM), and the other is the power conversion system (PCS).

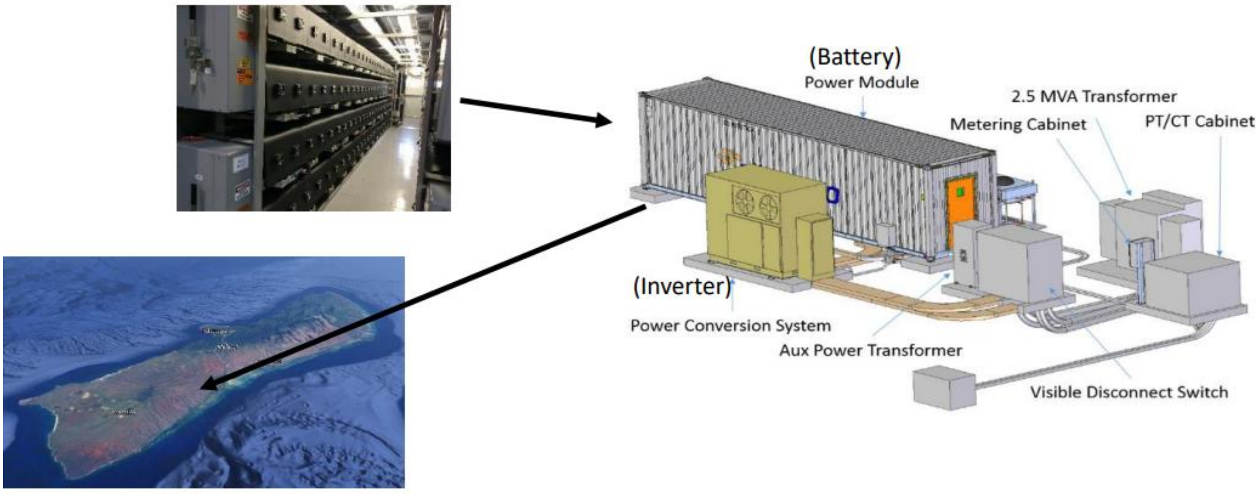

Figure 1.15. Example of a MW-scale BESS [10].

1.5. BESS development challenges in the context of the Cuban power system

Note: The material in this section is based on author's papers published in [6] *,* [43] *and* [5]*.*

Since 2014, the Republic of Cuba has pursued a plan to transform its energy matrix through the introduction of renewable sources into the electricity system. The main goal of the transformation plan is to achieve 30% of electricity generation from renewable sources by 2030 [48], [49].

This ambitious plan responds to one of the world's environmental protection goals, which is to reduce CO_2 emissions into the atmosphere. It is estimated that by 2030, Cuba will have a total of 2000 MW of photovoltaic generation and approximately 700 MW of wind generation [50].

According to [50], renewable generation must coexist with conventional generation, which could pose a problem for the frequency stability of the Cuban power system. Given this situation, it is necessary to use BESS to support frequency regulation. Because of this situation, studies are being conducted to determine the capacity of BESS needed by the electrical grid [50].

For the power system, the use of BESS for frequency control is a necessary challenge, as we also recently analysed in [5]. This application of BESS in the Cuban power system opens the possibility of using BESS in other applications such as steel mills.

1.5.1. Use of BESS in Cuban electric steel mills

In the Republic of Cuba, the past few years have presented significant challenges to the operation of the electrical power system. Frequent blackouts, mainly caused by a generation capacity deficit, are largely due to extended maintenance cycles of the main power plants and fuel shortages [51], [52]. This combination of factors creates a complex operational scenario that severely limits the efficient management of the power system, particularly regarding frequency control. These limitations are further exacerbated by the presence of EAFs in the Cuban electricity system, which are highly demanding and variable loads that require direct and constant intervention by the system operator [5], [53]. Proper management of these loads is essential for maintaining power system frequency stability, although their simultaneous operation has a negative impact on industrial productivity.

Figure 1.16 illustrates the typical behaviour of the power system frequency during EAF operation, showing that during most of the industrial process, the frequency remains outside the dead band range (represented by the black dashed lines) established for the Cuban power system (59.7–60.2 Hz) [5]. These values were obtained from the National Load Dispatch Centre's SCADA system records in 2023.

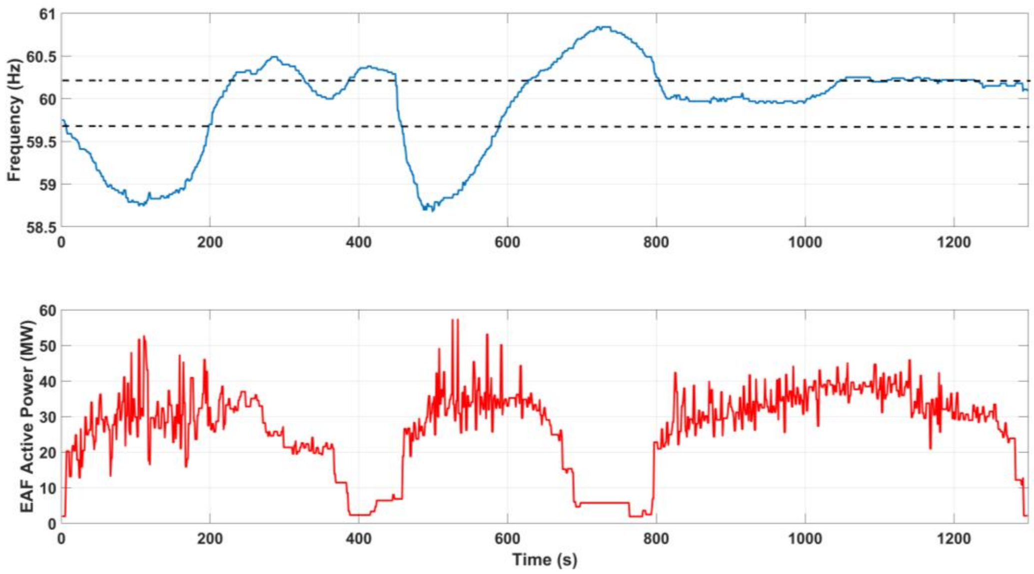

Figure 1.16. Frequency behaviour of the Cuban power system under the action of EAFs (experimental measurements).

Operating EAFs within the system highlights a significant weakness in the Cuban power system's ability to control frequency. In order to avoid the collapse of the power system during the operation of EAFs, the system operator imposes restrictions on the maximum power that can be demanded by the furnaces. This measure is beneficial for the grid, but as a consequence it affects the productivity and efficiency of the steel plant by increasing melting times and contributing to an increase in energy consumption [4]. Therefore, new solutions have been investigated to ensure the operation of the steel industry under Cuban power system conditions. One solution proposed by the author is the use of BESS in parallel with the EAF, aimed at supporting the transition rates between different melting processes, which place significant stress on the power system. Figure 1.17 shows the proposed integration of BESS within the EAF electrical infrastructure, where a specific Cuban steel mill was considered. The BESS is connected on Bus 2 at a voltage of 34.5 kV.

Regarding grid interaction, as discussed in Section 1.3.2.1, the choice between GFL and GFM control strategies mainly depends on the grid SCR at the PCC. Given the strong connection of the EAF to the transmission system through two parallel transformers, the SCR level at the BESS PCC is relatively high (2000 MVA). Therefore, as previously explained, GFL control represents the optimal choice.

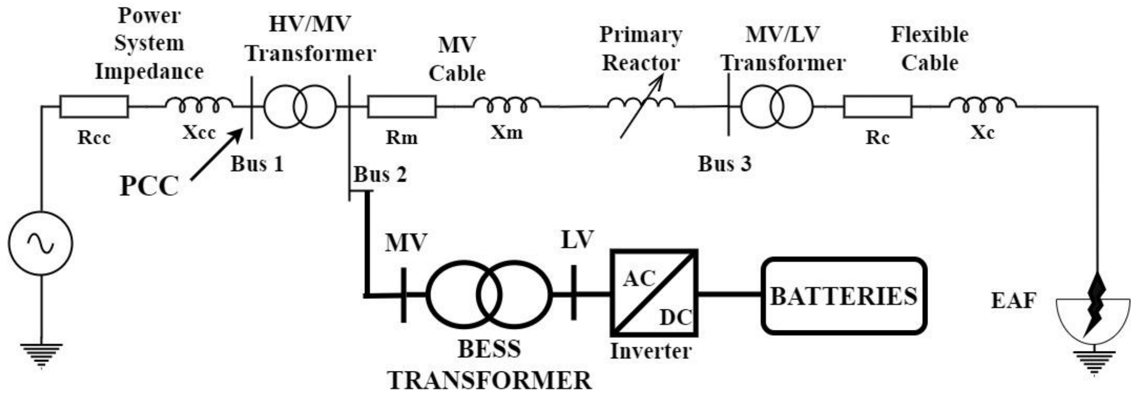

Figure 1.17. Single-line diagram of the power supply system of the steel mills in Cuba with integrated BESS.

1.6. Conclusions

The use of energy storage systems in power systems is a necessity today. The applications of these systems can be seen in any part of the electrical grid, which represents a change in the energy matrix that makes the electrical service more distributed. The Cuban power system, which is the focus of this thesis, aligns with the global trend of increasing reliance on renewable energy sources and, consequently, the integration of energy storage systems across the network.

Among the most common storage systems in use today are BESS, which are designed primarily to contribute to the stability of the power system and to facilitate the introduction of renewable energy sources, among other things. These systems feature bi-directional converters that allow for the fast and efficient conversion of direct current to alternating current and vice versa.

Battery storage projects are increasing every year due to the number of applications these systems present. The most common services provided by BEES in electric grids are electricity bill management, energy time shifting, frequency regulation, microgrid capacity, renewable generation switching, and renewable capacity firming.

In terms of control functions, these systems can use two main technologies, GFL and GFM, although GFL is currently the most widely used. The efficient use of these technologies in electrical networks depends on the strength of the power system with respect to it short-circuit power. In weak networks where the short-circuit ratio is between 2<SCR<4, the use of GFL technology is not recommended, while in the case of strong networks where the short-circuit ratio is SCR>4, the use of GFM technology is not recommended.

Another peculiarity of the control systems in the BESS is that they must be capable of handling transient events that occur in the power system. Under this premise there are two fundamental controls, the VFRT and the frequency control.

The various BESS projects around the world, as well as the study of the state of the art of these storage systems, make it possible to find new niches for future applications within the power system. One such application is the use of BESS in electric arc furnaces to improve the electrical efficiency of steel mills in conjunction with supporting frequency regulation in a weak power system.

CHAPTER 2 . Advanced control implementation of a BESS-based compensator for electric arc furnaces in weak power systems

Electric arc furnaces play an important role in electric steel mills during the steelmaking process. These are used to produce various types of steel, mainly for the construction industry and other sectors of society. A sustainable electric arc is formed inside these furnaces, which provides the thermal energy needed to melt the scrap metal. As a result of the non-linear behaviour of the electric arc, various problems occur in the power supply system. From a power quality point of view, these furnaces cause severe disturbances in the magnitude and waveform of the voltage, in addition to worsening the power factor of the industry [2]. Furthermore, EAFs cause voltage and current unbalances as well as harmonics [2], [54]. Concerning the system's stability, if the power system is weak in terms of the frequency regulation capacity (as is the current case of the Cuban power system), the operation of EAFs can cause severe perturbations and even the total disconnection of the system [4], [17]. This is one of the major obstacles to installing large EAFs in the investigated power system.

The electrical power supply problems caused by EAFs are solved in various forms. Every solution implemented in steel mills addresses specific issues, yet none offers a comprehensive approach that effectively mitigates all problems. Among the solutions described in the literature, and thanks to advances in power electronics, the implementation of industrial-scale BESS systems is emerging as a comprehensive alternative for addressing the electrical challenges faced by steel mills. Their application would not only help to mitigate adverse electrical phenomena but also increase the efficiency of the industrial process [4]. Based on these premises, the objective of this chapter is to present the implementation of control systems for a BESS that acts as a compensator for a high-power EAF within the Cuban power system.

2.1. Challenges arising in the Cuban power system caused by electric arc furnaces

Note: The material in this section is based on author's paper published in [5].

The operation of EAFs in the Cuban power system is a very complex task, mainly due to the reduced frequency regulation capacity, making the process inefficient and difficult to control. Likewise, if the operation of the EAFs is not controlled and limited, the system could lose stability [53]. This phenomenon, together with the low power factor caused by the continuous changes in the current demand by the EAF, are the fundamental problems affecting the Cuban power system today.

2.1.1. Power factor

The power factor is a measure of the performance of the electrical energy supply in an installation. In the Republic of Cuba, for the supply of electrical energy to be efficient, it must be carried out with a power factor of 0.9 or higher; values lower than 0.9 represent an economic penalty for the consumer [55]. The power factor in a steel plant is typically below 0.9 and varies with the loading of the EAF. Depending on the position of the furnace transformer tap, and the inductive elements present in the steel mill circuit, a certain power factor will be obtained. To achieve efficient operation of the EAF, it is necessary to establish parameters that are set during the melting process, which are achieved by constantly monitoring the electrical equipment that supplies the EAF at each stage of work. The low power factor can occur not only when the EAF is in operation, but also when the steel mill does not work for various technical reasons where the voltage drop-in high-power elements cause large losses of reactive power, and because of this the worsening of the power factor. For these reasons, steel mills must take measures to continuously counteract the deterioration of the power factor.

2.1.2. Fluctuations at the power system frequency

In the case of the Republic of Cuba, there are two important steel mills with high-power EAFs; one is the Las Tunas steel mill, and the other is Antillana de Acero. These two EAFs introduce significant oscillations in the frequency of the Cuban power system. The operation of these companies is limited precisely because of the severe oscillations that could compromise frequency stability. Furthermore, the intensity of these fluctuations can become so pronounced that midway through the melting process, the system frequency becomes difficult to control, compelling the system operator to initiate a shutdown of the steel plant. This is one of the most severe scenarios affecting the production process due to the loss of tons of steel that are not fully melted in the EAF. It is imperative to ensure complete melting, as interrupting the process midway leads to steel that doesn't meet technical specifications, necessitating a restart. The repercussions of an abrupt steel mills shutdown encompass both economic and electrical losses, not to mention the time lost in recommencing production.

2.2. Solutions adopted by the Cuban industry and remaining challenges

Note: The material in this section is based on author's paper published in [5].

The Cuban steel industries have taken different solutions to mitigate the electrical problems caused by EAFs. These solutions have been fundamentally aimed at mitigating voltage flickers, improving the power factor, reducing the harmonic currents produced by the EAF, and reducing the over- and under-frequency peaks that could endanger the stability of the power system. Other issues, such as current and voltage unbalances, have not yet been solved, primarily because of the absence of regulatory policies addressing this phenomenon, which is not currently considered an economic priority.

The main actions taken by the Cuban steel mills were:

- The increase of the short-circuit power in the PCC to reduce the problem of voltage fluctuations and flicker.
- The installation of passive filters to reduce harmonics and improve the power factor.
- Soft start and soft ending of the EAF to improve the problems of frequency fluctuations in the power system.

2.2.1. Increase of short-circuit power at the PCC

Voltage flicker represented a problem for the Cuban steel mills, which was solved by increasing the short-circuit power at the Bus 2 in Figure 1.17 with the installation of high-power parallel transformer. The measure significantly reduces voltage fluctuations on this bus, to which consumers near the steel mill are connected, and therefore also reduces flicker. These new transformers are specifically designed with a high-power rating, and a low short-circuit reactance. For the installation of high-power parallel transformers with low short-circuit reactance, transformers with special windings have been used. The 125 MVA transformers replaced the old 60 MVA transformers with a reduced short-circuit impedance of about 5.76%. It is important to mention that such a low short-circuit impedance value is not typical for high-power transformers according to IEC 60076-5, which states that for transformers over 100 MVA the impedance should be around 15%. The characteristic of having such a low short-circuit impedance allows the voltage drop at the medium voltage busbar to be very low and, therefore, voltage fluctuations and flicker are mitigated.

2.2.2. Installation of passive filters

To solve the problem of harmonics caused by the EAF, as well as to improve the power factor, passive filters were used in Cuban steel mills until a few years ago. These filters were connected to the steelwork's medium voltage busbar at a voltage level of 34.5 kV.

After over forty years of operation, the filters employed in the Cuban steel mills had deteriorated to the point where they were no longer capable of compensating for harmonics. Another important aspect is that these filters were exposed to over currents and over voltages due to their switching when EAF was operating. In addition, the harmonic spectrum for which these filters were designed became insufficient, because the equivalent impedance of the supply network was changed by employing low reactance parallel transformers that allow the harmonics to circulate along a more feasible path to the power system.

Regarding the harmonics that contaminate the power system, it is important to say that Cuba currently lacks a standard regulating harmonic pollution at high-voltage levels, a phenomenon that can be aggravated by the operation of EAFs without adequate harmonic compensation. Meanwhile, the low power factor continues to be a problem for the metallurgical industries, which are economically penalized by the system operator for maintaining an inadequate power factor.

2.2.3. Soft start and soft ending of the EAF

The Cuban power system currently does not have enough high-power generators that perform effective frequency control; for this reason, large loads such as steel mills are closely controlled by the system operator [53].

The control of the EAFs is achieved with a soft start and ending in the form of a power ramp. These ramps are managed by the system and furnace operator. The tap changers of the furnace transformer and the primary reactor are used to perform the different ramps at the start and stop of the EAF (Figure 2.1). Changing the reactor and furnace transformer taps causes changes in the power demand of the EAF on the system, and thus also controls the frequency.

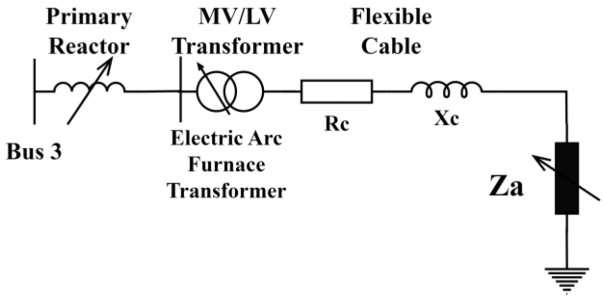

Figure 2.1. Primary reactor and furnace transformer as arc power control in the EAF.

The soft startup and shutdown of the EAF contribute to maintaining the stability of the Cuban power system. While this benefits the system operator, it disadvantages the industry, as it negatively impacts production efficiency. Figure 2.2 shows the idea of the soft start and soft ending of the EAF, as compared to the normal starting and ending that the EAF should follow for an efficient melting process. If we compare the two graphs, we can see that the soft start and soft ending make the melting time longer compared to the normal entry and exit, while the melting time is much shorter in the normal entry and exit.

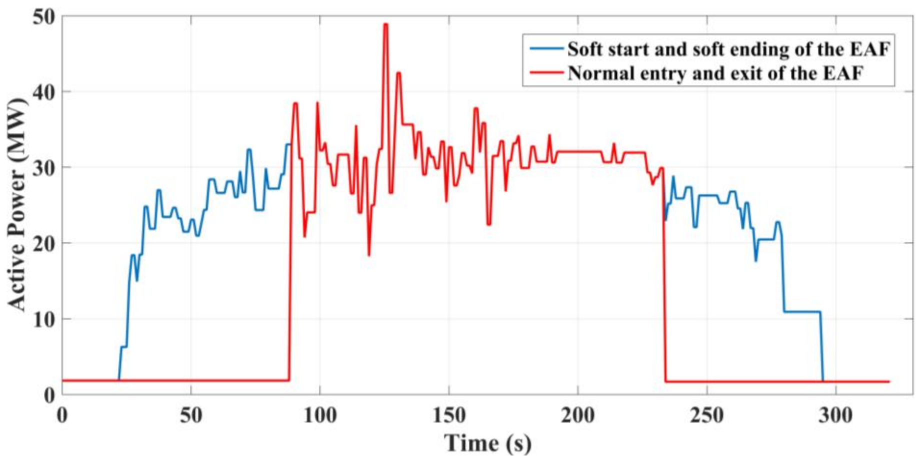

Figure 2.2. Soft start and soft ending of the EAF vs. normal EAF operation.

2.2.4. Remaining challenges in Cuban steel mills

The solutions explained above have not comprehensively solved all the challenges that are present in the Cuban steel mills. Problems such as the low power factor, as well as the low efficiency of the production process caused by the input and output of the EAF in the form of a ramp, have not been solved so far.

The economic losses resulting from penalties for low power factor, together with the increase in energy consumption caused by the staggered operation of EAFs, highlight the need to implement technical and definitive solutions to address these problems. Furthermore, harmonic pollution in these Cuban industries has not been studied in depth, which has limited the installation of comprehensive solutions that address all existing problems. Based on these challenges, the following sections will present the different control systems of a BESS, which is proposed as a comprehensive solution to the difficulties outlined above.

2.3. BESS control system configuration

Note: The material in this section is based on author's papers published in [6], [43], [56], [57].

Due to the current conditions of the Cuban power system—characterized by low inertia, a wide frequency dead band, and weak primary and secondary control—high-power consumers, such as steel mills, face significant challenges in operating efficiently. To address this issue, the solution proposed by the author in [4], [5] involves integrating a 25 MVA BESS in parallel with the 50 MVA EAF, primarily for active power compensation. As discussed in [4], selecting the battery involves balancing performance and cost based on requirements of the EAF under the specific conditions of the Cuban power system. It was determined that a battery capable of supplying 50% of the EAF's maximum demand is sufficient to support its transitions between different operational states while minimizing disturbances to the power system (Figure 2.3).

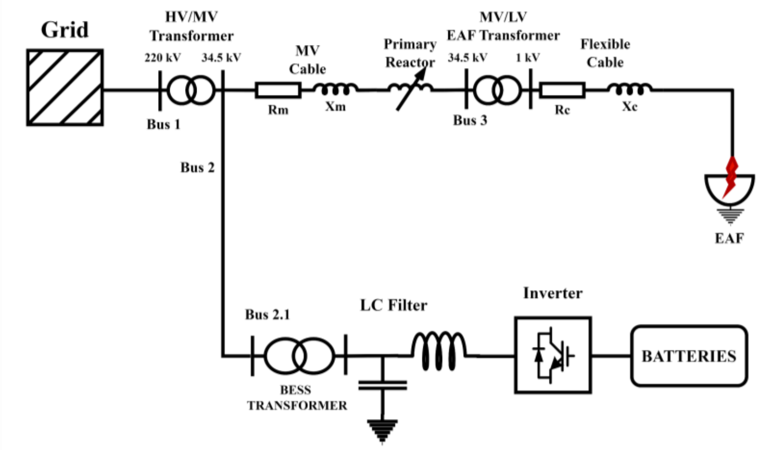

Figure 2.3. Single-line diagram of the power supply system of a 50 MVA EAF in combination with a BESS.

At this power level, a BESS generally operates with multiple converters in parallel. In order to analyse the behaviour of the BESS inverter a control system based on multiple loops has been designed, modelling the inverter as a voltage source (VSI). This control system (Figure 2.4) has been implemented in a three-phase, two-stage inverter that keeps the DC voltage constant during grid disturbances. The analysis focused exclusively on the response of the inverter, assuming a constant DC voltage provided by the battery.

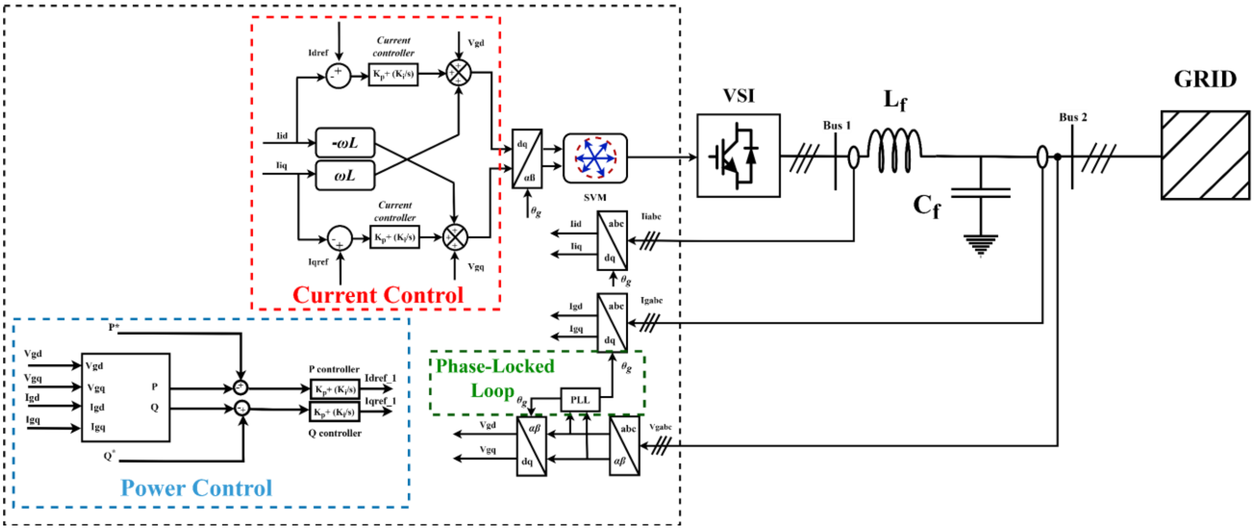

Figure 2.4. General diagram of the VSI connected to the network.

In general terms, the control of a VSI system consists mainly of two control loops: an internal loop and an external loop. The internal loop is responsible for current control, while the external loop, shown in Figure 2.4, is responsible for power control. However, additional controllers can be incorporated into this external loop, which will be described in the following sections.

2.3.1. Current control (internal loop)

The main function of current control is to regulate the current that the inverter injects into the grid. Once the PLL determines the phase reference, the measured currents are transformed to the synchronous dq frame, allowing independent control of the components associated with active power (I_d) and reactive power (I_q). The controller compares the actual currents (I_d, I_q) with their references (I_{dref}, I_{qref}) and adjusts the inverter's modulation signals to correct any deviations [58].

2.3.2. Power control (external loop)

Power control is responsible for setting the references for the current control loop. This block determines the desired values of I_{dref} and I_{qref}, in accordance with the system's operating objectives, such as maintaining a certain active power flow *(P)* and power factor or reactive power level *(Q)*. In the case of a BESS, this control defines the active and reactive power based on the needs of the grid operator or the energy management strategies implemented [58].

2.3.3. Phase-locked loop

The purpose of the PLL is to synchronise the converter with the electricity grid. Since the inverter does not generate its own voltage (as in a grid-forming system), it needs to 'follow' the frequency, phase and magnitude of the existing grid in order to inject power properly. The PLL measures the three-phase voltage of the grid and estimates the phase angle (θ) and instantaneous frequency (ω) of the system.

2.3.4. Voltage fault ride-through

The occurrence of network faults can significantly affect the stability of the power system, and in electrically weak systems, it can even cause total disconnection. Based on international experiences where stability has been compromised by such events, this section proposes an adaptive fuzzy control system for VFRT, designed to comply with the requirements of the Cuban GC, as outlined in [43]. This system considers the voltage and frequency variations that occur during voltage sags or swells in the electrical network. The proposed control was implemented within the VSI inverter control system (Figure 2.5), and its detailed structure is shown in Figure 2.6.

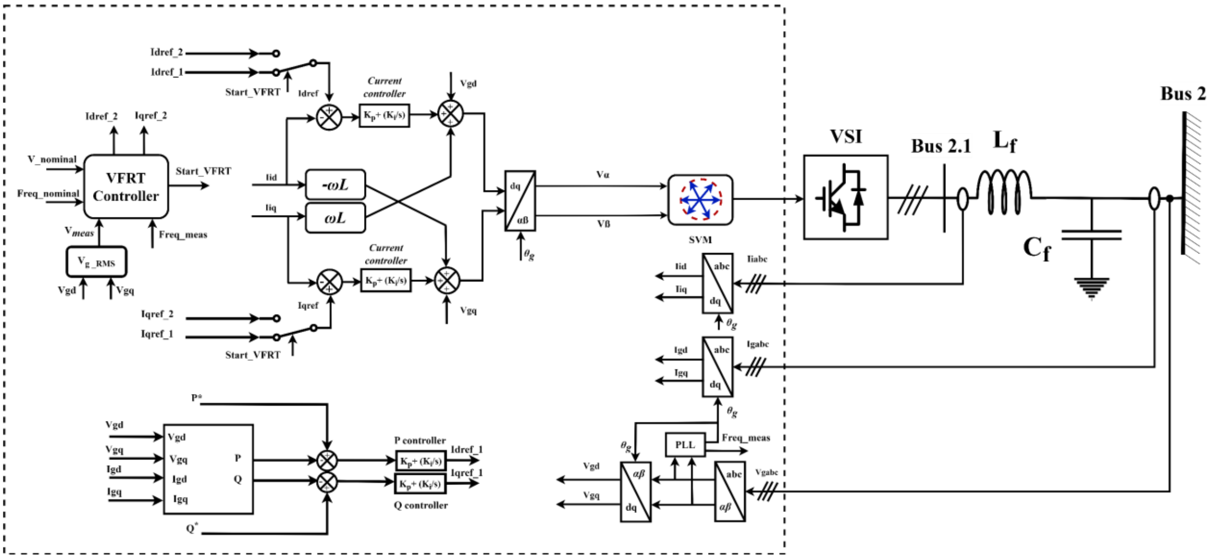

Figure 2.5. Diagram of the VSI connected to the network, together with its control system and the VFRT control scheme.

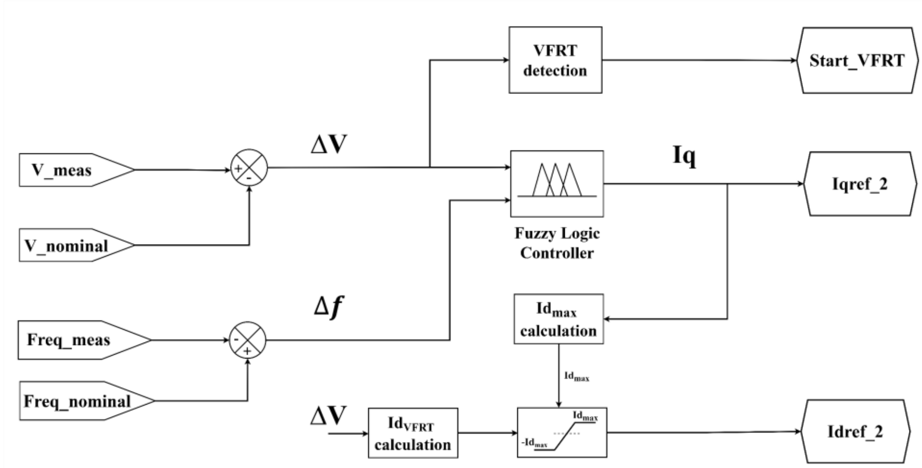

Figure 2.6. VFRT controller.

To detect the presence of sags or swells in the power system, the RMS voltage of the grid is monitored and when these conditions are verified, the VFRT controller is activated. Its purpose is to adapt to the network conditions by detecting the voltage variations together with the frequency behaviour to improve the voltage profile and contribute to the stability of the system in case of sags or swells.

2.3.4.1. VFRT detection

The voltage variations exceeding the normal range of ± 10 % are identified through the calculation of the RMS voltage at PCC using the reference frame dq [59]:

$$V_{gRMS} = \sqrt{{V_{gd}}^2 + {V_{gq}}^2} \tag{2.1}$$

where V_{gRMS} is the grid voltage, while V_{gd} and V_{gq} are the voltage components on the direct and quadrature axis.

The RMS value of the grid voltage is fed into the $V_{\_meas}$ input of the VFRT regulator, as shown in Figure 2.6, allowing the presence of dips or swells in the grid to be detected. When voltage fluctuations occur, this controller changes the inverter's operating state from the normal state to the activation of the VFRT state.

2.3.4.2. Reactive current injection during VFRT

Once the VFRT control is activated in the inverter, the converter must inject or consume reactive current to help restore the voltage profile after the event. Although there are several methods for controlling the reactive current output of the inverter [60], [61], this work presents a method that not only complies with the Cuban GC standard but also adds a substantial improvement by considering grid frequency deviation, making it an ideal candidate for future revisions of the standard. If, during a voltage fluctuation in the power system, the frequency remains within the tolerable limits set by the system operator, the reactive current will strictly follow the specifications of the GC. However, if the frequency exceeds these limits, the reactive current behaviour is adjusted differently. This adaptive capability is the key feature of the VFRT control proposed in this study, the operation of which will be detailed in the following section.

The reactive current (I_q) obtained from the VFRT control, as shown in Figure 2.6, limits the inverter's ability to deliver active current (I_d). As a result, the active current component during VFRT is limited by the following equation:

$$I_d = \sqrt{{I_{max}}^2 - {I_q}^2} \tag{2.2}$$

where I_d is the reference active current and I_q is the reference reactive current that the VSI can deliver to the grid, while I_{max} is the maximum current allowed by the inverter [61].

2.3.4.3. Fuzzy controller design

The adaptive capability of these FLCs has led to the development of a new VFRT controller in this work (Figure 2.6), which aims to calculate the reference reactive current I_{qref2} to be sent to the inverter current controller under VFRT conditions. The VFRT control is activated when the voltage drop in the grid exceeds the dead band established in [43]. Once activated, the FLC receives as inputs the voltage deviation *(ΔV)* and the frequency deviation *(Δf).* Based on these values, the system generates as output the reference reactive current I_{qref2} of the inverter in p.u. and the reference active current I_{dref2}, whose calculation is based on the maximum active current I_{dmax} obtained from (2.1) and the calculated active current I_{dVFRT}, which depends on the voltage drop and is always less than or equal to I_{dmax}. The value of I_{dVFRT} is calculated to minimize active power fluctuations at the PCC during VFRT by partially or fully compensating for the EAF power reduction caused by voltage variations.

Design of membership functions (Fuzzification)

The design of the membership functions for the input and output variables of the FLC was based on Z-shaped, S-shaped and generalised bell-shaped functions, selected based on application-specific knowledge and shown in Figure 2.7. The frequency membership functions were designed based on the dead band established in Cuba, while the voltage membership functions were developed in accordance with the Cuban GC regulations. Together, these functions satisfy the requirements of the GC and the frequency control criteria of the Cuban power system.

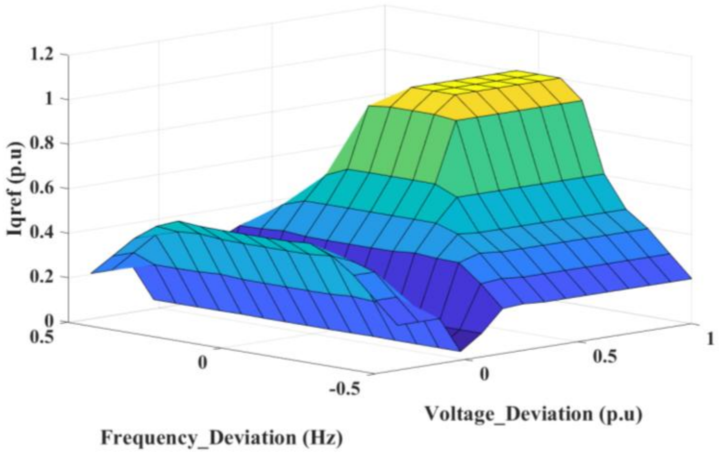

Figure 2.7. Surface plot which shows the relationship between the input and output functions of the FLC.

Fuzzy rules

The main objective of the FLC is to obtain the most effective value of reactive current in response to voltage variations. To do this, it is necessary to establish the relationship between the input and output functions by means of a series of simple if-then rules [62], as shown in Table 2.1. The rules presented in Table 2.1 offer an insight into how the fuzzy controller manages the inverter's reactive current reference (I_{qref2}) when there are sags or swells in the power system.

Table 2.1. Fuzzy rules of the FLC

Voltage deviation (ΔV)	Frequency deviation (Δf)	Reactive current (Iqref2)
SLV	FL	IqL
SLV	FN	IqL
SLV	FH	IqL
HLV	FL	IqL
HLV	FN	IqH
HLV	FH	IqL
HV	FL	IqL
HV	FN	IqH
HV	FH	IqL

2.3.5. Unbalance control

In power systems, the occurrence of certain transient events such as voltage sags, connection of unbalanced loads and short-circuits can cause negative sequence currents and voltages. Negative sequence currents circulation affects the normal operation of rotating machines because the induced currents in the rotors can lead to overheating, insulation failures and mechanical problems [63]. Due to the above reasons some standards such as IEEE Std 1159-2019 and IEC 61000-4-30 limit the unbalance caused by negative sequence circulation in the network.

For converters used in renewable sources, the occurrence of sags and short-circuits with the presence of negative sequence can cause the injection of unbalanced currents, in addition to the appearance of uncontrollable oscillations in the active and reactive powers delivered by the converter to the grid [58]. The solution to this problem is the use of a current regulator with two reference frames that rotate in positive and negative directions at the fundamental frequency of the grid (Figure 2.8).

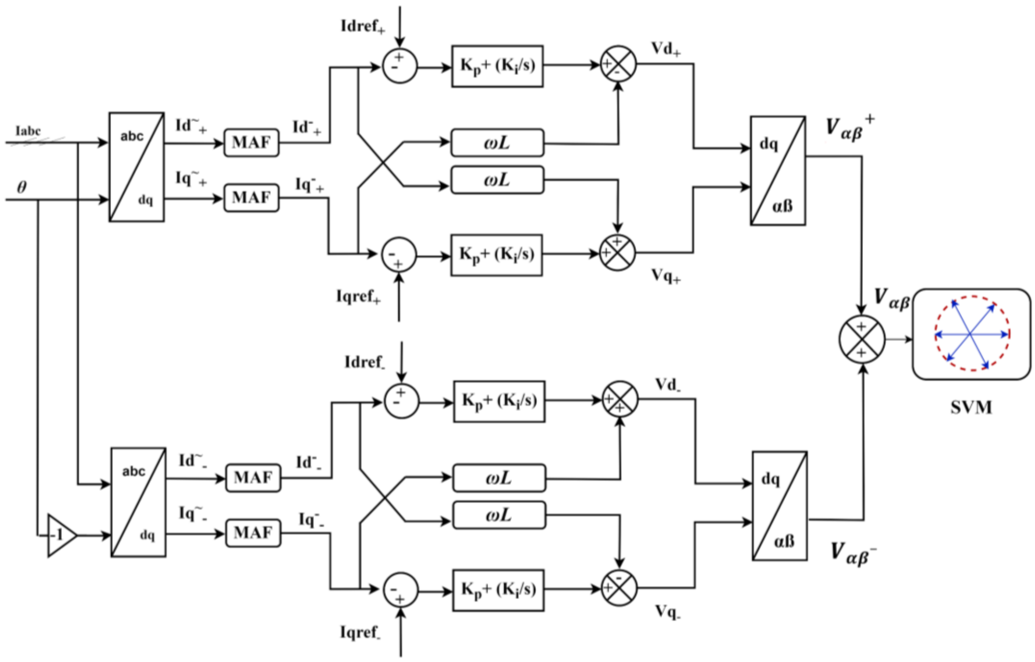

Figure 2.8. Double synchronous reference frame current controller.

The oscillations caused by the interactions of the dq-axis currents are twice the fundamental frequency of the power system. Because of these oscillations, it is necessary to use filters that help to ensure that the current reference signal sent to the PWM does not have negative sequence components so that the current delivered by the converter to the grid in the presence of a disturbance has a low percentage of unbalance [64].

2.3.6. Harmonic control

Due to the non-linear behaviour of the electric arc in EAFs, harmonics are generated in the current that deteriorate the power quality of the installation, in turn affecting the voltage waveform. This phenomenon forces steel mills to implement compensation measures, such as the use of a BESS system that acts as an active filter, the application of which in a mill is shown in this section (Figure 2.9).

In order to mitigate the harmonic currents generated by the EAF, the implemented BESS will act as an active filter, using rotating frames for each of the typical harmonic frequencies of the EAF [58]. The general control scheme based on these rotating frames is shown in Figure 2.10.

Figure 2.10 shows that the harmonic control detects the harmonic currents present on Bus 2 in Figure 2.3, which need to be compensated by the BESS. Each harmonic frequency is adjusted according to the reference frame set in the control model.

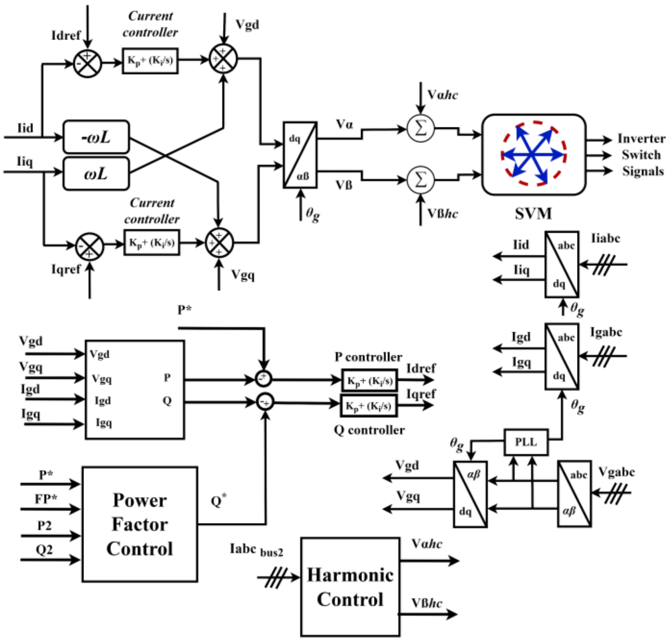

Figure 2.9. BESS control scheme for harmonic mitigation and power factor correction through VSI.

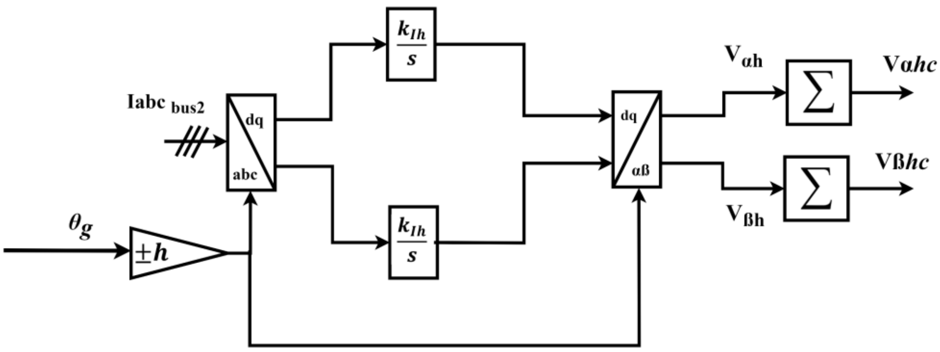

Figure 2.10. Harmonic compensation control in the BESS.

2.3.7. Power factor control

The power factor control of the BESS is based on its rated power (Figure 2.11). To regulate the power factor, priority is given to active power compensation by the BESS, while the remaining capacity of the BESS inverter is used to inject the necessary reactive power to correct the power factor. However, when the BESS reaches its maximum active power supply capacity, the power factor control is limited.

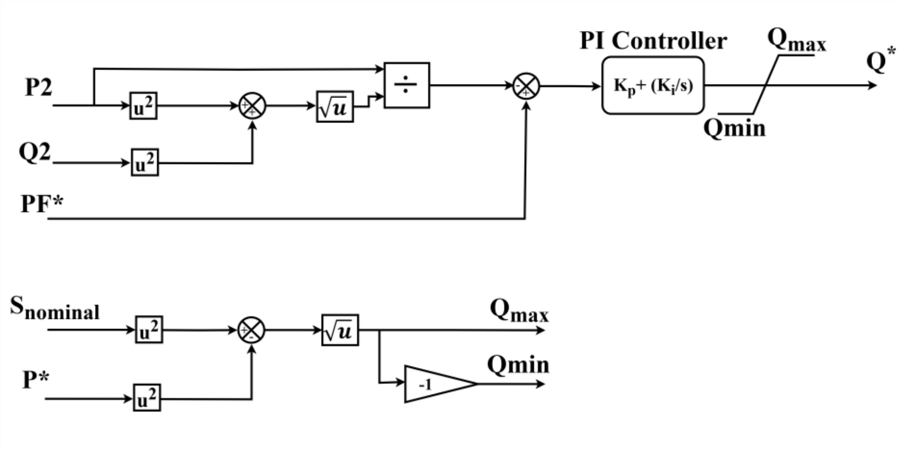

Figure 2.11. Power factor control in the BESS.

The BESS power factor control diagram, shown in Figure 2.11, measures the active and reactive power on bus 2 to determine the actual power factor during the melting process. This value is compared with the reference power factor *(PF*)* and the difference is applied to a PI controller. The controller adjusts the reactive power injection required to achieve the desired power factor, which is set to 0.9.

2.3.8. Control system for the compensation of power fluctuations in an EAF

Previous sections indicated that the short-circuit power on Bus 2 in Figure 2.3 reaches a high value, close to 2000 MVA, which allows for the implementation of GFL control (as explained in section 1.5.1) in the BESS. Given that the main function of the BESS is to compensate for the demand of the EAF, a controller is required that considers the power of the EAF and, simultaneously, maintains the frequency stability of the power system (Figure 2.12). As shown, at Bus 2 current and voltage measurement sensors are placed to obtain the EAF power consumption. The calculated EAF power is used as a reference for the BESS compensator, which is responsible for compensating the EAF power according to the proposed method. This system consists of a filter that can be adaptive or not, depending on its configuration. The operation of the filter in conjunction with the EAF will be discussed in detail in the following sections.

The BESS control also includes a state of charge (SOC) controller that ensures the battery SOC to be restored to the reference value. To achieve this, a SOC compensation power (ΔP_{SOC}) is added to the reference power provided by the BESS compensator (P_{COMP}). It is important to note that the SOC controller is activated only during the EAF's break periods to avoid interfering with the main BESS compensator. The SOC controller receives the SOC by means of the BMS, and generates the signal ΔP_{SOC} based on the system conditions [65]. Furthermore, the reference power *(P*)* of the BESS used by the inner GFL control is constrained by the limits set for the battery SOC (SOC_{min} and SOC_{max}) to prevent overcharging or over-discharging.

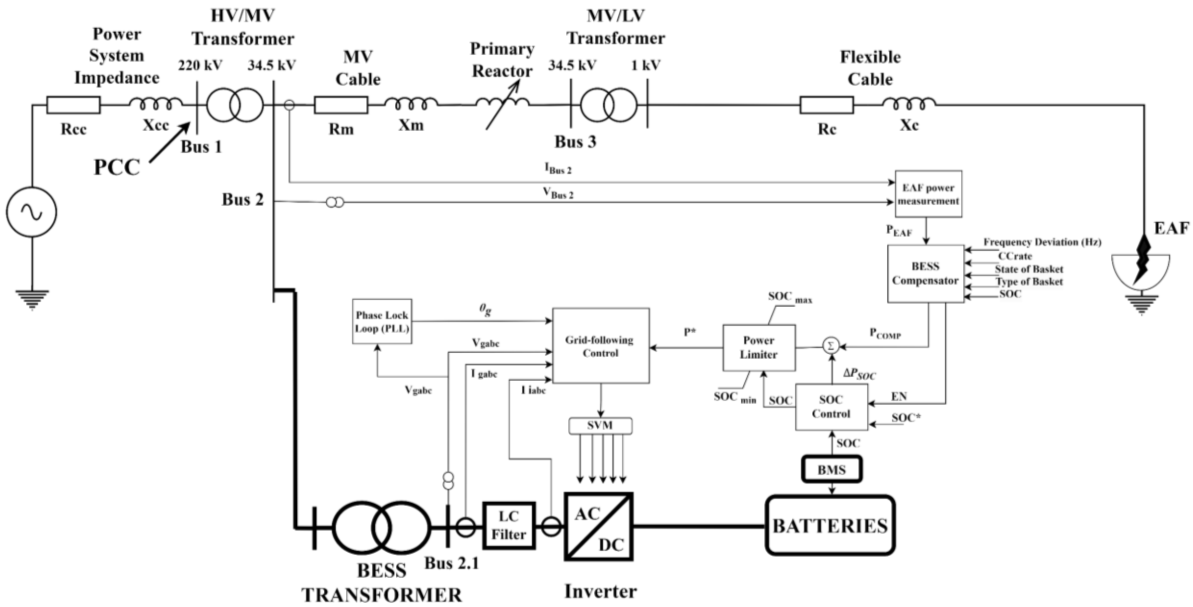

Figure 2.12. BESS control block diagram.

2.3.8.1. Equivalent power system model for analysing frequency behaviour

To analyse the frequency behaviour in the Cuban power system, an equivalent model was developed, as shown in Figure 2.13 [21]. This allows replicating the previously described frequency behaviour, based on the parameters involved in frequency control – primary (λ_p) and secondary (K_s) control gains, along with the power system's inertia (H) and damping coefficient (D). This model will also be used in the experimental tests to emulate the power system.

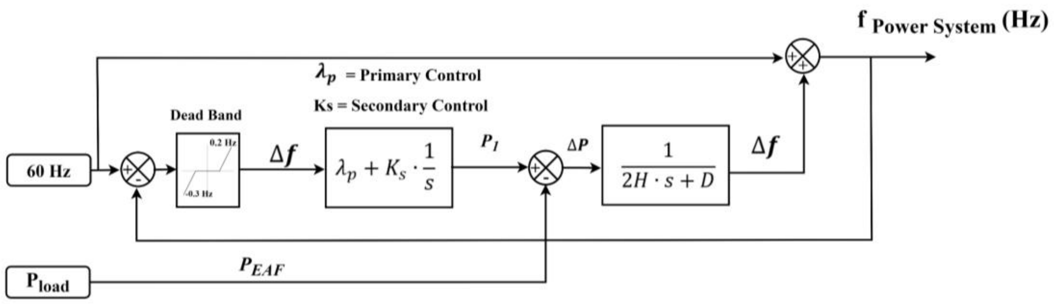

Figure 2.13. Equivalent power system model for analysing frequency behaviour.

2.3.8.2. Non-adaptive filter-based BESS compensator

As shown in Figure 2.12, the BESS active power reference is provided by a compensator that tracks the power variations of the EAF. The first implementation is based on a non-adaptive filter that has as input the active power of the EAF (P_{EAF}) measured in the point indicated in Figure 2.12. This non-adaptive filter serves as the basis for developing the improved compensator, discussed in the next section.

Figure 2.14 shows the block diagram of the non-adaptive filter, which essentially functions as a high-pass filter. The action of the filter control loop is fundamental because it classifies the amount of power that the BESS will deliver to the power system. This filtering technique is one of many that are used to smooth the output power using a BESS; mainly in applications to control the variability of the output power of photovoltaic systems [66], [67], [68].

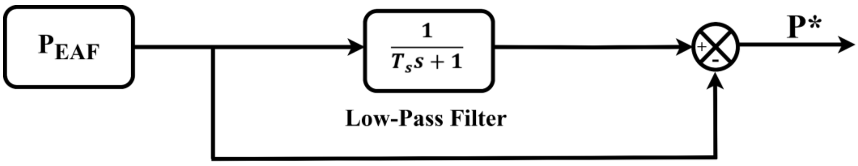

Figure 2.14. Block diagram of the non-adaptive compensator.

Selection of the LPF time constant

To determine the optimal time constant of the low pass filter (LPF) (T_s), the following performance indicators were considered the integral of the absolute frequency error (IAE), as defined in (2.3), and the energy cycled by the BESS in a melting process, as defined in (2.4). From these indices, the optimal T_s of the filter was determined for the weakest states of the Cuban power system, characterised by an inertia of H = 58 MWs²/rad and a damping of D = 25 MW/rad/s [6].

$$IAE = \int_0^T |e(t)|\, dt \tag{2.3}$$

$$E_{BESS} = \int_0^T |P_{BESS}(t)| dt \tag{2.4}$$

where $e(t) = \Delta f(t)$ is the error of the power system frequency (frequency deviation from nominal), P_{BESS} is the power output of the BESS battery during the smelting process, and T is the duration of the melting process.

The results obtained under the above conditions are shown in Figure 2.15. For this analysis, T_s was adjusted within a range to determine its optimum value, ensuring that the frequency remained within the specified limits during EAF operation.

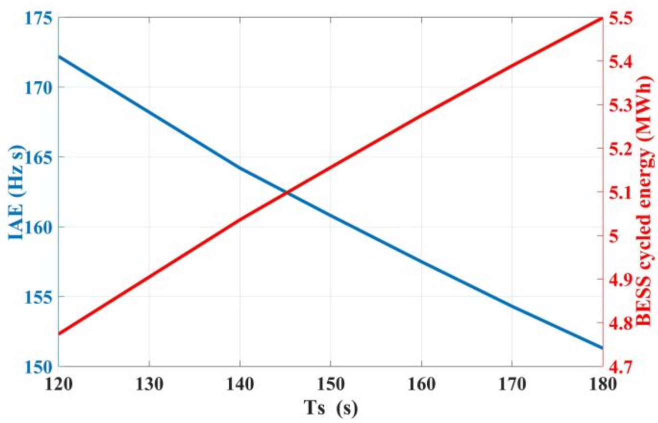

Figure 2.15. Relationship between IAE and BESS cycled energy for different filter time constant values.

As shown in Figure 2.15, increasing the filter time constant reduces the absolute frequency error, but this results in an increase in the energy processed by the BESS. For this reason, the optimum value of T_s was considered around the intersection of the two curves, resulting in a value between 140 and 150s. Therefore, a value of T_s=150s was chosen as a reference for the proposed adaptive method described in the following section.

2.3.8.3. Implementation of a fuzzy-logic adaptive BESS compensator

Although the use of a non-adaptive filter is one of the most widely used techniques by researchers due to its low complexity, it has the disadvantage that by using a fixed T_s defined by the user, it can cause overloading of the BESS battery, which is reflected in a reduction of its useful life [68]. Based on these drawbacks, several authors have studied different adaptive techniques to extend the battery life. Among these techniques is the use of a fuzzy controller to select the time constant of an LPF in applications to smooth the power output of photovoltaic systems [67], [68], [69]. In this section develops an adaptive control based on the application of fuzzy logic to select the time constant of an LPF used to compensate the output power of an EAF in a weak grid, particularly in the Cuban power system (Figure 2.16).

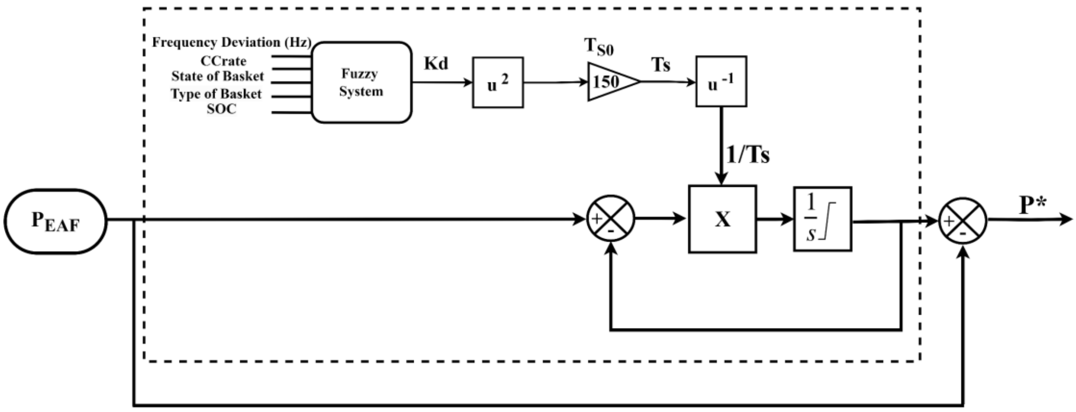

Figure 2.16. Block diagram of the BESS compensator with FLC.

As shown in Figure 2.16, the input variables to the fuzzy controller (FLC) will be the frequency deviation (Δf), the cumulative C-rate of the battery ($CC_{rate}(t)$) , the state and type of the EAF basket that is melting and the SOC. The input variables describing the operation of the EAF are mainly based on its operation cycle, which is divided into three phases: charging, melting and refining. Regarding $CC_{rate}(t)$ this variable, introduced by the author, it indicates the relation between the maximum power of the BESS and the working time of the battery. The higher this rate, the longer the battery will consume or deliver power close to its maximum value. The values of the $CC_{rate}(t)$ are expressed in per unit values based on the nominal battery C-rate of 2.5:

$$CC_{rate}(t) = \frac{1}{T_f s + 1} \cdot \frac{|P_{BESS}|}{E_{r\_BESS}} \cdot \frac{1}{2.5} \quad (2.5)$$

where P_{BESS} is the power output of the BESS battery, E_{r_BESS} is the rated capacity of the battery and T_f is the time constant of a low-pass filter used to average P_{BESS} over a convenient window. All these variables are aimed at obtaining the most efficient output of the FLC, which will have the least effect on battery life and will not allow the system frequency to reach unacceptable values outside the dead band for long periods. In this research, the application of the adaptive filter time constant has been designed from a fixed time constant, which can change its value depending on the existing conditions in the power system and the EAF. This behaviour allows the time constant to be modified over a range of values greater or less than the fixed T_s. The relationship between the adaptive and fixed time constant is expressed in (2.6).

$$T_s = {K_d}^2 \cdot T_{s0} \tag{2.6}$$

where T_s is the adaptive constant of the filter, K_d is the FLC's output variable, and T_{s0} is the fixed constant, in this study considered equal to 150 s as discussed previously.

Figure 2.17 shows the surface plots of the relationship between the FLC's input and output variables. The value of K_d increases when the frequency is outside the dead band, although the value of this coefficient can be reduced depending on the EAF's basket type, the cumulative C-rate and the SOC. The relationship between the input variables and the output of the fuzzy controller can be observed through a table of rules based on the IF-THEN format.

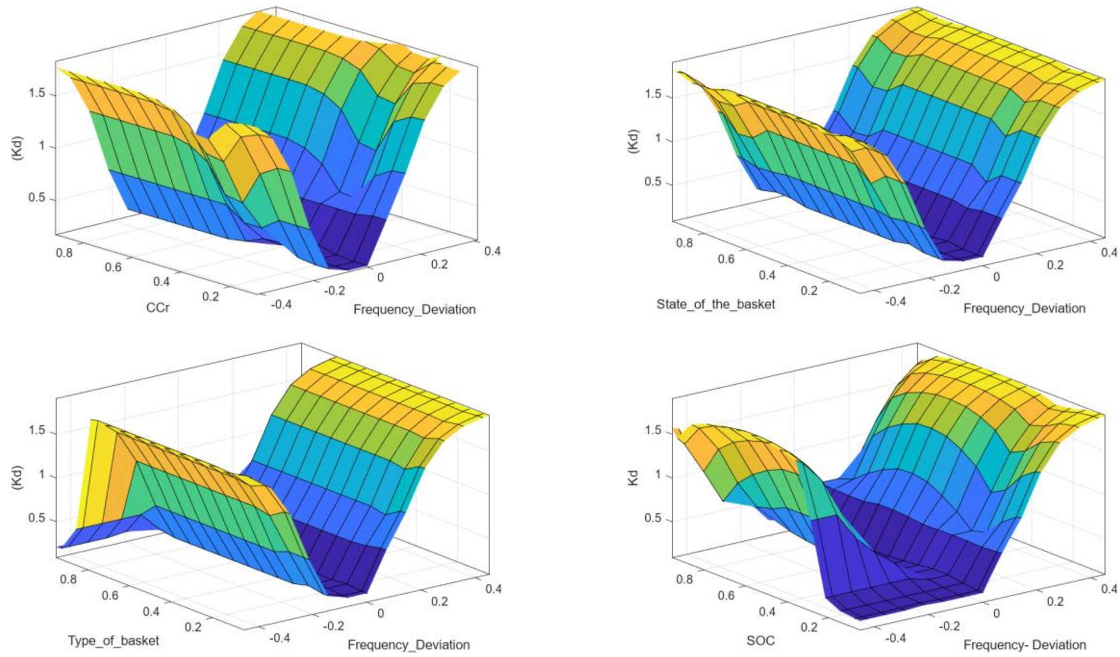

Figure 2.17. Surface plots showing the relationship between the input variables and the output adaptive variable.

2.4. Conclusions

The work carried out in this chapter proposed a comprehensive solution based on the incorporation of a BESS equipped with advanced control architecture. The BESS was designed with internal and external controls, aimed at simultaneously addressing various electrical problems present in the operation of the EAF. The control systems presented are designed to mitigate imbalance, improve power factor and reduce harmonics, as well as compensate for power fluctuations to contribute to frequency stability in the electrical system.

The main contributions of this chapter are summarized as follows:

- Highlighting the key challenges faced by the Cuban power system during the operation of large EAFs and proposing a modern solution that integrates a BESS to compensate for rapid EAF power fluctuations;
- Developing a control strategy for the inverter interfacing the BESS with the power system, based on GFL control principles;
- Analysing and improving the BESS power compensator to maximize its impact on EAF performance while minimizing battery usage;
- Proposing a novel adaptive filter for the BESS compensator based on fuzzy-logic techniques;
- Providing additional functionalities for power quality improvement, including power factor correction, harmonic mitigation, and voltage unbalance compensation.

CHAPTER 3 . Performance evaluation of the proposed BESS control system

Note: The material in this chapter is based on author's papers published in [6], [56], [57] *.*

The primary purpose of employing a BESS within the steelworks is to compensate for the EAF demand in order to prevent stability problems in the power system. However, beyond this function, the BESS's inverter can also be used to enhance the power quality in the PCC of the EAF. The simulation of these control strategies, as well as their coordinated operation, constitute the main objectives of this chapter, which are summarized as follows:

- Analysis of the BESS response for EAF active power compensation to reduce the EAF impact on the frequency stability in the Cuban power system,
- Analysis of the BESS response to sags and swells in the power system.
- Modelling of the EAF for harmonic and power factor analysis,
- Behaviour of the BESS as a power factor compensator,
- Analysis of the behaviour of the BESS as an active filter in the presence of harmonics in the steelworks network.

3.1. Analysis of BESS response for active power compensation in EAF to maintain power system frequency stability

Note: The material in this section is based on author's paper published in [57]*.*

To analyse the BESS compensation capability under different power system conditions, several performance indices were employed to characterize both the power system and the BESS battery usage. The indices that were used to analyse the behaviour of the power system were the frequency deviations and the maximum rate of change of the frequency ($ROCOF_m$) defined as [20], [70]:

$$ROCOF_m = \frac{f(t_0 + T) - f(t_0)}{T} \tag{3.1}$$

where $f(t_0), f(t_0 + T)$ are two consecutive frequency measurements and T is the time between two measurements, typically defined in grid codes (for the purpose of this research, T =0.5 s).

On the other hand, to evaluate the battery usage behaviour, the power output of the BESS, the energy consumed during the charging and discharging processes, the number of full cycles equivalents per year (FCE/a) defined in (3.2) and (3.3), the variation of the state of charge (ΔSOC) during the process defined in (3.4) and the average value of the C-rate curve, defined as the cumulative C-rate ($CC_{rate}(t)$) in [57], were observed.

The value of FCE related to the lifetime of the battery is determined by the equation given in [71]:

$$FCE = \frac{\sum_k |E(t_k)|}{2C} \tag{3.2}$$

where $E(t_k)$is the total energy during a battery operation cycle and C is the battery capacity. For the evaluation of (FCE/a) in (3.3), it is assumed that the load profile is repeated an average of 15 times during the 260 working days of a year.

$$FCE/a = \frac{\sum_k |E(t_k)|}{2C} \cdot 15 \cdot 260 \tag{3.3}$$

The variation of the SOC can be expressed as:

$$\Delta SOC = SOC_{max1} - SOC_{min1} \tag{3.4}$$

where SOC_{max1} and SOC_{min1} are the maximum and minimum values of the battery charge during one cycle of EAF operation respectively.

The use of a first-order filter in [57] allows the trend of the battery C-rate to be known to avoid high variations in the measurement. The increase or decrease in the cumulative C-rate gives a measure of the battery usage during the EAF compensation process.

Furthermore, to quantify the battery usage over one cycle of the EAF operation, the average cumulative C-rate value is defined as follows:

$$ACC_{rate} = \frac{1}{T_c} \int_0^{T_c} CC_{rate}(t) \cdot dt \tag{3.5}$$

where T_c is the time of one EAF cycle, and $CC_{rate}(t)$ is the cumulative C-rate defined in [57].

Case studies and comparison baseline

In order to test the effect of the proposed solution in the EAF compensation process, three case studies have been developed for different power system conditions. The compensator used in the BESS has a defined time constant of 150 s, as discussed in the section 2.3.8.2.

The defined power system parameters are selected for different values of inertia and load damping, hereinafter defined as Case 1 to Case 3. Case study 1 presents values of inertia (H = 58 MWs^2/rad) and damping (D =25 MW/rad/s) that are very similar to the current weaker conditions of the Cuban power system, unlike the other values that were estimated as future scenarios where the power system conditions would be more robust. The future scenarios, called Cases 2 and 3, present inertia values of 58 MWs^2/rad and 100 MWs^2/rad, while the damping values are 50 MW/rad/s and 100 MW/rad/s, respectively. The use of the different conditions within the power system will allow the effect of the BESS control to be characterised in detail.

As a baseline for comparison, the three defined cases are first analysed without BESS. Table 3.1 presents the performance parameters used to evaluate the various BESS control strategies, in the conventional EAF operation without BESS.

Table 3.1. Power system frequency parameters in different case studies without the use of BESS			
Parameters	**Case 1**	**Case 2**	**Case 3**
Maximum frequency (Hz)	60.785	60.515	60.298
Minimum frequency (Hz)	59.333	59.527	59.706
Time above 60.2 Hz (s)	307	222	103
Time below 59.7 Hz (s)	216	87	0
$ROCOF_m$ (Hz/s)	0.296	0.255	0.148

The table above highlights the need to implement a frequency compensation mechanism in the power system, since in each case study the behaviour of this variable represents a challenge for system stability. In response to this problem, the following sections present different compensation strategies based on the use of a BESS, considering both non-adaptive and adaptive control schemes.

BESS control with non-adaptive LPF

The results of the different simulations (Figure 3.1) show the frequency behaviour of the power system, BESS active power, active power behaviour of the power system, as well as the cumulative C-rate throughout the process. Table 3.2 shows the overall results of the simulations, where the base value for the representation of the active powers in p.u. was 50 MW. In general, the BESS maintains the electrical frequency within the dead band under various power system conditions, as well as $ROCOF_m$ values within the security thresholds of the various international standards [20], [70]. Across all three case studies, the power of BESS, the active power of the power system and cumulative C-rate values remained approximately constant, which may result in unnecessary battery usage under more robust power system conditions when the EAF requires less compensation. In terms of battery charging and discharging energy, full cycles equivalents per year and state of charge variations, the behaviour is similar in the three scenarios, showing once again that the compensator based on the fixed time constant filter does not allow the BESS to adapt to the varying conditions that frequently occur in the power system and in the behaviour of the EAF. Consequently, an adaptive compensator was developed to adapt to changes in grid conditions and EAF operation characteristics while minimizing battery wear.

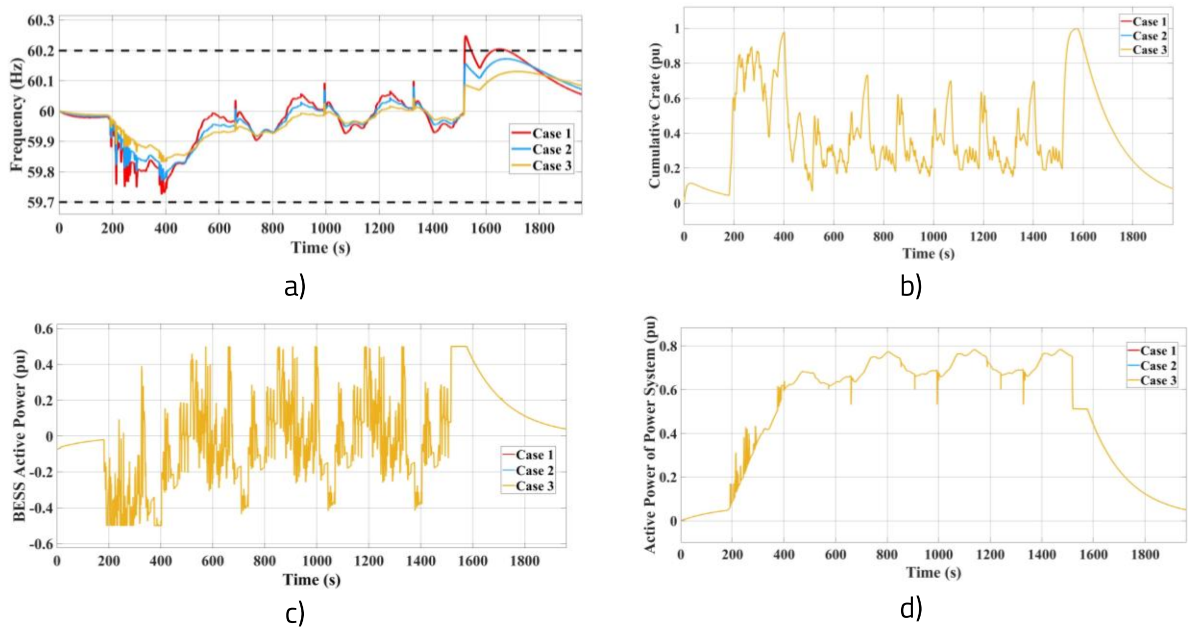

Figure 3.1. System operation with a non-adaptive compensator (T_s = 150 s): a) Frequency of the power system, b) Cumulative C-rate, c) BESS Active power, d) Active power behaviour of the power system.

3.1.1. BESS adaptive compensator based on fuzzy logic

To test the proposed adaptive control, the case studies defined previously were simulated. The simulation results (Figure 3.2) show the behaviour of the power system frequency, BESS and power system active powers, as well as the variation of the cumulative C-rate throughout the process. In addition to these variables, Figure 3.2e shows how the time constant is changed by the fuzzy controller in the three cases.

Table 3.2. Overall performance analysis with BESS including non-adaptive compensator (Ts=150 s)

Parameters	LPF with Ts=150 s		
	Case 1	Case 2	Case 3
Average power (pu)	0.196	0.197	0.196
Maximum frequency (Hz)	60.248	60.172	60.130
Minimum frequency (Hz)	59.722	59.770	59.832
Time above 60.2 Hz (s)	66.612	0	0
Average cumulative *C-rate* (pu)	0.384	0.385	0.384
FCE/a	1058	1058	1058
ΔSOC (%)	16.82	16.82	16.82
$ROCOF_m$ (Hz/s)	0.097	0.090	0.052

As shown, the FLC keeps the frequency within the dead band in the different conditions of the power system, as well as $ROCOF_m$ values within the security thresholds of the various international standards [20], [70]. Unlike the previous control strategy with a non-adaptive compensator, the proposed controller makes it possible to reduce the average output power of the BESS, meaning that the battery is used less, without compromising the stability of the power system during the EAF operation. To achieve optimum performance, the controller continuously varies the value of the LPF time constant to select the best response to the BESS output. Initially, the time constant is maintained below the reference value of 150 s, while towards the end of the process, it becomes necessary to increase the time constant above this threshold. This adjustment is required due to the abrupt power reduction of the EAF, which induces the frequency deviation, limited by the fast action of the BESS.

The variation of CC_{rate} for the three case studies decreases as system conditions improve. This behaviour is also reflected in the BESS output power, which decreases as the system becomes more robust (Case 2 and 3), better meeting the EAF power demand. In terms of battery charging and discharging energy, as power system conditions improve, the battery's energy usage is reduced, even though the charging process consumes the most energy due to the abrupt power reduction of the EAF. In addition, the full cycles equivalents per year and state of charge variations decrease with improved grid conditions, meaning that this control system helps to extend battery life.

In general, the behaviour of the adaptive control reduces BESS battery usage as the power system conditions improve, thus avoiding accelerated battery degradation. In addition, unlike the non-adaptive control approach presented in 2.3.8.3, which relies on an LPF with a fixed time constant, the adaptive control accounts not only for power system conditions but also for the state of the EAF in corelation with the working conditions of the BESS, thus making it a more general and efficient control strategy.

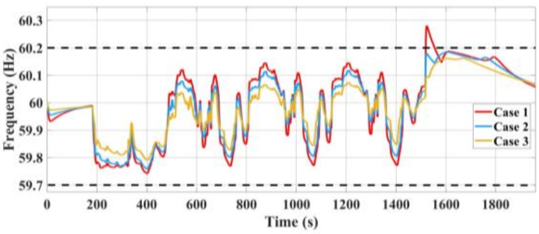

a)

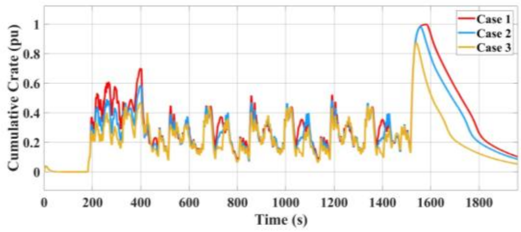

b)

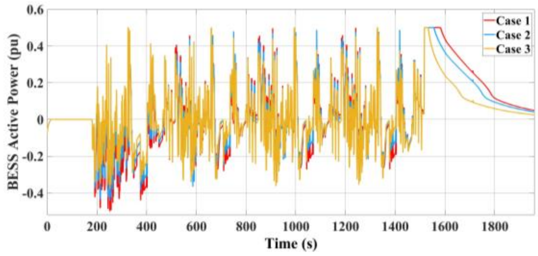

c)

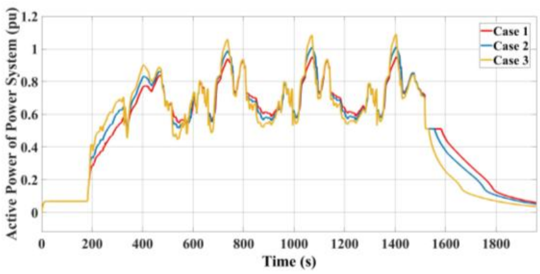

d)

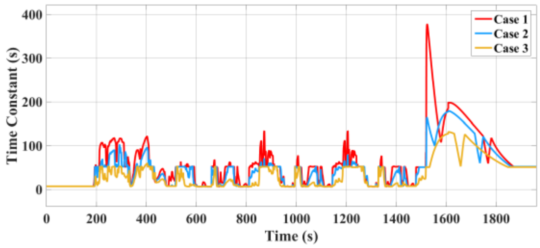

e)

Figure 3.2. System behavior using a fuzzy adaptive compensator: a) Frequency of power system, b) Cumulative C-rate, c) BESS Active power, d) Active power behaviour of the power system, e) Behaviour of the adaptive time constant.

3.1.2. Comparative analysis of BESS control strategies for EAF compensation

Table 3.3 shows the comparisons of the results obtained by each of the discussed control approach, namely the non-adaptive and the fuzzy-based filters. The analysis focuses on three previously considered cases (Case 1 to Case 3), using the same performance parameters as before.

Table 3.**3**. Comparison between the different control methods used in the EAF compensation BESS

Parameters	Case 1			Case 2			Case 3		
	CM0	CM1	CM2	CM0	CM1	CM2	CM0	CM1	CM2
Average power (pu)	-	0.20	0.15	-	0.20	0.13	-	0.20	0.11
Maximum frequency (Hz)	60.78	60.25	60.28	60.51	60.17	60.18	60.30	60.13	60.16
Minimum frequency (Hz)	59.33	59.72	59.74	59.53	59.77	59.76	59.71	59.83	59.77
Time above 60.2 Hz (s)	307	66.61	33.46	222	0	0	103	0	0
Time below 59.7 Hz (s)	216	0	0	87	0	0	0	0	0
Average cumulative *C-rate* (pu)	-	0.38	0.30	-	0.38	0.27	-	0.38	0.22
Charge energy (MWh)	-	2.63	2.74	-	2.63	2.48	-	2.63	1.93
Discharge energy (MWh)	-	2.79	1.71	-	2.79	1.45	-	2.79	1.29
FCE/a	-	1058	867	-	1058	766	-	1058	627
ΔSOC (%)	-	16.82	17.84	-	16.82	15.49	-	16.82	9.67
$ROCOF_m$ (Hz/s)	0.30	0.10	0.12	0.25	0.09	0.10	0.15	0.05	0.06

CM0: no BESS; CM1: LPF with Ts=150 s; CM2: LPF with Fuzzy System

The data presented in the table above demonstrate the technical superiority of the adaptive compensator over the non-adaptive one. The reduction in the evaluated parameters optimises the operating regime of the BESS battery and reduces frequency fluctuations. As a result, operational constraints in the steelworks' smelting process are eliminated.

3.1.3. BESS SOC dynamics for a daily EAF power demand profile

To ensure the long-term sustainability of the BESS in the face of the continuous and variable demand from an EAF adapted to the load constraints of the Cuban electricity system an active state of charge (SOC) restoration strategy was evaluated during the breaks between casting batches. Through five case studies that varied the initial SOC (SOC_i) and the target reference value (SOC*), via the flexible use of a controller, the effectiveness of this proposal was demonstrated; whereas when the controller was deactivated (Case 1) the final SOC reaches nearly 100%, limiting the BESS's capacity for subsequent cycles, the activation of the control in Cases 2 to 5 (shown in Figure 3.3) ensures that the SOC systematically returns to its reference value at the end of the operating day, guaranteeing the availability and reliability of the storage system for the following day's production.

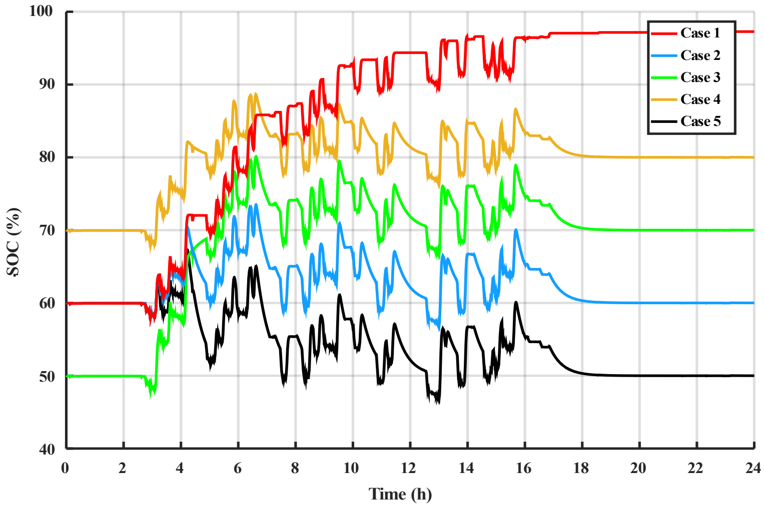

Figure 3.3. Daily SOC variation of the BESS for the considered cases.

3.2. Predictive state of charge management in battery energy storage systems integrated with electric arc furnaces

Note: The material in this section is part of a journal paper which has been submitted by the author for review to Journal of Energy Storage.

Currently, the integration of BESS into power systems has been increasingly influenced by the implementation of demand forecasting models based on artificial intelligence (AI). In this context, this section proposes a novel methodology based on EAF demand forecasting for the dynamic optimisation of the SOC of a BESS. Unlike conventional approaches, the proposal incorporates a Bilayer Neural Network (BNN) model aimed at accurately predicting demand peaks associated with the industrial process. In this way, the BESS can proactively adjust its SOC, ensuring sufficient energy reserves are available to mitigate power ramps and contribute to maintaining frequency stability in a weak power system.

3.2.1. Proposed control strategy

This work adopts a methodology based on combining a demand prediction system and an energy storage system, with the aim of mitigating the power variations associated with the operation of an electric arc furnace (Figure 3.4). Future demand is estimated using prediction algorithms, which allow the future SOC of the battery to be calculated, considering both the expected demand and the restrictions imposed by the system's ramp rate limits.

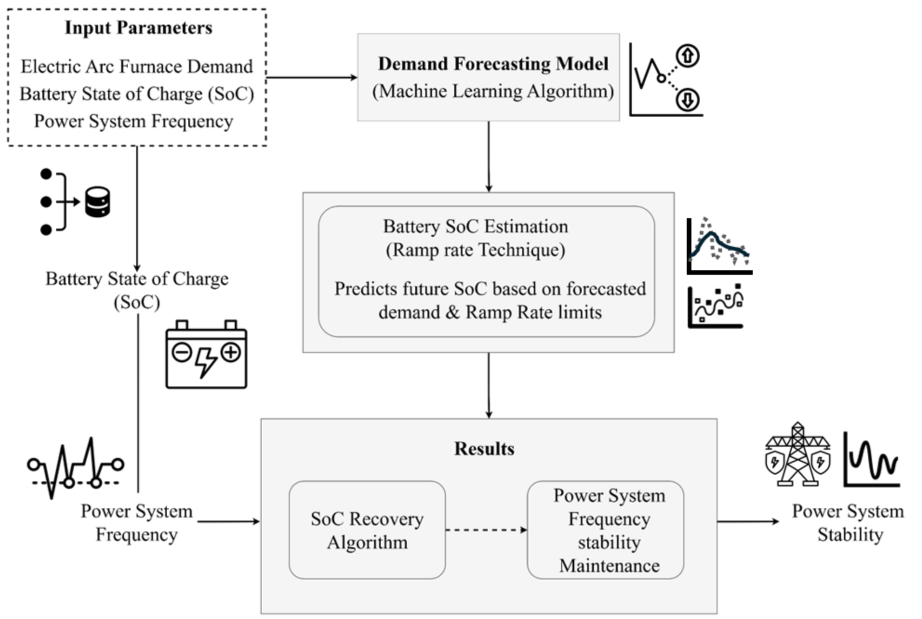

Figure 3.4. Flowchart of the methodological proposal.

3.2.1.1. Power smoothing system

In order to mitigate the negative impact of power fluctuations from an EAF on the frequency of a weak power system, a conventional ramp rate filter is initially implemented to limit sudden changes in power; however, this rigid mechanism tends to increase battery usage and generate losses due to its lack of flexibility. The SOC of this BESS is determined in real time by calculating the energy accumulated during charge and discharge cycles based on a reference power, whilst being strictly controlled within a safe operating range of 5% to 95% to prevent cell saturation or premature discharge. To validate this strategy under a real-world, highly chaotic and non-linear load regime, the operational records of a Cuban steelworks were used as a basis; this facility has a 50 MVA furnace connected to a 220 kV circuit, which operates in parallel with a 25 MVA BESS specifically designed to mitigate the asymmetric nature of industrial demand and counteract the tendency for batteries to discharge progressively.

3.2.1.2. SOC prediction adjustment

In order to optimise the energy management of the storage system, it became necessary to develop a method for the predictive adjustment of the SOC, whereby the energy available in the BESS is determined in advance based on demand estimates provided by the neural network model. This stage enables the control scheme to assess the battery's temporal dynamics and implement preventive corrective actions should the SOC be projected to fall below the 50% reference limit. Next, the charge recovery algorithm is introduced, which replaces the stiffness of the traditional filter with an adaptive ramp rate technique (RR_t); this strategy dynamically adjusts the filter constraints based on the accumulated energy error and the operational conditions of the grid frequency, segmenting its behaviour for dead band, over-frequency and under-frequency scenarios.

Given that an inflexible charging process could compromise the stability of the electricity system under critical conditions, a gradual termination criterion based on conditional logic is incorporated. To ensure a smooth transition and reduce the battery power without causing disturbances in the grid, two state variables coupled via an AND logic function are monitored in real time; this function is formally defined by the expression:

$$G(t) = C_1(t) \cdot C_2(t) \quad (3.6)$$

where the value $G(t) = 1$ indicates valid charging operation in the interval $SOC_{min} < \mathrm{SOC} < 50\%$.

Once both requirements are met simultaneously, a proportional control loop is activated, which gradually reduces the battery's power output until the restoration cycle is complete, thereby ensuring full compatibility between the device's energy recovery and the maintenance of frequency stability in the power system.

3.2.1.3. Evaluation of the prediction model

The validation of the control strategy began with an evaluation of various machine learning architectures against classical regression techniques for the short-term forecasting of electric arc furnace (EAF) demand. The models evaluated included Narrow Neural Networks (NNN), Bilevel Neural Networks (BNN), Support Vector Machines (SVM), Wide Neural Networks (WNN) and Robust Linear Regression (RLR).

The behaviour of the models was divided into four critical operational windows to verify the load-following capability at different stages of the smelting process: the initial arc-striking stage (Zone 1), the electric arc stabilisation period (Zone 2), and the phases of gradual reduction in the demand slope as the smelting process comes to an end (Zones 3 and 4) (Figure 3.5).

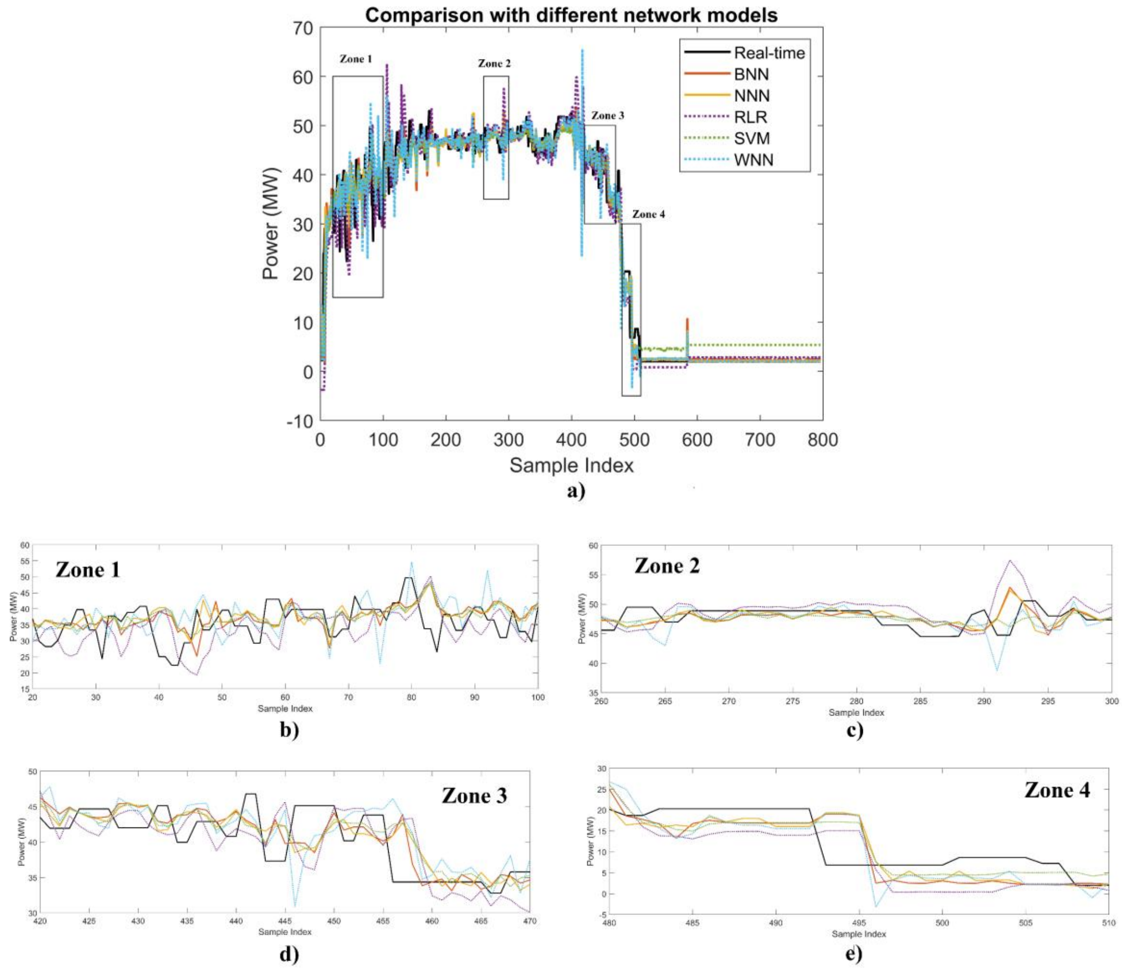

Figure 3.5. Comparison of forecasting models, (b) Zone 1, (c) Zone 2, (d) Zone 3 and (e) Zone 4

Although the analysis of statistical performance metrics (RMSE, R^2, MSE and MAPE) showed the NNN network to be slightly superior in terms of point-by-point accuracy for active power, the integration of these data streams into the BESS closed-loop control revealed a cumulative error phenomenon. When the predictions were subjected to ramp-rate filtering, the localised errors of the NNN network were amplified, causing systematic deviations in the estimation of the state of charge (Figure 3.6). In contrast, the BNN demonstrated a much more consistent handling of uncertainty. As can be seen from the dynamic behaviour of the SOC and the analysis of the ±5% tolerance bands, the BNN architecture consistently kept the load state estimation error within the technical safety limits, establishing itself as the ideal operational predictor for the application (Figure 3.7).

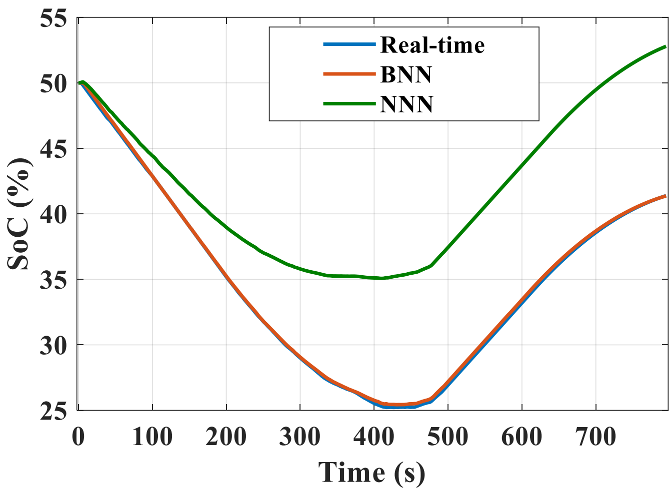

Figure 3.6. SOC behaviour for the different prediction models in conjunction with the actual value to be estimated.

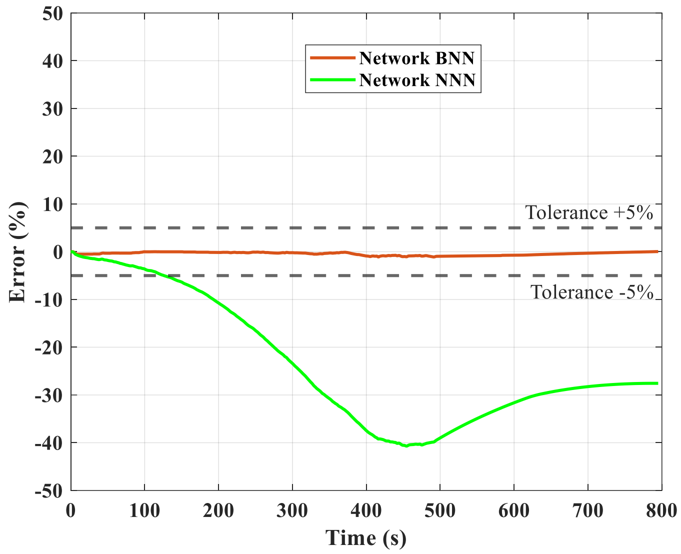

Figure 3.7. Percentage error between the actual SOC value and its estimated value in real time for the different prediction models.

Once the BNN predictor had been selected, the combined impact of the adaptive recovery algorithm on internal battery management and power grid stability was assessed. The results show that the use of a conventional (non-adaptive) ramp rate filter causes a progressive and irreversible discharge of the storage system, leaving the SOC below the minimum safety threshold of 50% at the end of the industrial cycle. In contrast, the proposed predictive and adaptive strategy makes optimal use of periods of low variability to initiate a gradual and smooth energy restoration of the battery, successfully returning the storage to optimal charge levels (above 50%) to face the next production cycle without degrading the useful life of the system (Figure 3.8).

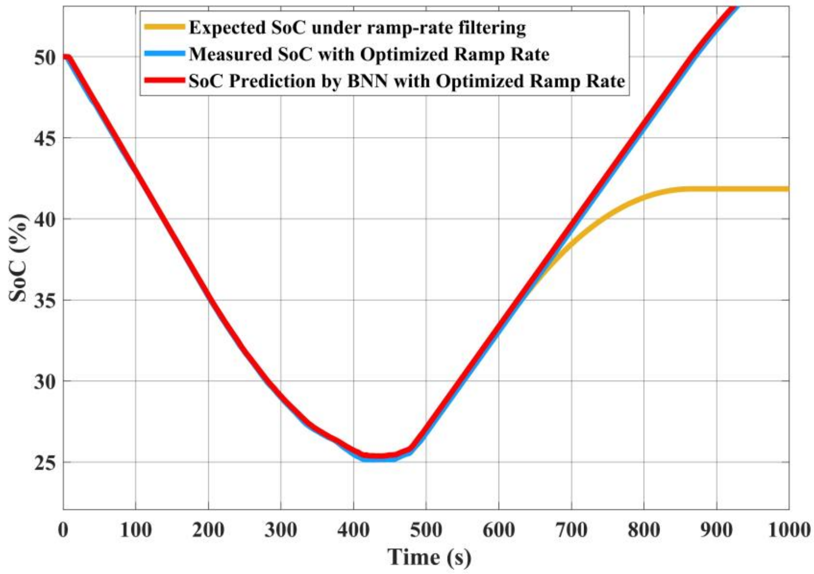

Figure 3.8. Comparison of battery SOC under conventional ramp-rate control and optimised ramp-rate strategy.

Finally, the impact of this strategy on the frequency of the Cuban power system (characterised by its status as a weak, low-inertia grid) was assessed. The dynamic simulation demonstrated that the coordinated power injection from the BESS absorbs the load fluctuations of the EAF. The adaptive predictive control loop not only prevents critical drops in grid frequency but also permanently confines oscillations within the safe operating dead band, significantly overcoming the operational limitations of RR filter (Figure 3.9).

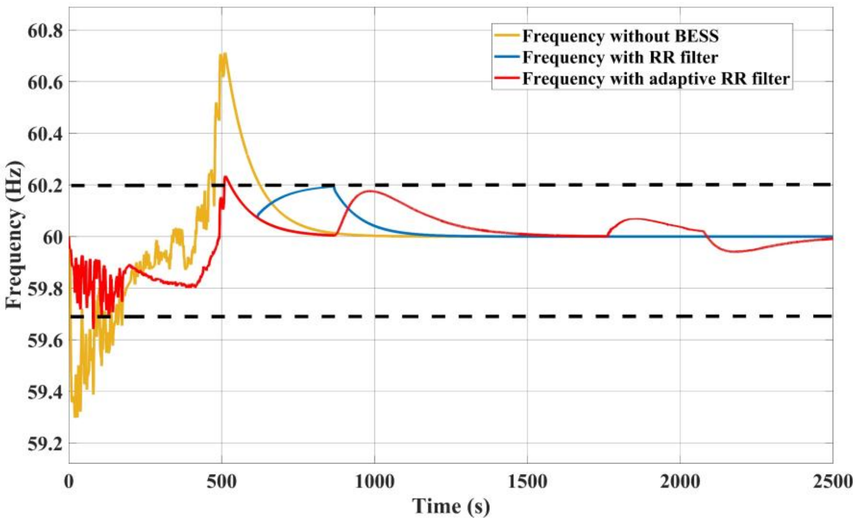

Figure 3.9. Power system frequency behaviour under different control strategies.

3.3. Analysis of the BESS response to sags and swells in the power system

Note: The material in this section is based on author's paper published in [6].

In order to evaluate the behaviour of the developed VFRT controller discussed in section 2.3.4, several simulations were carried out in Matlab/Simulink software. The occurrence of various events, including swell, single-phase, two-phase and three-phase sags with different durations, were considered, modelling the EAF as a constant impedance load due to the short time period analysed. Different voltage magnitudes were used to evaluate the events, analysing the effect of the BESS under two control schemes: one corresponding to the conventional Cuban GC (CGC) conditions and the other with the proposed FLC, developed in this work. The main variables analysed were the frequency deviation (Δf), the active (P_{PCC}) and reactive (Q_{PCC}) power at the PCC and the active (I_{dBESS}) and reactive (I_{qBESS}) currents of the BESS. The inertia and damping parameters used for the frequency analysis were H = 58 MWs²/rad and D = 25 MW/rad/s, obtained from a study of the Cuban power system conditions in recent years. To evaluate the proposed solution under a challenging scenario, the initial power of the BESS prior to the voltage variation was set to 0 MW. For the consistency of the analysis, all powers were expressed in p.u. with a base value of 50 MVA.

3.3.1. Performance of the VFRT controller under asymmetric voltage sags

Voltage sags in power systems mainly occur due to faults and the switching of large loads. The most common of these are asymmetrical faults, such as single-phase and two-phase short circuits, which can cause significant voltage dips. To replicate the dynamics of real faults in simulation, sags of different depths and durations were applied. Typically, these sags are almost instantaneous, as the system protections swiftly isolate the fault. The temporal extent of each sag is determined by the settings of these protection devices [72].

3.3.1.1. Single-phase sag

The occurrence of a voltage decrease in one phase of the power system was simulated to analyse the behaviour of the conventional CGC with respect to FLC proposed in this work. Four single-phase instantaneous sags with magnitudes of 0.8 p.u., 0.5 p.u., 0.2 p.u. and 0.8 p.u. with durations of 0.3 s, 0.1 s, 0.1 s and 0.1 s respectively were simulated continuously (Figure 3.10).

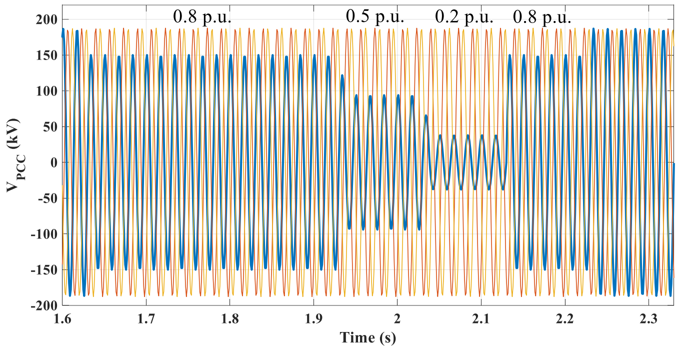

Figure 3.10. Single-phase instantaneous sags.

Figure 3.11 shows that, despite the significant voltage drop, the frequency remains within the dead band. Both controllers exhibit identical reactive current behaviour, improving the voltage profile in accordance with Cuban GC standards. While the frequency does not undergo significant destabilisation, the FLC mitigates slight oscillations by consuming active power to prevent degradation. Starting from an initial value of 59.997 Hz within the dead band, the maximum frequency deviation with the CGC reached 0.092 Hz. Using the FLC reduced the frequency deviation to 0.08 Hz, highlighting the ability of the fuzzy controller to assist in frequency control when there is operational margin.

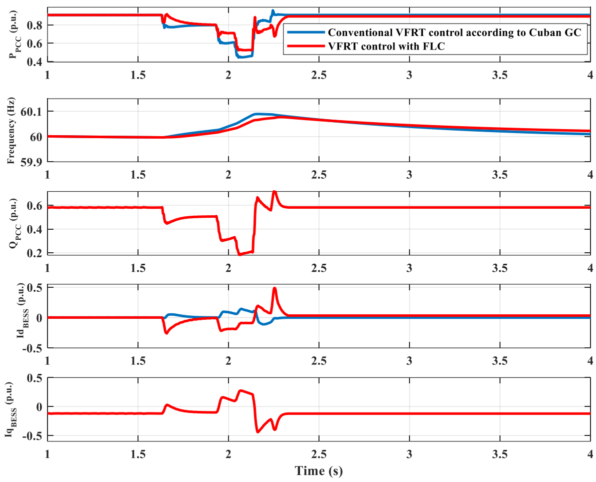

Figure 3.11. Behaviour of the different VFRT controllers in the presence of single-phase sags.

3.3.1.2. Two-phase sag

The simulation of the two-phase sags was carried out in the same way as for the single-phase sags, except that in this case two phases have their nominal voltage reduced. For the comparison between the CGC and the FLC, four instantaneous two-phase sags were developed with magnitudes of 0.8 p.u., 0.5 p.u., 0.2 p.u. and 0.8 p.u. with durations of 0.3 s, 0.1 s, 0.1 s and 0.1 s respectively (Figure 3.12).

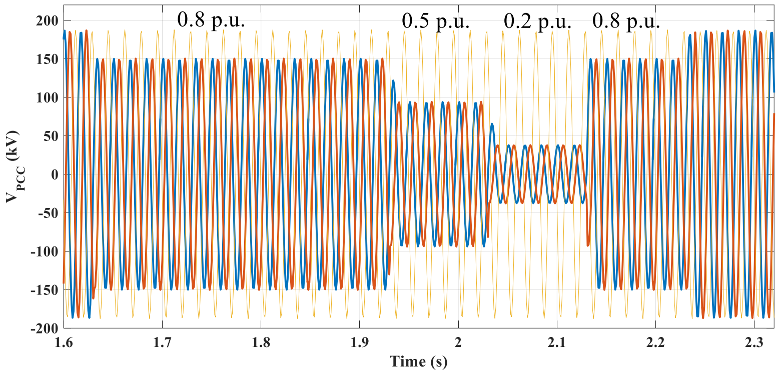

Figure 3.12. Two-phase instantaneous sags.

Figure 3.13 shows how the key variables behave during two-phase sags. As in the single-phase case, the system frequency remains within the dead band, with both controllers equivalently injecting reactive current to fill the voltage gap. Although the frequency is not significantly destabilised, the FLC attenuates the slight oscillation by consuming active power, thereby helping to maintain stability. Under the CGC scheme, the maximum frequency deviation from an initial value of 59.997 Hz within the dead band was 0.161 Hz; with the FLC, this was reduced to 0.093 Hz. This demonstrates the FLC's ability to contribute to frequency control when it has operational margin.

3.3.1.3. Three-phase sag

Three-phase voltage sags in power systems are a random phenomenon that can create critical conditions for the system frequency. The magnitude of these sags determines the reduction in power supplied to loads, which can jeopardise overall stability. Therefore, it is essential to simulate scenarios involving three-phase sags that affect stability more severely than asymmetrical sags. In this study, three sag simulations of varying magnitudes were conducted, as illustrated in Figure 3.14, to analyse the frequency response of the power system when subjected to CGC and FLC controllers. Figures 3.15 to 3.17 show the behaviour of the various VFRT controllers in the event of three-phase voltage sags.

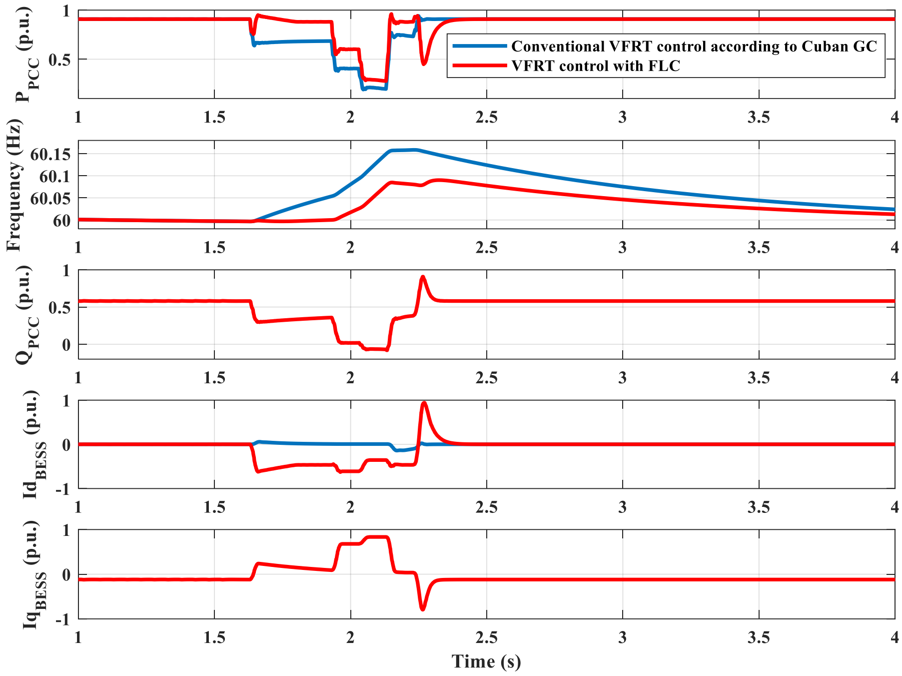

Figure 3.13. Behaviour of the different VFRT controllers in the presence of two-phase sags.

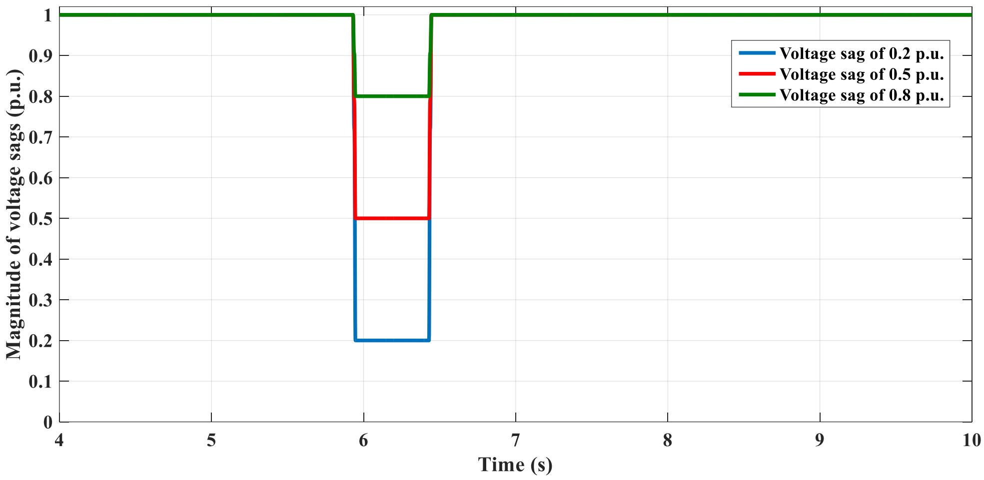

Figure 3.14. Different voltage sags implemented in the simulations.

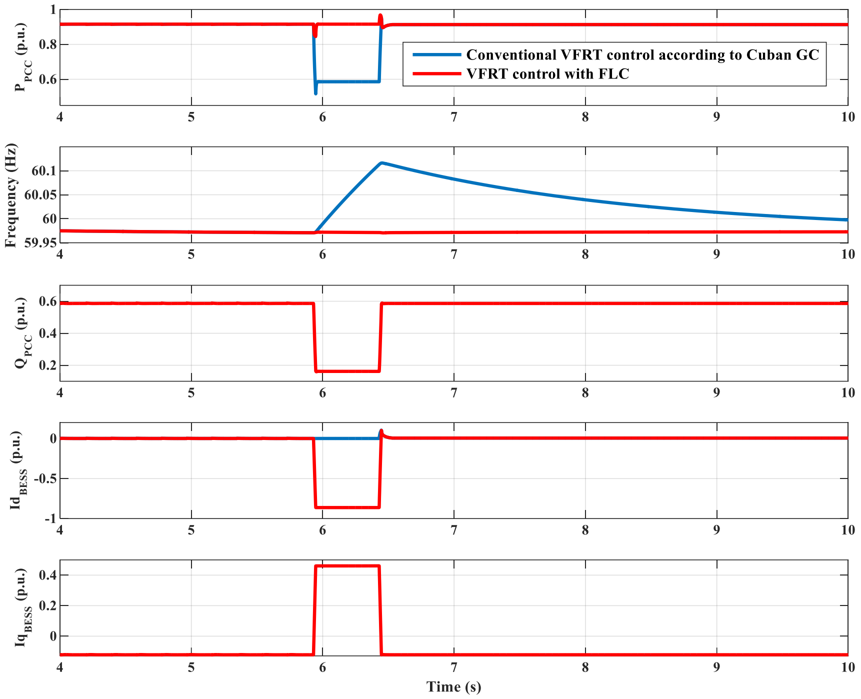

Figure 3.15. Behaviour of the different VFRT controllers in the presence of a voltage sag of 0.8 p.u.

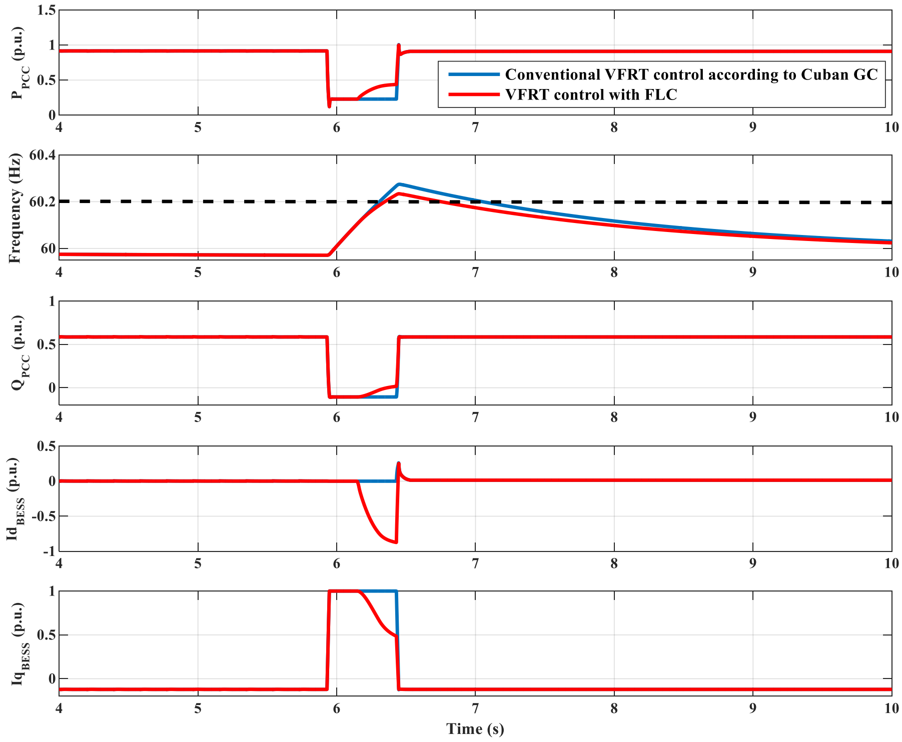

Figure 3.16. Behaviour of the different VFRT controllers in the presence of a voltage sag of 0.5 p.u.

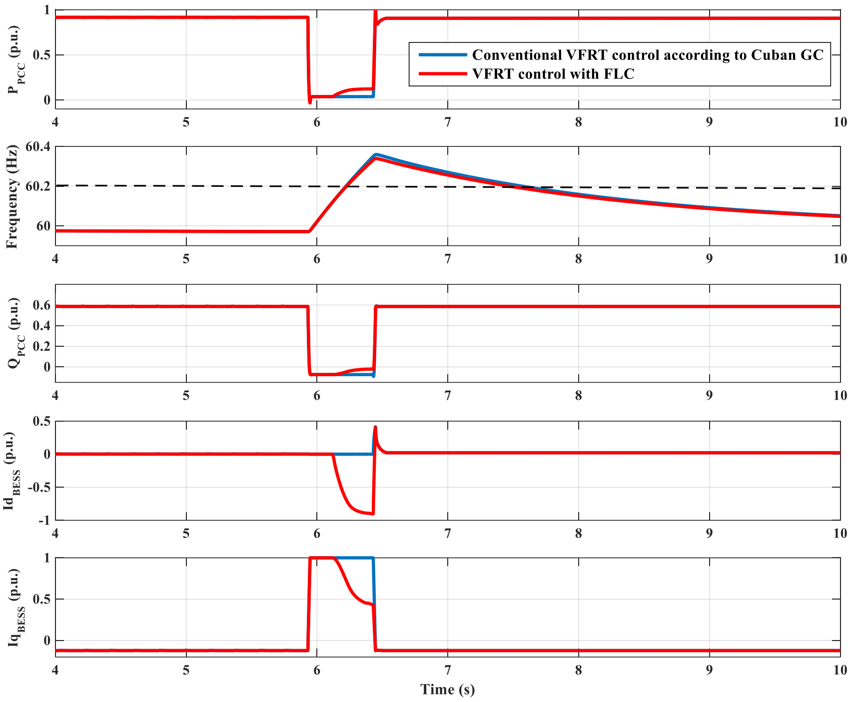

Figure 3.17. Behaviour of the different VFRT controllers in the presence of a voltage sag of 0.2 p.u.

3.3.1.4. Comparative analysis

The use of the two controllers in the system under study allows different comparisons to be made with respect to the frequency deviation (Δf), the active ($P_{PCC\ (\Delta fmax)}$) and reactive power ($Q_{PCC\ (\Delta fmax)}$) and the active ($I_{dBESS\ (\Delta fmax)}$) and reactive ($I_{qBESS\ (\Delta fmax)}$) currents of the BESS values obtained when the maximum frequency deviation occurs. Three-phase voltage sags from the previous section were chosen for this comparison, as they generate a higher frequency deviation and allow the different controllers to be evaluated, as shown in Table 3.4. As shown, the CGC controls only the reactive current, while the BESS active current remains unchanged from its pre-sag value. Similarly, the FLC injects reactive power in all cases; however, under the proposed approach, it adapts its output based on frequency variations, enabling active current control as well.

Consequently, the proposed FLC allows the BESS to consume power in all scenarios, helping to mitigate frequency variations to a certain extent depending on the voltage sag. The maximum frequency deviation in each case in Table 3.4 is calculated as the difference between the peak value recorded during the sag and the initial value of 59.983 Hz. As expected, the most significant frequency improvement occurs when the voltage sag is 0.8, allowing the BESS to maintain active power at the PCC during the sag at a level close to the value before the event.

Table 3.4. Comparison of different VFRT controllers under three-phase voltage sags						
Parameters	Voltage sag (0.8 p.u.)		Voltage sag (0.5 p.u.)		Voltage sag (0.2 p.u.)	
	CGC	**FLC**	**CGC**	**FLC**	**CGC**	**FLC**
Δf *(Hz)*	0.116	0.001	0.274	0.234	0.360	0.340
$P_{PCC\ (\Delta fmax)}$ *(p.u.)*	0.586	0.925	0.229	0.438	0.037	0.123
$Q_{PCC\ (\Delta fmax)}$ *(p.u.)*	0.163	0.163	-0.107	0.016	-0.074	-0.020
$Id_{BESS\ (\Delta fmax)}$ *(p.u.)*	0.000	-0.863	0.000	-0.874	0.000	-0.903
$Iq_{BESS\ (\Delta fmax)}$ *(p.u.)*	0.460	0.460	1.000	0.490	1.000	0.428

Overall, the use of the fuzzy system has several advantages over the conventional control based on the Cuban GC. Unlike the conventional controller, the fuzzy system makes it possible to reduce the frequency variation in a weak power system, as is the case with the Cuban system. In addition, this BESS controller offers the possibility of injecting or consuming active power according to the conditions of the power system. Similarly, the fuzzy controller allows the reactive power injection to be adjusted, with a value that can be modified according to the frequency behaviour. The flexibility of the proposed FLC offers the potential to enhance the operation of the Cuban power system in the future as the penetration of RES and BESS increases.

3.3.1.5. Performance of VFRT controllers under voltage swells

The occurrence of swells in power systems is defined by voltages greater than 1.1 p.u., with durations ranging from 0.5 cycles to 1 minute. Their typical magnitudes are between 1.1 p.u. and 1.2 p.u. Although swells are less frequent than sags, they are mainly caused by faults in the network, as well as by the sudden disconnection of high-power loads or capacitor banks [72].

The severity and amplitude of a swell depend on the location of the fault, the impedance of the system and the grounding scheme. For example, in isolated systems, a single-phase ground fault can generate over-voltages of up to 1.73 p.u. on the unaffected phases, whereas in effectively earthed systems, the same faults do not cause over- voltages on the unaffected phases.

In order to compare the CGC with the FLC, a three-phase swell of 1.2 p.u. and 1 s duration was simulated (Figure 3.18). In the occurrence of this strong over-voltage in the three phases (Figure 3.19), it is observed that the frequency in the case of the CGC presents a strong decrease, unlike the FLC where it does not vary too much. In addition to this, both controllers show the same behaviour in reactive current, which means that both contribute to the improvement of the voltage profile.

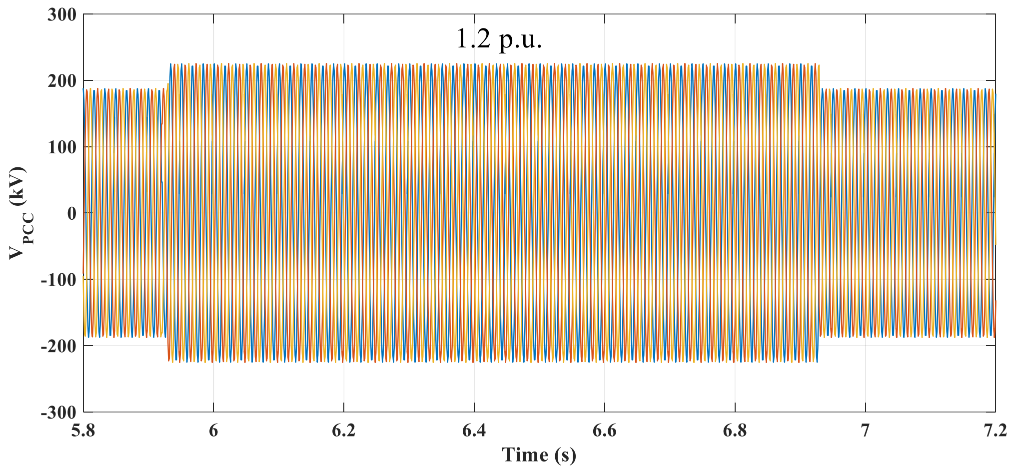

Figure 3.18. Three-phase swell.

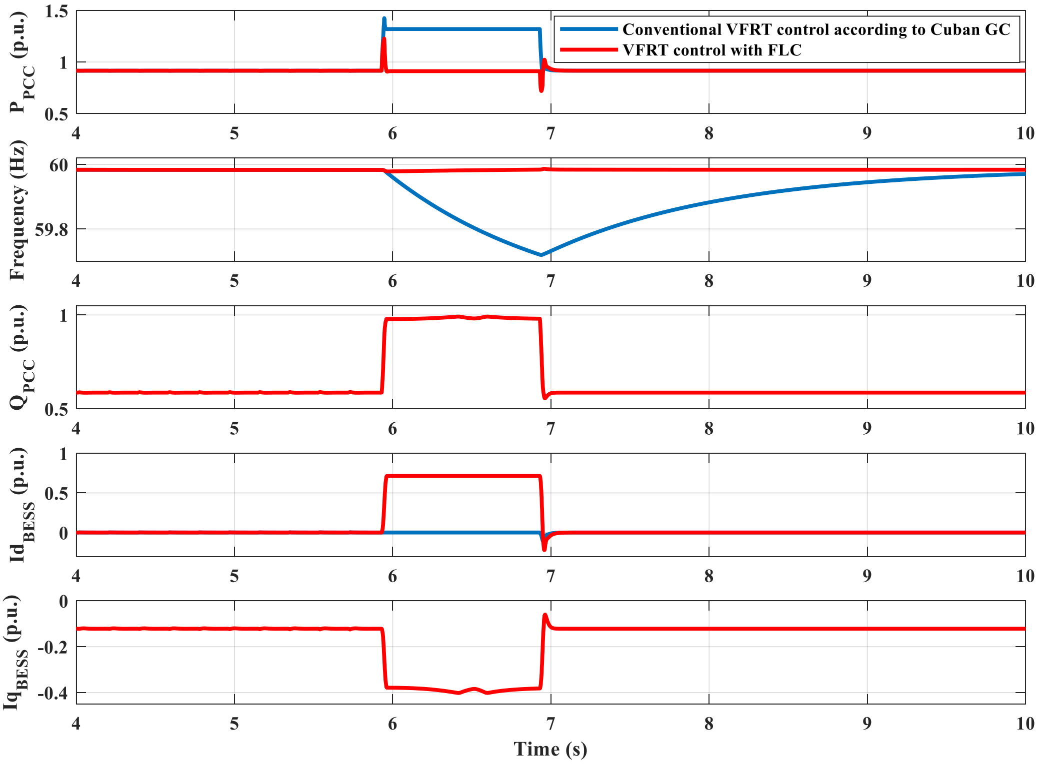

Figure 3.19. Behaviour of the different VFRT controllers in the presence of three-phase swell.

3.4. Modelling of the EAF for harmonic and power factor analysis.

Note: The material in this section is based on author's paper published in [56].

This work analyses the behaviour of harmonics in the steelworks, as well as the response of the BESS acting as an active filter, using a model in the frequency domain. In addition, this model allows the behaviour of the power factor within the circuit to be studied. To explain its operation, a brief theoretical description of the model will be presented, followed by the unbalanced model, which makes it possible to represent an EAF under conditions closer to practice.

3.4.1. EAF model

The adopted model provides a simplified representation of the nonlinear behaviour of an EAF. It is based on the approximation of the V-I characteristic of the electric arc, resulting in a reduced equivalent circuit, as illustrated in Figure 3.20, which produces a square waveform in the furnace voltage [73]. Besides the arc model, the impedances between the furnace and the bus to which the BESS is connected (i.e. Bus 2) are also included.

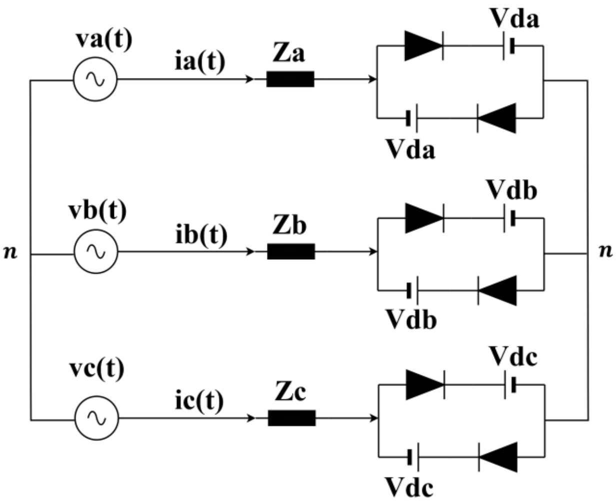

Figure 3.20. Electrical circuit of the EAF model.

3.4.2. EAF unbalanced model

The behaviour of the electric arc in each phase of the EAF is not balanced in practice. The electric arc presents a quasi-random characteristic, which is caused by the different positions of the scrap inside the furnace. Consequently, an unbalance is observed between the phases of the circuit, which can be mathematically represented by considering different impedances within the EAF. To approximate the behaviour of the electric arc within the EAF, an arc voltage control model was developed based on the previously described model. Figure 3.21 shows a per-phase model designed to mimic the electrical characteristic of an EAF.

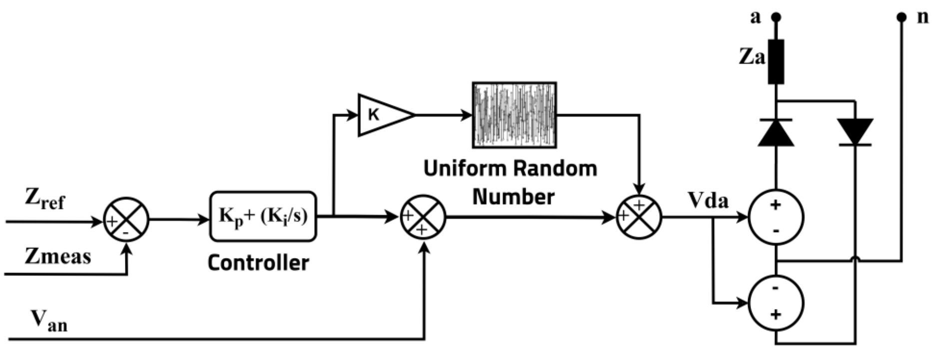

Figure 3.21. Per-phase model of the EAF.

To control the arc voltage V_{da}, the system includes control of the arc impedance to be maintained within the furnace and the value of the nominal phase voltage at the EAF input. In addition, the impedance control incorporates a gain K which reflects the distortion rate of the arc current [74],

[75]. This gain is multiplied by a uniform function of random numbers, simulating the random nature of the arc in the furnace.

3.5. Use of BESS as an active filter to compensate for EAF harmonic compensation

Note: The material in this section is based on author's paper published in [56].

For the analysis of the BESS behaviour in the steelworks circuit in the presence of harmonics, all control and circuit components were modelled in Matlab/Simulink (Figure 2.3). The harmonic current analysis was performed in accordance with IEEE Std 519-2022, which uses Total Demand Distortion (TDD) to measure the harmonic content present in the system. TDD is defined as the ratio of the root mean square harmonic content to the maximum demand load current (I_l), expressed as a percentage [76]. The maximum demand load current in the steel mill circuit is 146 A; a value obtained from periodic measurements over three months of operation.
The current distortion limits in the 220 kV system were determined using the ratio between the short-circuit current at the PCC and the peak demand load current. In our case study, this ratio resulted in a value of 48, which allowed us to determine the distortion limits shown in Table 3.5, according to IEEE Std 519-2022.

Table 3.5. Maximum harmonic current distortion - IEEE Std 519-2022					
Individual harmonic order - % of I_l					
2 ≤ h < 11	*11 ≤ h < 17*	*17 ≤ h < 23*	*23 ≤ h < 35*	*35 ≤ h ≤ 50*	*TDD [%]*
2	1	0.75	0.3	0.15	2.5

3.5.1. Analysis of harmonic currents in the EAF circuit without compensation measures

For the analysis of a high-power melting profile in the EAF, an impedance of 10 mΩ was set in the electrode movement control, which is approximately equivalent to a 50 MW demand of the EAF. Analysis of harmonic behaviour in the PCC showed that, at a voltage level of 220 kV, currents with a high percentage of harmonics can be generated, which is unacceptable for the electrical system in accordance with the standard IEEE Std 519-2022 (Figure 3.22).

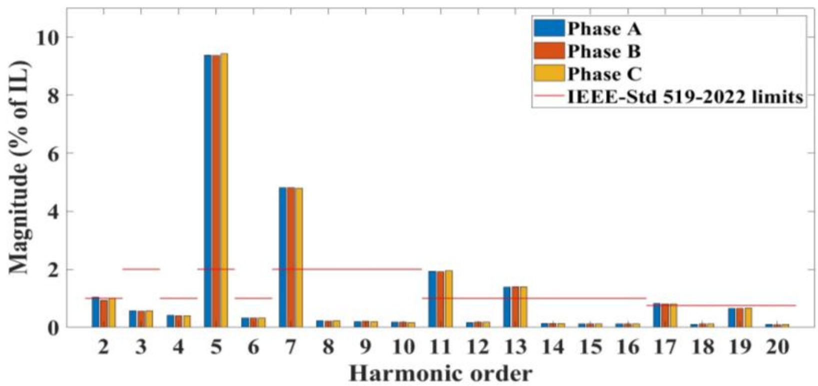

Figure 3.22. Harmonic current spectrum at PCC (without compensation).

3.5.2. Analysis of harmonic currents in the steel mill circuit with compensation measures

The integration of the BESS within the EAF system was previously established as necessary to ensure continued steel mill operation under the specific conditions of the Cuban power system. In addition to its primary function, the BESS can be leveraged to improve power quality at the PCC, particularly through the mitigation of EAF-generated harmonic distortion.

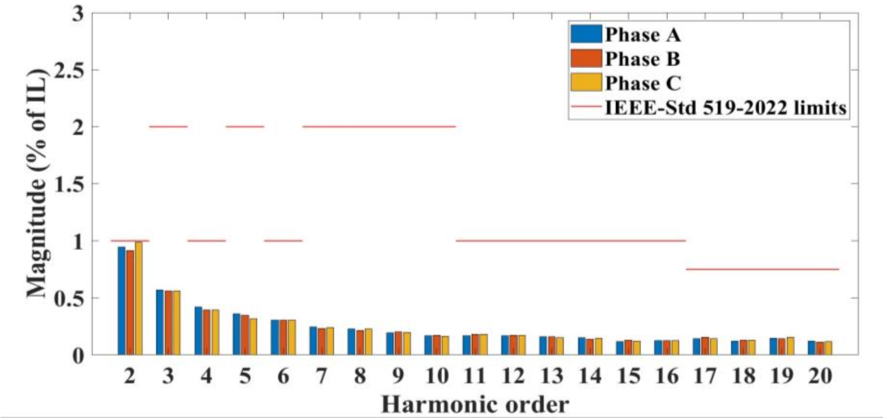

Figure 3.23. Harmonic spectrum at the PCC with BESS compensation.

The analysis of the harmonic spectrum in Figure 3.23 allows a general comparison to be made between the TDD index observed without compensation and that obtained with compensation. The results of this comparison are shown in Table 3.6, in conjunction with the waveforms of the currents shown in Figure 3.24. As shown, the BESS can reduce harmonics in the PCC to levels well below the standard limits, both for individual harmonics and for the TDD. However, the level of harmonic compensation is limited by the remaining inverter capacity.

Table 3.6. Total demand distortion per phase at the PCC

	TDD Phase A [%]	TDD Phase B [%]	TDD Phase C [%]
Without compensation	10.94	10.92	10.98
With compensation	1.86	1.82	1.86
IEEE Std 519-2022 limit	2.5		

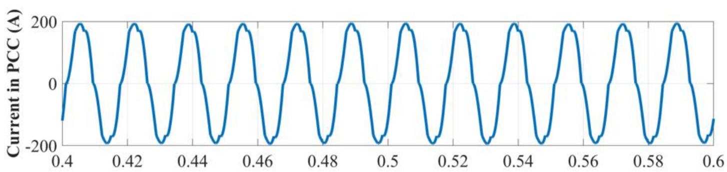

a)

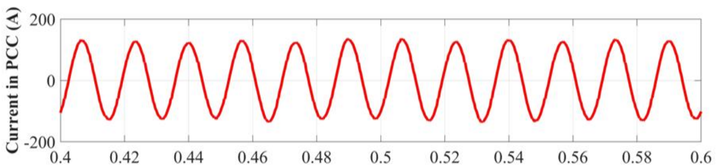

b)

Figure 3.24. Current at the PCC: a) without harmonic compensation; b) with harmonic compensation.

3.6. Use of BESS as a reactive power compensator to improve EAF power factor

Note: The material in this section is based on author's paper published in [56].

In addition to harmonic compensation, power factor improvement is another ancillary function that the BESS can provide. The analysis of the power factor behaviour on bus 2 (Figure 2.3) was based on the same melting profile used for the study of harmonics in the network. The EAF impedance was set at 10 mΩ for a maximum power of 50 MW. In general, the power factor analysis corresponding to this melting profile yielded a value of 0.85, which highlights the need to implement a compensation method to improve power quality in the industry. Table 3.7 summarises the power factor performance on bus 2 for each of these scenarios.

Table 3.7. Power Factor on bus 2 for various power levels supplied by BESS

BESS active power (MW)	BESS reactive power (MVAr)	Power factor on bus 2
0	6.63	0.9
5	9.17	0.9
10	11.72	0.9
15	14.29	0.9
20	15.00	0.88
25	0.00	0.6

As can be seen from the results in Table 3.7, the power factor is effectively compensated up to the 15 MW level, reaching and maintaining a value of 0.9. This level meets the requirements of the Cuban regulations and avoids penalties to the industry for low power factor [55]. However, beyond the mentioned limit, the power factor can no longer be fully corrected because the BESS prioritises the supply of active power, reducing its ability to compensate for reactive power.

3.7. Conclusions

In this chapter, the BESS was simulated along with all the parameters of the steelworks' electrical circuit, including a model of the EAF designed to faithfully reproduce the actual conditions of the process. Different control systems were evaluated, demonstrating that the BESS can function as a comprehensive solution for electrical compensation in a steelwork.

The main contributions of this chapter are summarized as follows:

- Validation of the adaptive filter for the BESS compensator based on fuzzy logic techniques;
- Implementation of the BESS VFRT control system in the case of grid voltage fault events;
- Validation of the BESS control system as an active filter for compensating harmonics produced by the EAF in conjunction with power factor compensation for the steel mill;
- Design and implementation of an EAF model for harmonic simulation and power factor analysis.

CHAPTER 4 . Experimental validations

Note: The material in this chapter is based on author's papers published in [6], [57].

The aim of this chapter is to experimentally validate the proposed BESS designed for improving EAF operation in the conditions of the Cuban power system, as presented in the preceding chapters. For this purpose, a laboratory setup at the R&D Institute of Transilvania University of Brasov, was employed. A Power Hardware-in-the-Loop (PHIL) approach was adopted, in which the power system dynamic was simulated, while the physical representation of the BESS PCC with the grid was implemented using a four-quadrant power converter as part of the PHIL system. In terms of power, the PHIL setup allows bidirectional power flow of up to 10kW, therefore the scaling factor relative to the real system is 1:5000. The BESS consisted of a 5kW-scale three-phase inverter supplied by a bidirectional DC source and connected on the AC side to the PHIL system. The BESS control was developed using a rapid control prototyping (RCP) system based in a dSPACE DS1103 board [77]. Details of the employed setup are provided in the following section.

The experimental validations closely follow the simulations, presented in chapter 3, Therefore, this chapter presents experimental validations of the proposed BESS for the following features that have been developed within this thesis:

1) Validating the inverter control, particularly in terms of power control, current harmonics and unbalances compensation.
2) Validating the developed adaptive support during the EAF power variations using the BESS to mitigate the impact of EAF operations on the Cuban power system.
3) Validating the BESS response under VFRT conditions.
4) Evaluating the performance of the BESS inverter as an active power filter for the mitigation of harmonic distortion generated by the EAF.

4.1. Experimental setup

The experiments were carried out using a laboratory scale PHIL testbench consisting of the elements shown in Figure 4.1. The main hardware setup consists of a 5kW VSI, an LC filter, and a 650 V DC supply at the DC link. A 10kW four-quadrant power converter (FQPC) emulates the frequency behaviour of the Cuban power system, whereas a controlled non-linear load emulates the harmonic behaviour characteristic of an EAF. The main parameters of the experimental setup are shown in Table 4.1. The control system developed for the BESS inverter is implemented using a dSPACE DS1103 board, which provides all the necessary analogue and digital interfaces required for the intended system [77].

Table 4.1. Main parameters of the PHIL system	
Parameters	**Values**
Inverter rated active power	5 kW
FQPC rated active power	10 kW
Rated AC voltage (line-to-line)	400 V
Rated frequency	60 Hz
DC inverter voltage	650 V
PWM switching frequency	10 kHz
Filter inductance	3 mH
Filter capacitance (star-connected)	10 μF
Non-linear load rated active power	9 kW

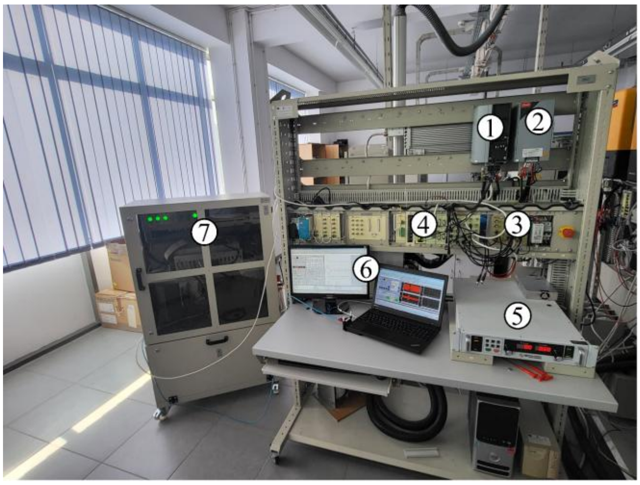

1.VSI (Voltage Source Inverter)

2.LC filter

3.V-I transducers

4.ADC (Analog interface)

5.DC Power Supply

6.MATLAB/Simulink and dSPACE/ControlDesk

7. Four-quadrant power converter

Figure 4.1. View of the laboratory PHIL setup.

The general control diagram developed in MATLAB/Simulink (Figure 4.2) consists mainly of three major subsystems: the data acquisition (Figure 4.3), inverter control (Figure 4.5) and PWM generation (Figure 4.4).

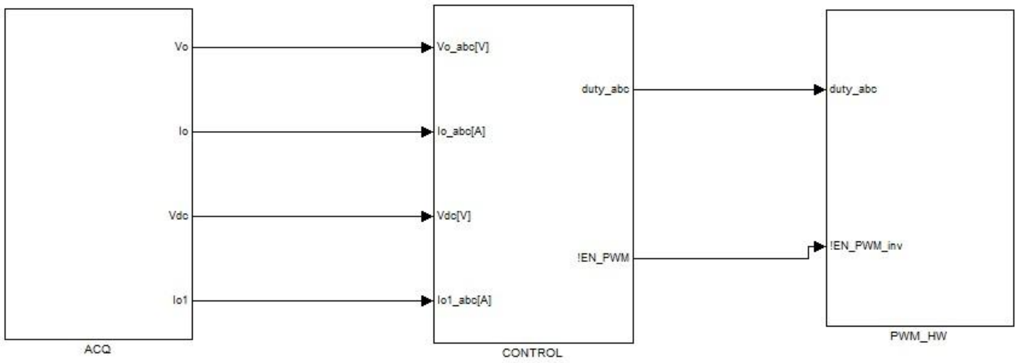

Figure 4.2. General control diagram.

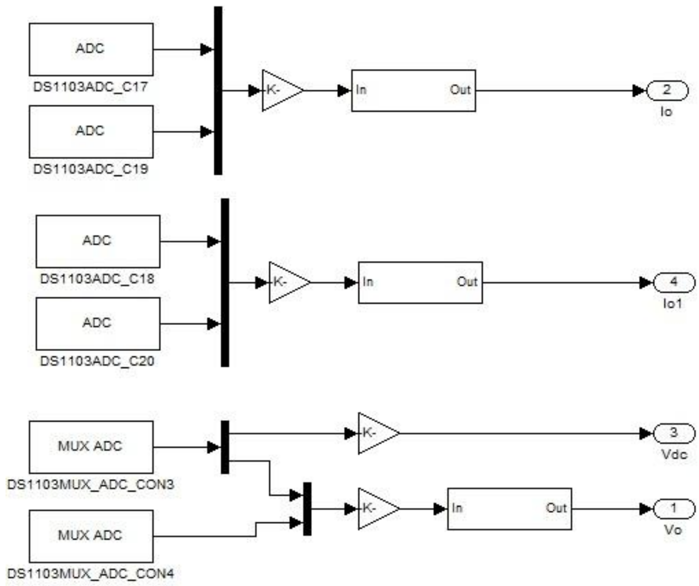

Figure 4.3. Data acquisition subsystem.

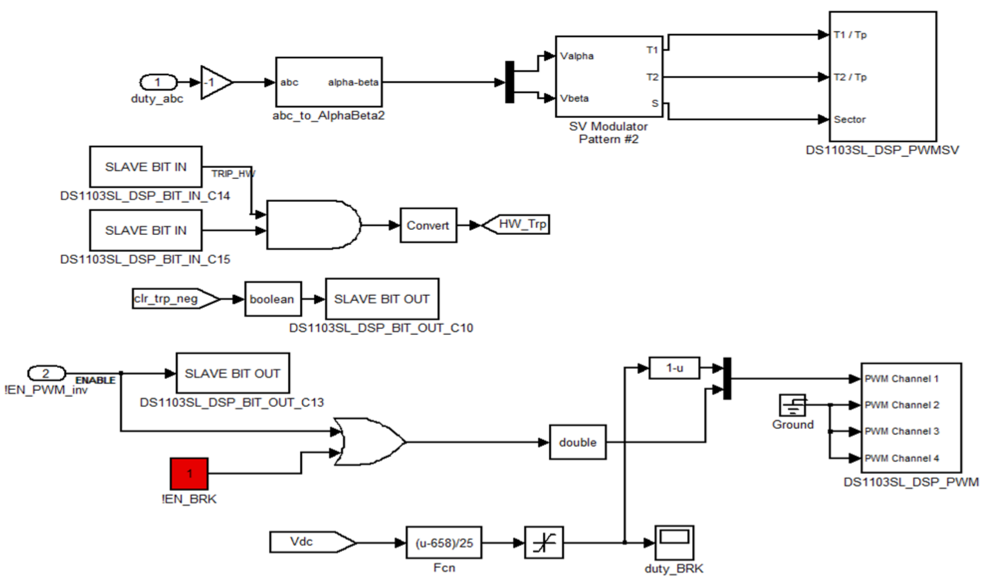

Figure 4.4. PWM generation subsystem.

In order to obtain the main results during the experiments, the programme interface shown in Figure 4.6 was designed using dSPACE ControlDesk. This interface consists of inverter control, measurements, inverter active and reactive power management, adjustment of the gains of some parameters within the inverter control, and the real-time plotting block.

Once all the parameters and controls of the experimental setup were correctly adjusted, the designed control systems were implemented. To carry out the experiments, they were divided into two stages: in the first stage, the inverter's inner control was tested while connected to the power system, without operating in parallel with the EAF emulator; in the second stage, the control systems were evaluated within the intended EAF application under the real operating conditions of the Cuban power system emulated by the FQPC.

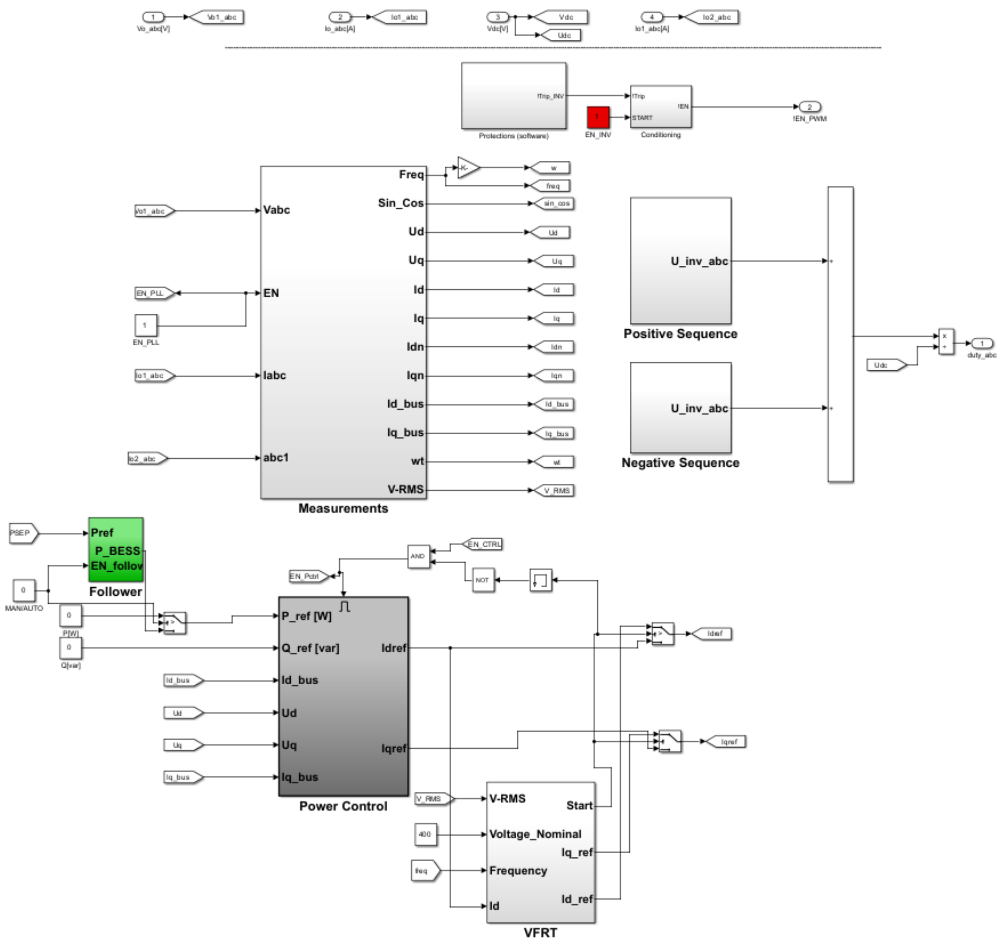

Figure 4.5. Inverter control subsystem.

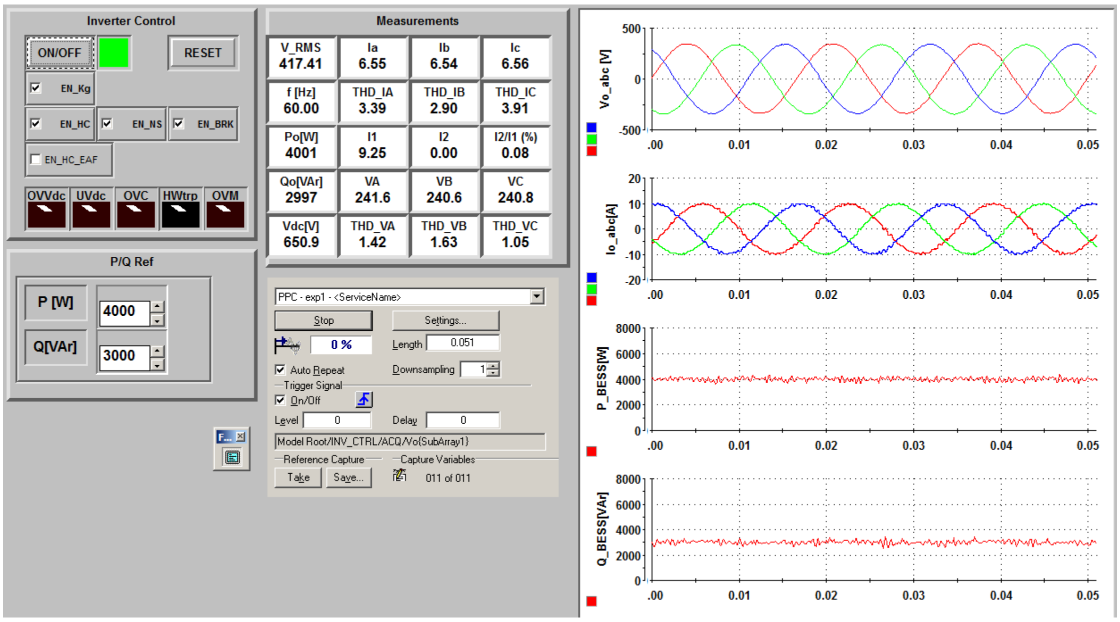

Figure 4.6. ControlDesk user interface.

4.2. Control Systems

The block diagram of the GFL current control is shown in section 4.2.2, where the internal current control loop provides the reference voltages to the space vector modulator that controls the BESS inverter. The goal of the internal current loop is to control the current flow through the inverter to follow the reference signal and contribute to the protection and power quality of the converter [24]. Additionally, there are five other control loops: power control, harmonics compensation, unbalanced current controller, VFRT control and another for the EAF compensator main control.

4.2.1. Power controller

Figure 4.7 presents the Simulink block diagram of the power controller, which employs two PI controllers acting on the error between the reference active and reactive powers (Pref, Qref) and the measured powers. The results in Figure 4.8 show that the power controller responds quickly, in around two to three cycles. Furthermore, the inverter operation in all four quadrants allows it to accurately emulate the behaviour of the BESS.

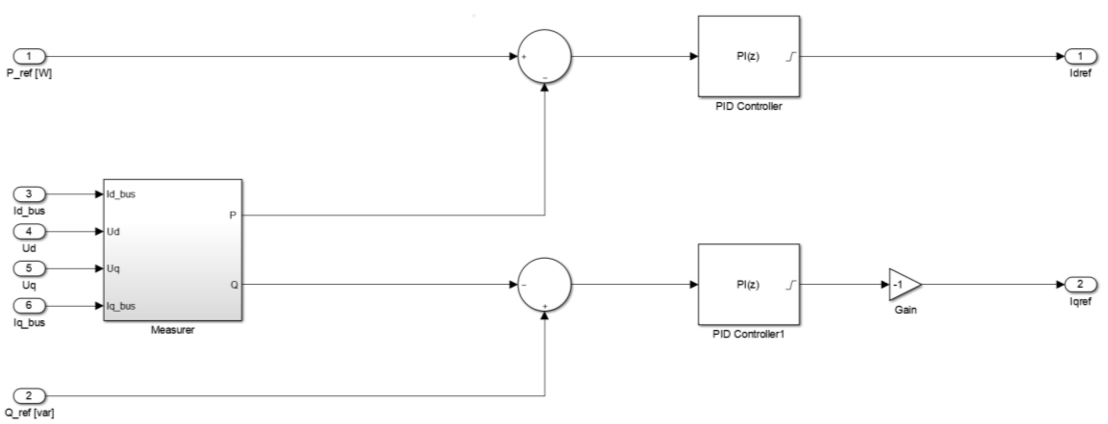

Figure 4.7. Power controller.

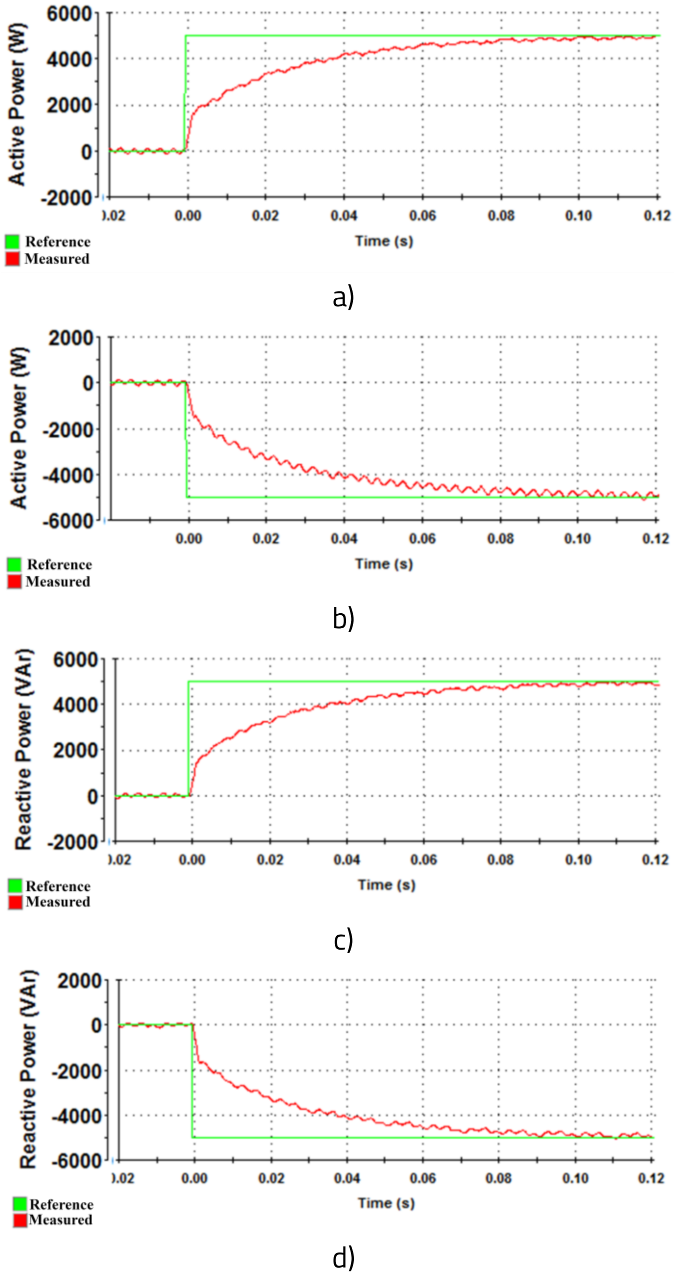

Figure 4.8. Inverter response to a step change in power references (generator rule): a) Pref=5kW; b) Pref=-5kW; c) Qref=5kVAr; d) Qref=-5kVAr.

4.2.2. Current control loop with harmonic compensation

The GFL control implies the use of an inner current control loop synchronised by a PLL, as discussed in section 2.3.1. Besides controlling the fundamental current component, the inverter must also ensure mitigation of current harmonics. For this purpose, one of the control loops designed to improve power quality at the inverter output is the harmonic compensation control (Figure 4.9).

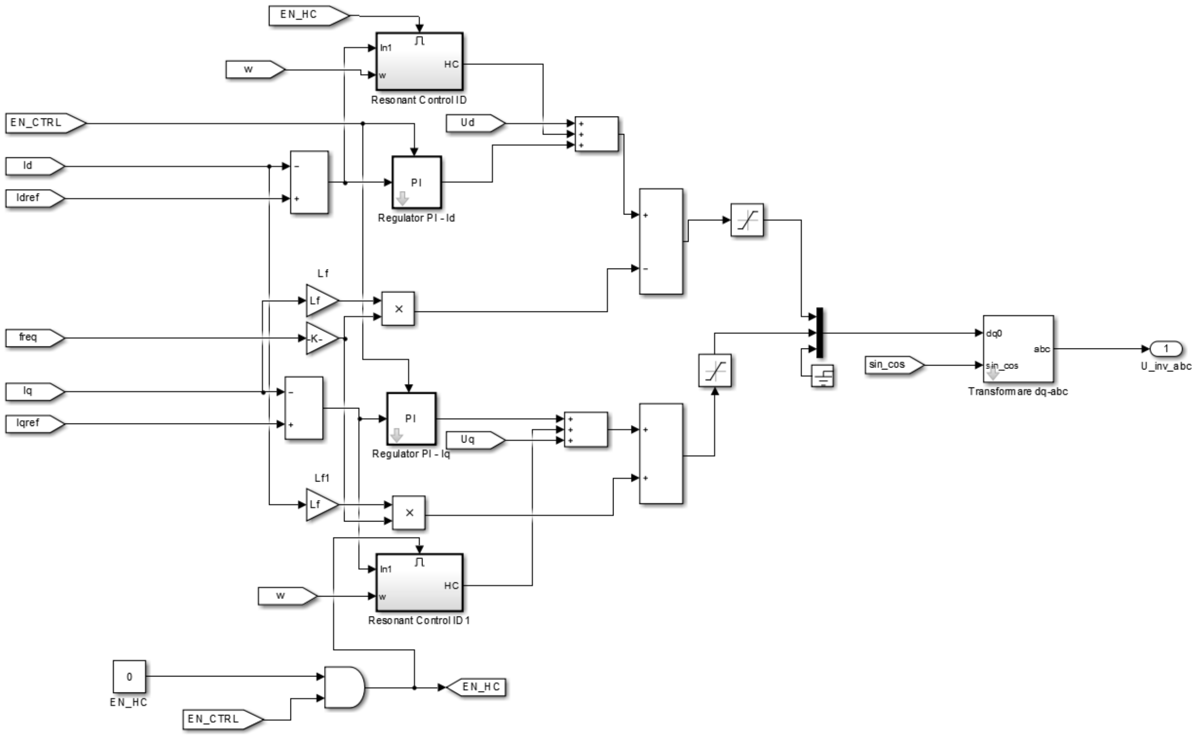

Figure 4.9. Current control implementation with harmonic compensation.

As shown in Table 4.2, the effect of the harmonic compensation control is to reduce the current THD per phase. This effect is highly beneficial for the power quality of the inverter with respect to the grid, as it ensures compliance with the IEEE 1547 and IEC 61727 standards, which set a maximum limit of 5% for the current THD. In this context, the implementation of the compensation controller keeps the THD always below this threshold. Furthermore, the accurate control of the harmonics allows enhancing the BESS with an active power filter functionality, as will be discussed in section 4.2.6.

Table 4.2. Harmonic compensation control general results

Case	THD_I_A (%)	THD_I _B (%)	THD_I _C (%)
P=5 kW without control	2.82	2.74	3.22
P=5 kW with control	1.99	2.14	1.56
P=-5 kW without control	5.51	5.07	5.90
P=-5 kW with control	1.97	2.15	2.22
Q=5 kVAr without control	3.79	3.29	3.69
Q=5 kVAr with control	2.52	2.29	2.16
Q=-5 kVAr without control	4.35	4.27	4.75
Q=-5 kVAr with control	1.99	2.15	2.89

4.2.3. Unbalanced current controller

This unbalanced current controller has been evaluated in the laboratory under unbalanced conditions at the output of the PHIL inverter. In these initial experiments, it was not necessary to consider the real conditions of the power system, but to observe the process of attenuation of the unbalanced currents at the output of the inverter. The results are shown in Table 4.3.

Table 4.3. Unbalanced current controller results

Parameters	I_a (A)	I_b (A)	I_c (A)	I_1 (A)	I_2 (A)	I_2 / I_1 (%)
Output current converter without unbalanced control	3.880	4.600	4.700	6.175	0.710	11.500
Output current converter with unbalanced control	4.380	4.380	4.380	6.175	0.005	0.081

As can be seen from Table 4.3, when the inverter is operated without an unbalance controller, the degree of unbalance in the output currents reaches 11.5%. However, by implementing the current unbalance controller, this value is significantly reduced to 0.081%. Under these conditions, the inverter complies with one of the power quality requirements of international GCs.

4.2.4. Implementation of a fuzzy-logic adaptive BESS compensator

A block diagram of the laboratory setup configuration employed for BESS compensation tests is shown in Figure 4.10. The following experimental results are obtained for one of the most severe scenarios, with the power system inertia of 58 MWs²/rad and damping constant of 25 MW/rad/s. Figure 4.11 shows the main experimental results, including the active powers of the EAF and BESS, as well as the power system frequency. The base value for active powers representation in p.u. was 10 kW for the real power, and 50 MW for emulated power. Additionally, the variation of the filter's Ts, as provided by the FLC, and the battery's CC_{rate} are shown.

Table 4.4 shows a comparison between the simulation and experimental results, based on previously introduced performance indices. As shown, all values are close, with the largest difference observed in the time the frequency exceeds the upper bound of 60.2 Hz during the furnace high rate of power reduction at the end of the smelting process. Regarding the frequency excursion, both experimental and simulation results show that the frequency consistently remains above 59.7 Hz throughout the entire process, thus achieving the primary objective.

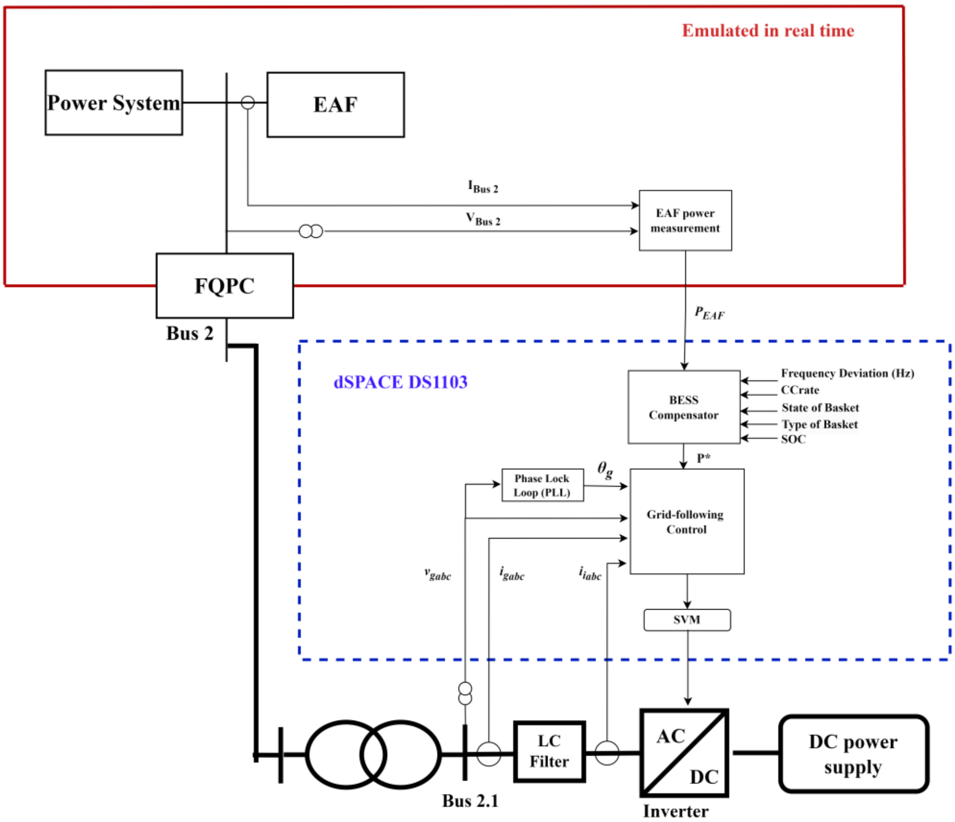

Figure 4.10. Block diagram of laboratory PHIL setup.

Table 4.4. Comparison between simulation and experimental results for the most challenging scenario		
Parameters	Simulation results	Experimental results
Average power (p.u.)	0.152	0.157
Maximum frequency (Hz)	60.280	60.286
Minimum frequency (Hz)	59.741	59.731
Time above 60.2 Hz (s)	33.461	73
Time below 59.7 Hz (s)	0	0
Average cumulative C-rate (pu)	0.304	0.316

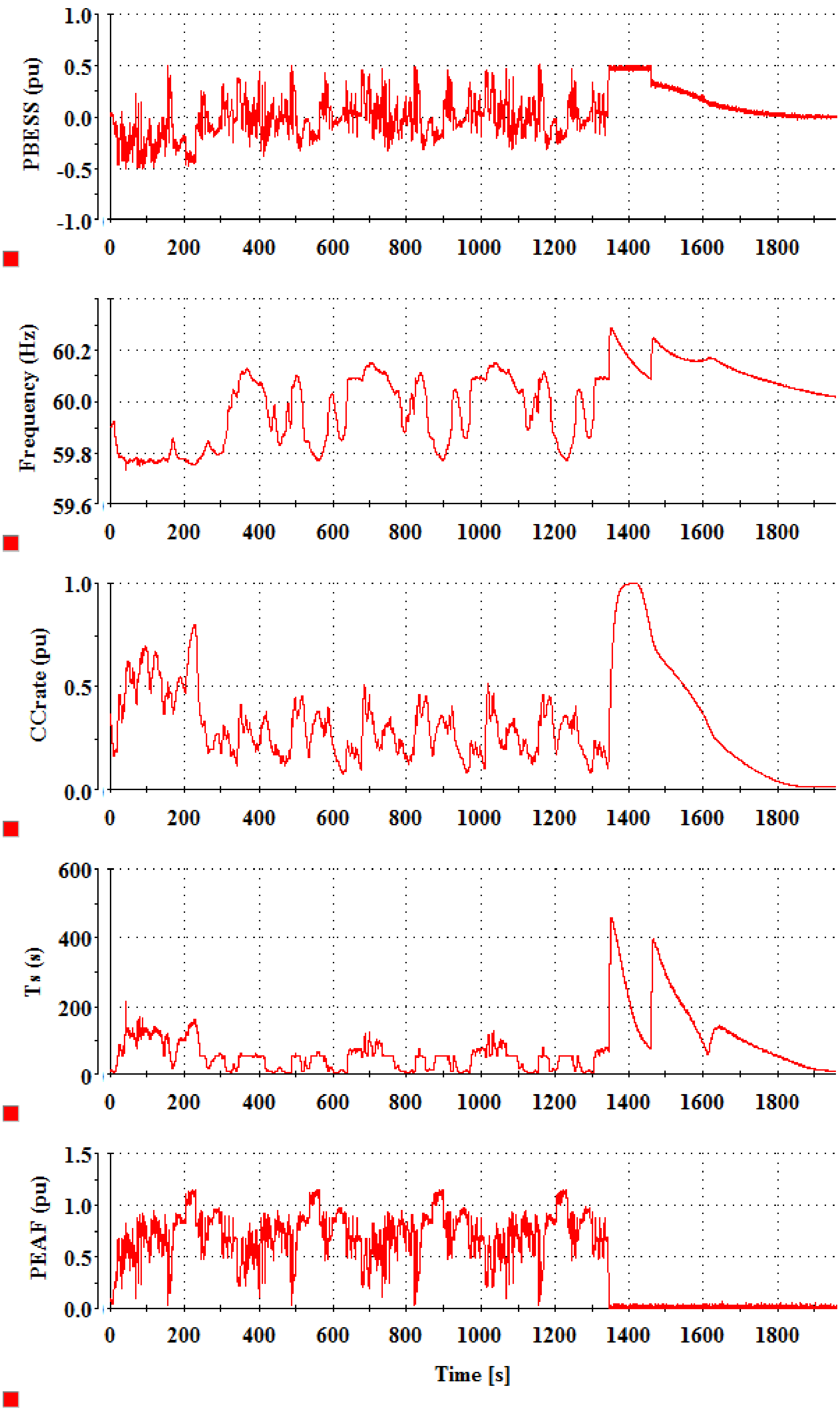

Figure 4.11. Experimental results for the most challenging scenario.

4.2.5. Voltage fault ride through controller

The experimental analysis aims to validate the implementation and feasibility of the fuzzy VFRT presented in this work. Detailed analyses have been carried out for the three sags, considering a power system inertia of 58 MWs²/rad and a damping constant of 25 MW/rad/s. The results of the different experiments are shown in Figure 4.12 – Figure 4.14, where the behaviour of the active and reactive currents of the BESS in conjunction with the frequency behaviour of the power system at the occurrence of the sag are included.

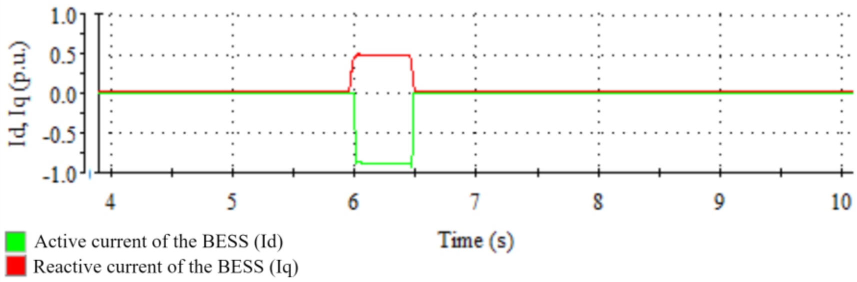

a)

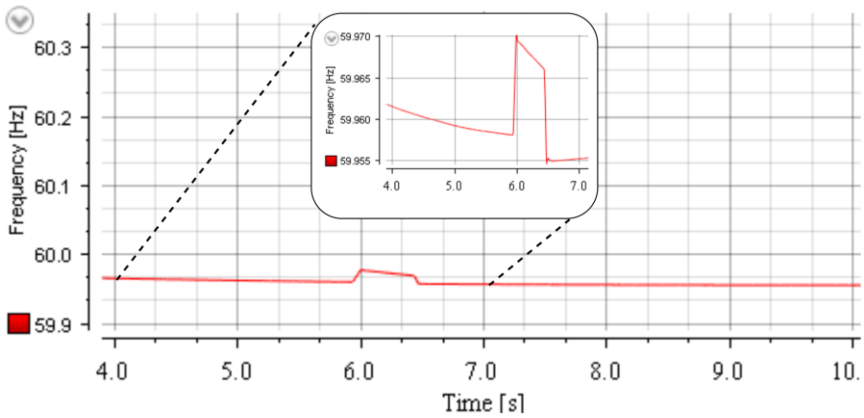

b)

Figure 4.12. System behaviour for a voltage sag of 0.8 p.u.: a) BESS active and reactive currents; b) power system frequency.

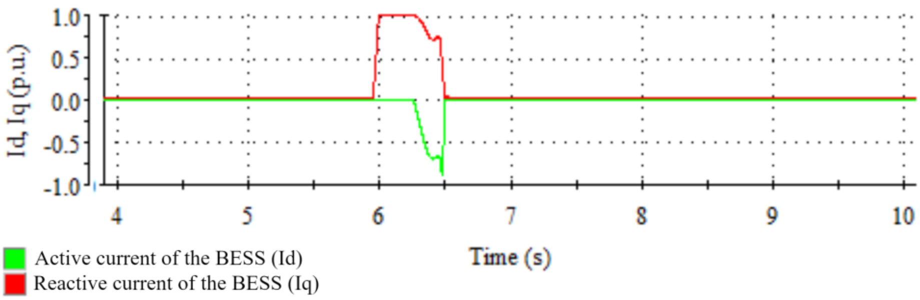

a)

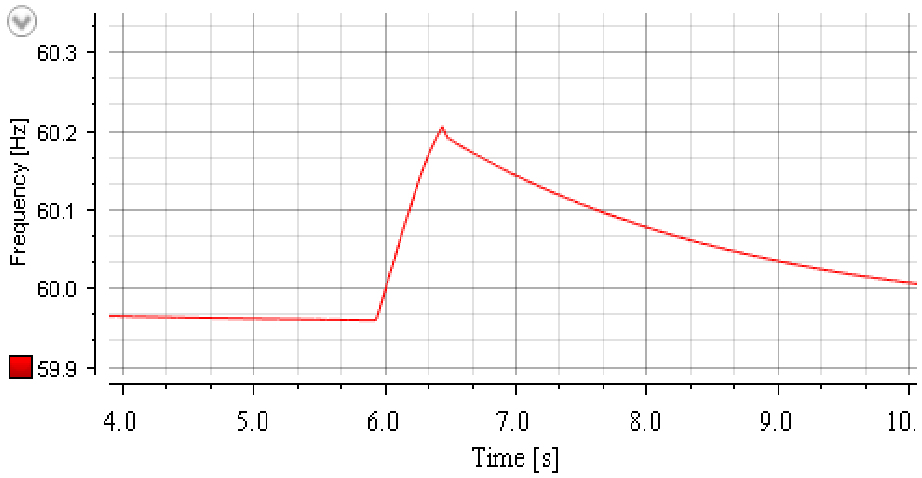

b)

Figure 4.13. System behaviour for a voltage sag of 0.5 p.u.: a) BESS active and reactive currents; b) power system frequency.

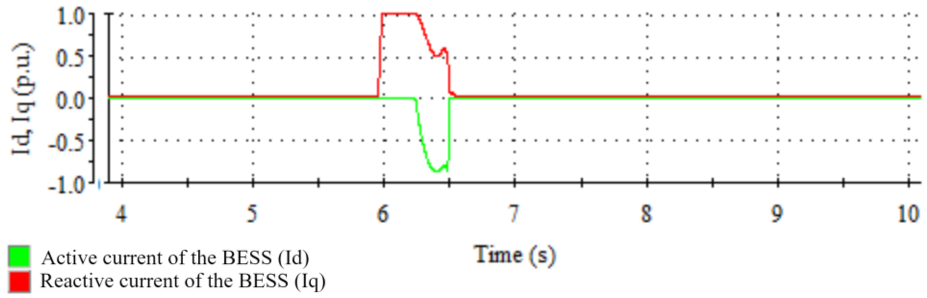

a)

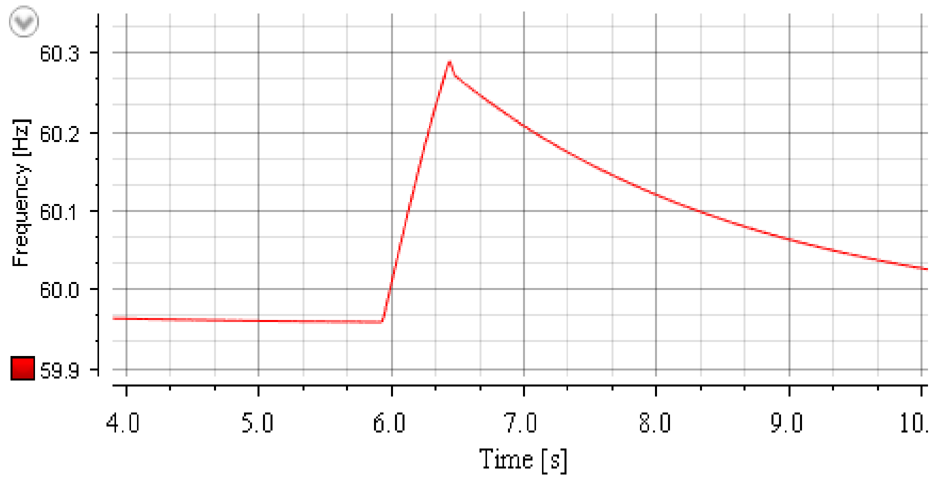

b)

Figure 4.14. System behaviour for a voltage sag of 0.2 p.u.: a) BESS active and reactive currents; b) power system frequency.

Table 4.5 shows a comparison between the results of the experimental analyses and those obtained by simulation in the scenarios where the maximum frequency deviation occurs in the power system. In general, the values are very similar, although there is a slight reduction in the maximum frequency deviation in the experiments compared to the simulations. These results demonstrate the effectiveness of the adaptive fuzzy VFRT controller presented in this study, which simultaneously contributes to reducing the frequency deviation and providing fault ride-through support through reactive current injection.

Table 4.5. Comparison between simulation and experimental results for the different scenarios

Parameters	Voltage sag (0.8 p.u.)		Voltage sag (0.5 p.u.)		Voltage sag (0.2 p.u.)	
	Simulation results	Experimental results	Simulation results	Experimental results	Simulation results	Experimental results
Δf (Hz)	0.030	0.040	0.234	0.203	0.340	0.290
$Id_{BESS\,(\Delta fmax)}$ (p.u.)	-0.863	-0.862	-0.874	-0.896	-0.903	-0.908
$Iq_{BESS\,(\Delta fmax)}$ (p.u.)	0.460	0.472	0.490	0.443	0.428	0.419

4.2.6. BESS as an active filter for harmonic compensation.

This section experimentally evaluates the ability of the BESS inverter to detect and minimise pre-existing harmonic distortions in the grid. The analysis is initially based on a rigorous statistical validation aimed at verifying the accuracy of the simulation model against the data obtained in the experimental setting. This evaluation specifically considers the characteristic harmonic spectrum of the EAF mathematical model detailed in [56]. Once the statistical robustness of the model has been established, a quantitative analysis is carried out of the harmonic compensation achieved in the laboratory tests, thereby validating the effectiveness of the BESS when operating as an active filter in industrial networks.

Experimental design and validation of the simulation model

The evaluation of harmonic compensation for the EAF was conducted using an experimental setup designed to emulate its non-linear behaviour in real time. This setup consisted of a 9kW programmable load connected to the PCC emulating the non-linear EAF model, integrated in parallel with the BESS inverter. The harmonic mitigation was executed through the control algorithm previously detailed in Section 2.3.6.

Validation database

To proceed with the discrepancy analysis, the current magnitude values (as a percentage of the fundamental) for harmonic orders 2 to 20 were measured across the three phases of the system. The individual harmonic distortion (IHD), defined as the ratio between the RMS value of a specific harmonic component and the RMS value of the fundamental component, was used as the evaluation metric. The current harmonic spectrum of the EAF, up to the 20^{th} harmonic and based on the model discussed in section 2.3.6, was replicated using the programmable load, and the measured values, compared with those obtained from simulations, are presented in Table 4.6.

Table 4.6. Comparative results for EAF current IHD [%]						
	PHASE A		PHASE B		PHASE C	
Harmonic order	**Experimental results**	**Simulation results**	**Experimental results**	**Simulation results**	**Experimental results**	**Simulation results**
2	1.011	1.174	1.118	1.021	0.615	1.126
3	0.097	0.642	0.622	0.618	0.787	0.628
4	0.237	0.474	0.084	0.434	0.248	0.434
5	7.984	10.534	7.604	10.321	7.743	10.433
6	0.430	0.358	0.116	0.355	0.270	0.357
7	4.282	5.415	4.219	5.293	4.195	5.319
8	0.226	0.263	0.127	0.238	0.302	0.247
9	0.441	0.221	0.274	0.227	0.270	0.222
10	0.118	0.200	0.179	0.203	0.097	0.190
11	2.055	2.176	2.141	2.108	2.017	2.152
12	0.097	0.193	0.179	0.191	0.075	0.193
13	1.313	1.561	1.445	1.542	1.596	1.559
14	0.054	0.155	0.148	0.142	0.151	0.149
15	0.258	0.123	0.169	0.134	0.377	0.125
16	0.043	0.127	0.074	0.124	0.129	0.127
17	0.775	0.921	0.875	0.886	0.625	0.895
18	0.097	0.118	0.084	0.124	0.097	0.122
19	0.204	0.737	0.084	0.708	0.173	0.732
20	0.075	0.111	0.000	0.101	0.065	0.106

As illustrated in the table above, the 5th and 7th harmonics show the highest levels of distortion. Generally, the experimental findings align with the simulation results, as the harmonics present in the experimental tests are of the same orders as those reported in [56].

Assessment of power quality without compensation

According to the preliminary analysis of Figure 4.15, the experimental results for current IHD reveal that harmonics 2, 5, 7, 11, 13, 17 and 19 exceed the limits set by the IEEE 519 standard. Beyond these percentage values, the waveforms obtained in the laboratory (shown in Figure 4.16) visually confirm severe distortion in each of the phases, as expected during the EAF operation.

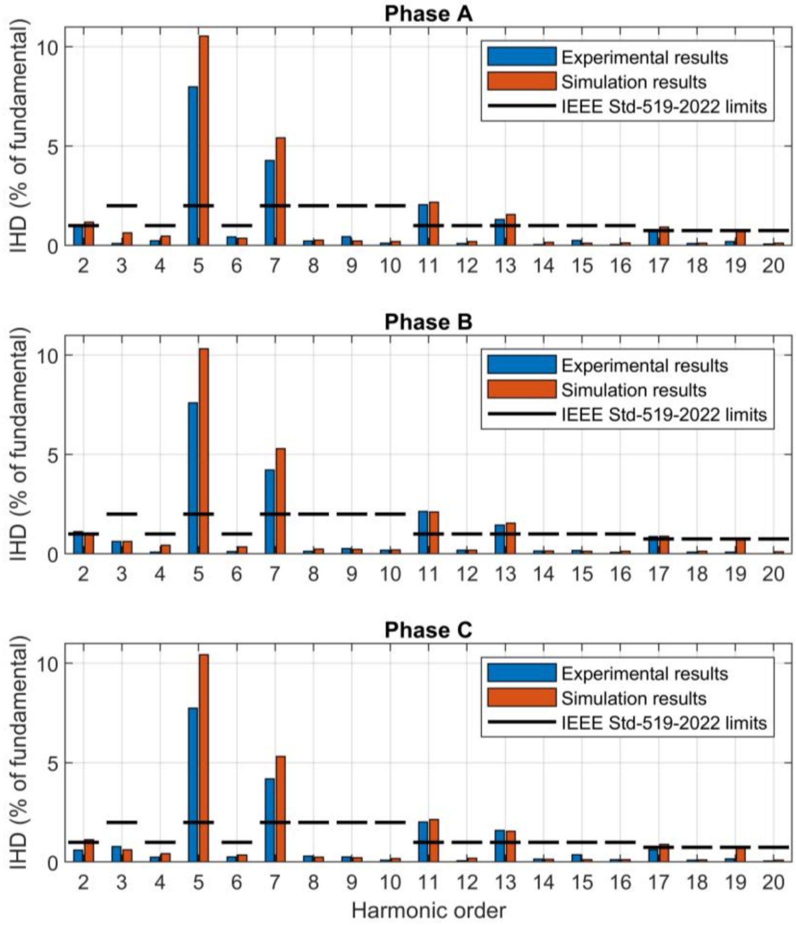

Figure 4.15. Phase-by-phase current harmonic spectrum vs. IEEE Std-519-2022 limits.

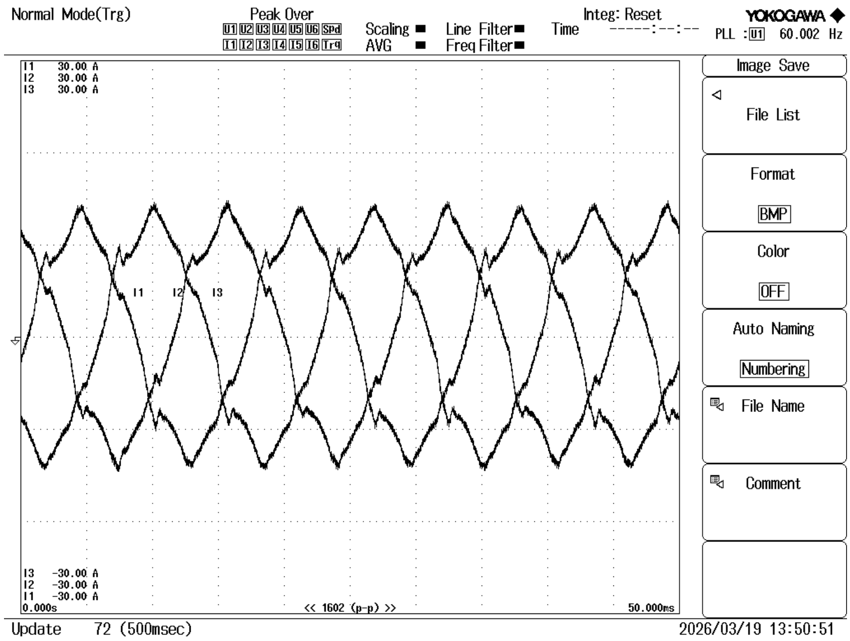

Figure 4.16. Phase current waveforms without harmonic compensation.

The similarity between the experimental waveforms and those obtained in simulations [56] validates the accuracy of EAF emulation. As also discussed in section 3.4.1, the per-phase TDD levels (exceeding 9%) surpass the 2.5% limit specified in IEEE 519 standard. Consequently, intervention by the compensation system at the PCC though the BESS, described in the following section, is necessary.

Implementation and experimental results of EAF harmonic compensation

As discussed in 2.3.6, in addition to its primary function, the BESS can also provide power quality improvement during the EAF operation. For this purpose, an active filtering control was implemented within the BESS inverter. The experimental tests of this scenario implied the use of the non-linear load that generates harmonic currents similar to an EAF. Figure 4.17 shows the phase current waveforms at PCC with harmonic compensation.

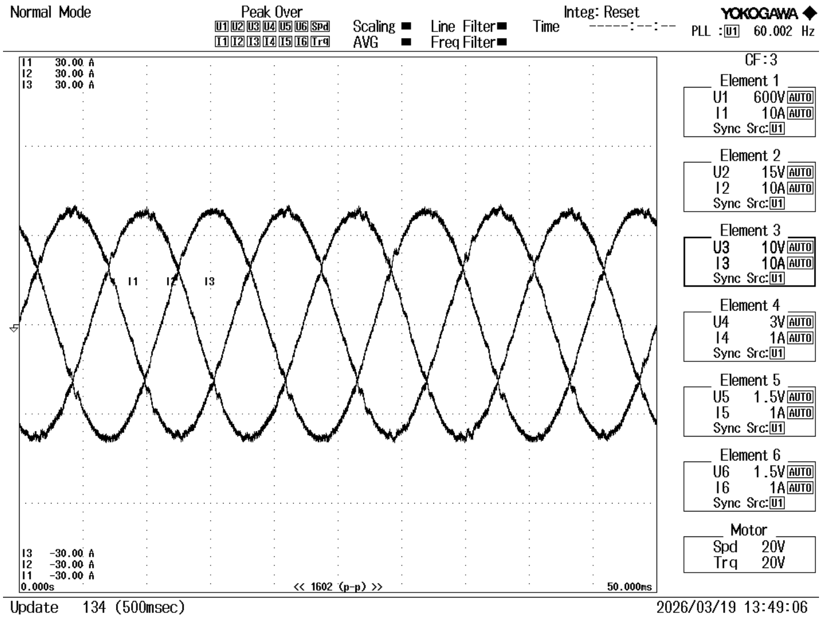

Figure 4.17. Phase current waveforms with harmonic compensation.

Regarding the TDD values per phase, readings of 1.26% (phase A), 1.19% (phase B) and 1.39% (phase C) were obtained, all of which were below the 2.5% limit set by the IEEE 519 standard. Figure 4.18 presents a comparison of the current harmonic spectrum obtained in both the simulation and the experimental tests against the regulatory thresholds. The results confirm that in both scenarios, harmonic mitigation is effective and strictly complies with the standard.

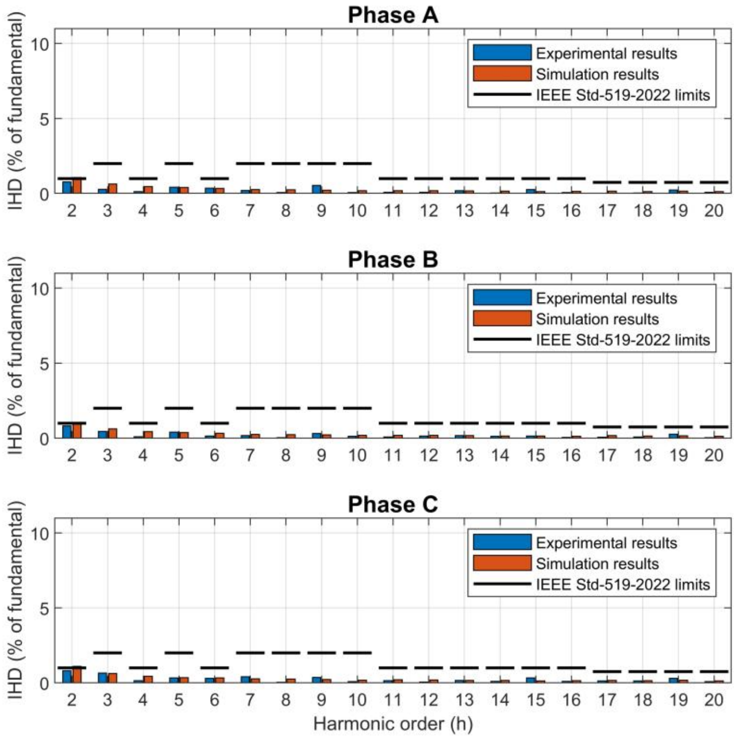

Figure 4.18. Harmonic current spectrum at PCC for each phase (experiment, simulation and IEEE Std-519-2022 limits).

4.3. Conclusions

This chapter has provided experimental validations of the proposed control system of the studied BESS operating in parallel to an EAF in the Cuban power system. The experimental implementation was carried out in laboratory and was based on a PHIL approach, with the main objective of validating the BESS inverter control under various scenarios occurring in the PCC of the EAF with the power system (frequency variations, voltage variations, unbalances, harmonics). The power system was emulated with a FQPC capable of generating frequency variations according to the power system dynamic model and voltage perturbations for VFRT testing. The control implementation was based on a dSPACE DS1103 real-time control board and the associated software.
The experimental of these control strategies, as well as their coordinated operation, constitute the main objectives of this chapter, which are summarized as follows:

- Analysis of the BESS response for EAF active power compensation to reduce the EAF impact on the frequency stability in the Cuban power system,
- Analysis of the BESS response to sags and swells in the power system.
- Modelling of the EAF for harmonic and power factor analysis,
- Behaviour of the BESS as a power factor compensator,
- Analysis of the behaviour of the BESS as an active filter in the presence of harmonics in the steelworks network.

FINAL CONCLUSION

This doctoral thesis has developed and validated a multifunctional control strategy for a BESS, specifically designed to mitigate the negative impact of EAFs on weak power systems. The Cuban power system serves as the primary case study, where EAF operation presents significant challenges to system stability and performance. The central objective was to ensure system frequency stability whilst simultaneously compensating for power factor and reducing harmonic distortion in the steelworks.

The structure of the research is outlined as follows:

- **Context and Rationale**: In the first phase, the relevance and critical applications of BESSs in modern power grids were analysed, highlighting their indispensable nature in systems with low frequency regulation capacity, such as the Cuban grid.
- **Modelling and Control:** The second and third parts focused on the design of control systems and the detailed mathematical modelling of the steelworks' circuit components. This included modelling the non-linear behaviour of the EAF and the integration of the BESS based on a grid-following inverter architecture. Under this approach, the system acts as a controlled current source that monitors the frequency and voltage at the PCC, facilitating harmonic mitigation and real-time power factor compensation whilst maintaining frequency stability within the power system.
- **Validation and Innovation:** The final stage consisted of the experimental and simulation-based validation of the proposed strategies. A notable scientific innovation is the implementation of fuzzy controllers in an industrial application environment, optimising the system's response to the stochastic nature of the electric arc. Furthermore, PHIL laboratory validation proved to be a powerful tool for the development and experimental tuning of BESS control strategies.

The results obtained confirm that the integration of a BESS into the electrical system of a steelworks connected to a weak grid is not only a technically viable option for preserving operational stability but also represents a substantial improvement in the industry's power quality indices and production efficiency.

Impact of the research

- **Impact on Industrial Efficiency:** The proposed solution enables the EAF to operate at full power from the start of the process without the 'soft ramp' restrictions imposed nowadays by the system operator in Cuba. This directly reduces melting time, specific energy consumption and premature wear of electrodes and refractories. Although the solution has been tailored to the present conditions of the Cuban power system, it also establishes a general operational framework for power quality enhancement in similar industrial applications.

- **Economic Impact:** The proposed BESS capability improves conditions of the steelwork industry, enabling continuous operation despite the constraints of the Cuban power system, while contributing to power quality improvement (e.g. power factor correction). This reduces the financial losses and improves the profitability of steelworks such as 'Antillana de Acero' which is considered as the reference case in this study.
- **Impact on System Operation:** By mitigating sudden power fluctuations at the PCC, the risk of frequency instability and potential total system blackouts is reduced, resulting in greater safety for the Cuban power system.
- **Technological Outlook:** This thesis establishes a technical roadmap for the transition from passive compensation solutions to flexible power electronics systems, demonstrating that energy storage is the most viable comprehensive solution for decarbonisation and industrialisation in electricity systems with limited regulation resources.

Scientific and technical contribution

- A fuzzy control model was developed for a BESS which compensate for EAF's active power fluctuations; in parallel with this control, the power factor is dynamically regulated during the melting stage in conjunction with harmonic compensation.
- The implementation of BESS-based control proved capable of raising the power factor from inefficient levels (0.83) to target values (0.93), overcoming the limitations of traditional passive filters, which suffer from obsolescence and a lack of adaptability.
- It was validated that the use of a 25 MW BESS allows the frequency to be maintained within the permitted dead band of the Cuban power system (59.7–60.2 Hz), reducing reliance on the system's primary control, which is currently insufficient in the studied context.

REFERENCES (Selective)

[1] M. M. Abadi, H. Tang, and M. M. Rashidi, "A review of simulation and numerical modeling of electric arc furnace (EAF) and its processes," *Heliyon*, vol. 10, no. 11, p. e32157, Jun. 2024, doi: 10.1016/j.heliyon.2024.e32157.

[2] Z. Łukasik and Z. Olczykowski, "Estimating the Impact of Arc Furnaces on the Quality of Power in Supply Systems," *Energ. 2020*, vol. 13, Mar. 2020, doi: 10.3390/en13061462.

[3] H. Andrei, C. Cepisca, and S. Grigorescu, "Power Quality and Electrical Arc Furnaces," 2011. doi: 10.5772/15996.

[4] J. E. Dominguez, J. Rekola, O. E. Torres Breffe, and C. R. Capablanca, "Use of Battery Energy Storage with Electric Arc Furnace to Improve Frequency Stability of Weak Power System," in *2021 IEEE PES Innovative Smart Grid Technologies Europe (ISGT Europe)*, Oct. 2021, pp. 1–5. doi: 10.1109/ISGTEurope52324.2021.9640151.

[5] J. E. Domínguez, O. E. Torres Breffe, I. Serban, C. B. González, and C. Revuelta Capablanca, "The Impact of Electric Arc Furnaces on the Cuban Power System: Existing Approaches and Future Prospects," in *2023 International Symposium on Fundamentals of Electrical Engineering (ISFEE)*, Nov. 2023, pp. 1–6. doi: 10.1109/ISFEE60884.2023.10637080.

[6] J. E. Domínguez, I. Serban, and O. E. T. Breffe, "Adaptive voltage fault ride-through control of a battery energy storage system according to the cuban grid code," *Energy 360*, vol. 4, p. 100033, Dec. 2025, doi: 10.1016/j.energ.2025.100033.

[7] G. G. Farivar *et al.*, "Grid-Connected Energy Storage Systems: State-of-the-Art and Emerging Technologies," *Proc. IEEE*, vol. 111, no. 4, pp. 397–420, Apr. 2023, doi: 10.1109/JPROC.2022.3183289.

[8] K. Prakash *et al.*, "A review of battery energy storage systems for ancillary services in distribution grids: Current status, challenges and future directions," *Front. Energy Res.*, vol. 10, 2022, Accessed: Nov. 27, 2023. [Online]. Available: https://www.frontiersin.org/articles/10.3389/fenrg.2022.971704

[9] W.-J. Kim, Y.-S. Lee, and Y.-H. Chun, "Assessment of Primary Control Reserve Requirement from Generator Considering a Battery Energy Storage System," *J. Electr. Eng. Technol.*, vol. 15, no. 1, pp. 315–324, Jan. 2020, doi: 10.1007/s42835-019-00319-2.

[10] K. Stein, M. Tun, K. Musser, and R. Rocheleau, "Evaluation of a 1 MW, 250 kW-hr Battery Energy Storage System for Grid Services for the Island of Hawaii," *Energies*, vol. 11, no. 12, Art. no. 12, Dec. 2018, doi: 10.3390/en11123367.

[11] D. Gamage, C. Wanigasekara, A. Ukil, and A. Swain, "Multi-level consensus based load frequency controller with multi-battery energy storage systems," *Electr. Power Syst. Res.*, vol. 239, p. 111208, Feb. 2025, doi: 10.1016/j.epsr.2024.111208.

[12] A. Saldarini, M. Longo, M. Brenna, and D. Zaninelli, "Battery Electric Storage Systems: Advances, Challenges, and Market Trends," *Energies*, vol. 16, no. 22, Art. no. 22, Jan. 2023, doi: 10.3390/en16227566.

[13] V. Virulkar and M. V. Aware, “Reactive and real power compensation with DSTATCOM and BESS for mitigation of flicker,” *Int. J. Power Energy Convers.*, vol. 1, Jan. 2009, doi: 10.1504/IJPEC.2009.029055.

[14] H. Toopchizadeh, M. Zallaghi, M. Moradi, and S. Shahmoradi, “An effective shunt active power filter based on novel binary multilevel inverter and optimal type-2 fuzzy system to accurately mitigate harmonic currents,” *Evol. Syst.*, vol. 14, no. 5, pp. 783–800, Oct. 2023, doi: 10.1007/s12530-022-09465-x.

[15] V. B. Virulkar and M. V. Aware, “DSTATCOM with BESS, an efficient means for flicker mitigation,” in *TENCON 2008 - 2008 IEEE Region 10 Conference*, Nov. 2008, pp. 1–6. doi: 10.1109/TENCON.2008.4766740.

[16] G. A. Orcajo, J. M. Cano, J. G. Norniella, F. P. G., C. H. Rojas, and J. R. D., “Hybridization of a Wind Farm and a Photovoltaic Plant in a Steelworks with an Energy Storage System,” in *2023 IEEE Industry Applications Society Annual Meeting (IAS)*, Oct. 2023, pp. 1–7. doi: 10.1109/IAS54024.2023.10406767.

[17] A. Fahren, K. Banjar Nahor, C. D. Widjaja, and N. Hariyanto, “Static Watt Compensator and Battery Energy Storage System for Frequency Stability Considering Smelter: A Comparison,” Dec. 2020. doi: 10.1109/PECon48942.2020.9314465.

[18] S. Sakib, Md. B. Hossain, M. A. Zamee, M. J. Hossain, and Md. A. Habib, “Role of battery energy storage systems: A comprehensive review on renewable energy zones integration in weak transmission networks,” *J. Energy Storage*, vol. 128, p. 117223, Aug. 2025, doi: 10.1016/j.est.2025.117223.

[19] F. Barrero-González, M. I. Milanés-Montero, E. González-Romera, C. Roncero-Clemente, and P. González-Castrillo, “El Control de Potencia y Frecuencia en los Sistemas Eléctricos Multiárea. Revisión y Nuevos Retos,” *Rev. Iberoam. Automática E Informática Ind. RIAI*, vol. 12, no. 4, pp. 357–364, Oct. 2015, doi: 10.1016/j.riai.2015.07.001.

[20] K. Prabhakar, S. K. Jain, and P. K. Padhy, “Inertia estimation in modern power system: A comprehensive review,” *Electr. Power Syst. Res.*, vol. 211, p. 108222, Oct. 2022, doi: 10.1016/j.epsr.2022.108222.

[21] P. Kundur and N. J. Balu, *Power System Stability and Control*. McGraw-Hill, 1994.

[22] R. Rajan, F. M. Fernandez, and Y. Yang, “Primary frequency control techniques for large-scale PV-integrated power systems: A review,” *Renew. Sustain. Energy Rev.*, vol. 144, p. 110998, Jul. 2021, doi: 10.1016/j.rser.2021.110998.

[23] A. Etxegarai, P. Eguia, E. Torres, A. Iturregi, and V. Valverde, “Review of grid connection requirements for generation assets in weak power grids,” *Renew. Sustain. Energy Rev.*, vol. 41, pp. 1501–1514, Jan. 2015, doi: 10.1016/j.rser.2014.09.030.

[24] R. Aljarrah, B. B. Fawaz, Q. Salem, M. Karimi, H. Marzooghi, and R. Azizipanah-Abarghooee, “Issues and Challenges of Grid-Following Converters Interfacing Renewable Energy Sources in Low Inertia Systems: A Review,” *IEEE Access*, vol. 12, pp. 5534–5561, 2024, doi: 10.1109/ACCESS.2024.3349630.

[25] “IEEE Guide for Planning DC Links Terminating at AC Locations Having Low Short-Circuit Capacities,” *IEEE Std 1204-1997*, pp. 1–216, Jan. 1997, doi: 10.1109/IEEESTD.1997.85949.

[26] T. Ahmad and D. Zhang, "A critical review of comparative global historical energy consumption and future demand: The story told so far," *Energy Rep.*, vol. 6, pp. 1973–1991, Nov. 2020, doi: 10.1016/j.egyr.2020.07.020.

[27] O. Smith, O. Cattell, E. Farcot, R. D. O'Dea, and K. I. Hopcraft, "The effect of renewable energy incorporation on power grid stability and resilience," *Sci. Adv.*, vol. 8, no. 9, p. eabj6734, Mar. 2022, doi: 10.1126/sciadv.abj6734.

[28] D. W. Gao, *Energy Storage for Sustainable Microgrid*. 2015, p. 142.

[29] O. Palizban and K. Kauhaniemi, "Energy storage systems in modern grids—Matrix of technologies and applications," *J. Energy Storage*, vol. 6, pp. 248–259, May 2016, doi: 10.1016/j.est.2016.02.001.

[30] M. G. Molina, "Energy Storage and Power Electronics Technologies: A Strong Combination to Empower the Transformation to the Smart Grid," *Proc. IEEE*, vol. 105, no. 11, pp. 2191–2219, Nov. 2017, doi: 10.1109/JPROC.2017.2702627.

[31] F. Nadeem, S. M. S. Hussain, P. K. Tiwari, A. K. Goswami, and T. S. Ustun, "Comparative Review of Energy Storage Systems, Their Roles, and Impacts on Future Power Systems," *IEEE Access*, vol. 7, pp. 4555–4585, 2019, doi: 10.1109/ACCESS.2018.2888497.

[32] M. Faisal, M. A. Hannan, P. J. Ker, A. Hussain, M. B. Mansor, and F. Blaabjerg, "Review of Energy Storage System Technologies in Microgrid Applications: Issues and Challenges," *IEEE Access*, vol. 6, pp. 35143–35164, 2018, doi: 10.1109/ACCESS.2018.2841407.

[33] J. Mitali, S. Dhinakaran, and A. A. Mohamad, "Energy storage systems: a review," *Energy Storage Sav.*, vol. 1, no. 3, pp. 166–216, Sep. 2022, doi: 10.1016/j.enss.2022.07.002.

[34] L. S. Xavier, W. C. S. Amorim, A. F. Cupertino, V. F. Mendes, W. C. do Boaventura, and H. A. Pereira, "Power converters for battery energy storage systems connected to medium voltage systems: a comprehensive review," *BMC Energy*, vol. 1, no. 1, Art. no. 1, Jul. 2019, doi: 10.1186/s42500-019-0006-5.

[35] G. Wang *et al.*, "A Review of Power Electronics for Grid Connection of Utility-Scale Battery Energy Storage Systems," *IEEE Trans. Sustain. Energy*, vol. 7, no. 4, Art. no. 4, Oct. 2016, doi: 10.1109/TSTE.2016.2586941.

[36] X. Gao, D. Zhou, A. Anvari-Moghaddam, and F. Blaabjerg, "A Comparative Study of Grid-Following and Grid-Forming Control Schemes in Power Electronic-Based Power Systems," *Power Electron. Drives*, vol. 8, no. 1, pp. 1–20, Jan. 2023, doi: 10.2478/pead-2023-0001.

[37] J. Rocabert, A. Luna, F. Blaabjerg, and P. Rodríguez, "Control of Power Converters in AC Microgrids," *IEEE Trans. Power Electron.*, vol. 27, no. 11, pp. 4734–4749, Nov. 2012, doi: 10.1109/TPEL.2012.2199334.

[38] Z. Xu, Y. Qin, Z. Li, C. Jiao, B. Zhai, and X. Chang, "Stability analysis of different control modes of grid-connected converters under different grid conditions," *Front. Energy Res.*, vol. 11, 2023, Accessed: Dec. 22, 2023. [Online]. Available: https://www.frontiersin.org/articles/10.3389/fenrg.2023.1242024

[39] R. Rosso, X. Wang, M. Liserre, X. Lu, and S. Engelken, "Grid-Forming Converters: Control Approaches, Grid-Synchronization, and Future Trends—A Review," *IEEE Open J. Ind. Appl.*, vol. 2, pp. 93–109, 2021, doi: 10.1109/OJIA.2021.3074028.

[40] X. Ji, D. Liu, K. Jiang, Z. Zhang, and Y. Yang, "Small-Signal Stability of Hybrid Inverters with Grid-Following and Grid-Forming Controls," *Energies*, vol. 17, no. 7, p. 1644, Jan. 2024, doi: 10.3390/en17071644.

[41] R. H. Lasseter, Z. Chen, and D. Pattabiraman, "Grid-Forming Inverters: A Critical Asset for the Power Grid," *IEEE J. Emerg. Sel. Top. Power Electron.*, vol. 8, no. 2, pp. 925–935, Jun. 2020, doi: 10.1109/JESTPE.2019.2959271.

[42] M. Yadav, N. Pal, and D. K. Saini, "Low voltage ride through capability for resilient electrical distribution system integrated with renewable energy resources," *Energy Rep.*, vol. 9, pp. 833–858, Dec. 2023, doi: 10.1016/j.egyr.2022.12.023.

[43] J. E. Domínguez, I. Serban, and O. E. T. Breffe, "Enhancing the Control of a DC/AC Converter for Voltage Perturbation Ride-Through in Compliance with the Cuban Grid Code," in *2024 6th Global Power, Energy and Communication Conference (GPECOM)*, Jun. 2024, pp. 68–73. doi: 10.1109/GPECOM61896.2024.10582679.

[44] P. Liu *et al.*, "High-voltage ride-through strategy for wind turbine with fully-rated converter based on current operating range," *Int. J. Electr. Power Energy Syst.*, vol. 141, p. 108101, Oct. 2022, doi: 10.1016/j.ijepes.2022.108101.

[45] J. Langstädtler, M. Schellschmidt, J. Scheffer, B. S. D. Brelie, S. Schrobsdorff, and C. Kahlen, "Relevance of high-voltage-ride-through capability and testing," 2015. Accessed: Nov. 30, 2024. [Online]. Available: https://www.semanticscholar.org/paper/RELEVANCE-OF-HIGH-VOLTAGE-RIDE-THROUGH-CAPABILITY-Langst%C3%A4dtler-Schellschmidt/33c816de888c098081d8184a3158b215422ea8bc

[46] U. Datta, A. Kalam, and J. Shi, "The relevance of large-scale battery energy storage (BES) application in providing primary frequency control with increased wind energy penetration," *J. Energy Storage*, vol. 23, pp. 9–18, Jun. 2019, doi: 10.1016/j.est.2019.02.013.

[47] "US Departmentof Energy, Global Energy Storage Database." Accessed: Jan. 16, 2024. [Online]. Available: https://gesdb.sandia.gov/

[48] M. Korkeakoski and M. L. Filgueiras Sainz de Rozas, "A look to the transition of the cuban energy matrix," *Ing. Energética*, vol. 43, no. 3, pp. 40–47, Dec. 2022.

[49] E. Alberto Alvarez, M. Korkeakoski, A. Santos Fuentefría, M. Lourdes Filgueiras Sainz de Rozas, R. Arcila Padura, and J. Luukkanen, "Long-Range Integrated Development Analysis: The Cuban Isla de la Juventud Study Case," *Energies*, vol. 14, no. 10, Art. no. 10, Jan. 2021, doi: 10.3390/en14102865.

[50] L. Guerra-Hernández, A. A. Martínez-García, M. Vilaragut-Llanes, Y. Salgado-Duarte, and J. Szpytko, "Prospective Estimation of BESS Nominal Values for Frequency Control with High PV and Wind Integration," in *2023 27th International Conference on Methods and Models in Automation and Robotics (MMAR)*, Aug. 2023, pp. 314–319. doi: 10.1109/MMAR58394.2023.10242553.

[51] D. C. Adams, "Cuba Suffers Second Power Outage in 24 Hours, Realizing Years of Warnings," *The New York Times*, Oct. 19, 2024. Accessed: May 10, 2025. [Online]. Available: https://www.nytimes.com/2024/10/19/world/americas/cuba-power-outage.html

[52] M. Soto Calvo, H. S. Lee, and S. W. Chisale, "A novel method for long-term power demand prediction using enhanced data decomposition and neural network with integrated uncertainty analysis: A Cuba case study," *Appl. Energy*, vol. 372, p. 123864, Oct. 2024, doi: 10.1016/j.apenergy.2024.123864.

[53] J. Luukkanen, A. Saunders Vázquez, A. Santos-Fuentefria, Y. Majanne, M. L. Filgueiras Sainz de Rozas, and J. Laitinen, *CUBAN ENERGY SYSTEM DEVELOPMENT– Technological Challenges and Possibilities. FFRC eBooks 2/2022*. 2022.

[54] Z. Olczykowski, "Electric Arc Furnaces as a Cause of Current and Voltage Asymmetry," *Energ. 2021*, vol. 14, Aug. 2021, [Online]. Available: https://doi.org/ 10.3390/en14165058

[55] Ministerio de Finanzas y Precios, "Official Gazette No. 26 Extraordinary of 2021/Gaceta Oficial No. 26 Extraordinaria de 2021," Apr. 13, 2021. [Online]. Available: https://www.gacetaoficial.gob.cu/es/gaceta-oficial-no-26-extraordinaria-de-2021

[56] J. E. Domínguez, I. Serban, and O. E. Torres Breffe, "Battery Energy Storage System for Power Quality Enhancement in Electric Arc Furnace Circuits," in *2025 International Aegean Conference on Electrical Machines and Power Electronics (ACEMP) & 2025 International Conference on Optimization of Electrical and Electronic Equipment (OPTIM)*, May 2025, pp. 1–6. doi: 10.1109/OPTIM-ACEMP62776.2025.11075254.

[57] J. E. Domínguez, I. Serban, and O. E. T. Breffe, "Fuzzy Logic-Based Control of a Battery Energy Storage System to Mitigate Frequency Excursions in the Cuban Power System Caused by Electric Arc Furnaces," *J. Electr. Eng. Technol.*, Apr. 2026, doi: 10.1007/s42835-026-02777-x.

[58] R. Teodorescu, M. Liserre, and P. Rodriguez, *Grid Converters for Photovoltaic and Wind Power Systems: Teodorescu/Grid Converters for Photovoltaic and Wind Power Systems*. 2011. doi: 10.1002/9780470667057.

[59] M. A. Khan and J. Kim, "Smart Sag Detection and Reactive Current Injection Control for a PV Microgrid under Voltage Faults," *Energies*, vol. 16, no. 19, Art. no. 19, Jan. 2023, doi: 10.3390/en16196776.

[60] Z. Hassan, A. Amir, J. Selvaraj, and N. A. Rahim, "A review on current injection techniques for low-voltage ride-through and grid fault conditions in grid-connected photovoltaic system," *Sol. Energy*, vol. 207, pp. 851–873, Sep. 2020, doi: 10.1016/j.solener.2020.06.085.

[61] K. H. Oon, C. Tan, A. H. A. Bakar, H. S. Che, H. Mokhlis, and H. A. Illias, "Establishment of fault current characteristics for solar photovoltaic generator considering low voltage ride through and reactive current injection requirement," *Renew. Sustain. Energy Rev.*, vol. 92, pp. 478–488, Sep. 2018, doi: 10.1016/j.rser.2018.05.001.

[62] R. R. Yager, "Fuzzy rule bases with generalized belief structure inputs," *Eng. Appl. Artif. Intell.*, vol. 72, pp. 93–98, Jun. 2018, doi: 10.1016/j.engappai.2018.03.005.

[63] J. Wang and R. Hamilton, "A review of negative sequence current," in *2010 63rd Annual Conference for Protective Relay Engineers*, Mar. 2010, pp. 1–18. doi: 10.1109/CPRE.2010.5469515.

[64] M. Mirhosseini, J. Pou, B. Karanayil, and V. G. Agelidis, "Positive- and negative-sequence control of grid-connected photovoltaic systems under unbalanced voltage conditions," in

2013 Australasian Universities Power Engineering Conference (AUPEC), Sep. 2013, pp. 1–6. doi: 10.1109/AUPEC.2013.6725406.

[65] E. G. Shehata, M. S. Gaber, K. A. Ahmed, and G. M. Salama, “Implementation of an energy management algorithm in DC MGs using multi-agent system,” *Int. Trans. Electr. Energy Syst.*, vol. 29, no. 4, p. e2790, 2019, doi: 10.1002/etep.2790.

[66] Md. R. Alam, I. Bhuiyan, and N. Mohammad, “A Feasibility Study of Solar Photovoltaic Power Smoothing Using Fuzzy Logic Approach,” vol. 14, pp. 124–135, Dec. 2023.

[67] A. Atif and M. Khalid, “Fuzzy logic controller for solar power smoothing based on controlled battery energy storage and varying low pass filter,” *IET Renew. Power Gener.*, vol. 14, no. 18, pp. 3824–3833, 2020, doi: 10.1049/iet-rpg.2020.0459.

[68] S. Sukumar, M. Marsadek, K. R. Agileswari, and H. Mokhlis, “Ramp-rate control smoothing methods to control output power fluctuations from solar photovoltaic (PV) sources—A review,” *J. Energy Storage*, vol. 20, pp. 218–229, Dec. 2018, doi: 10.1016/j.est.2018.09.013.

[69] D. Ochoa, S. Martinez, and P. Arévalo, “A Novel Fuzzy-Logic-Based Control Strategy for Power Smoothing in High-Wind Penetrated Power Systems and Its Validation in a Microgrid Lab,” *Electronics*, vol. 12, no. 7, Art. no. 7, Jan. 2023, doi: 10.3390/electronics12071721.

[70] X. Deng, R. Mo, P. Wang, J. Chen, D. Nan, and M. Liu, “Review of RoCoF Estimation Techniques for Low-Inertia Power Systems,” *Energies*, vol. 16, no. 9, Art. no. 9, Jan. 2023, doi: 10.3390/en16093708.

[71] J. Fleer and P. Stenzel, “Impact analysis of different operation strategies for battery energy storage systems providing primary control reserve,” *J. Energy Storage*, vol. 8, pp. 320–338, Nov. 2016, doi: 10.1016/j.est.2016.02.003.

[72] “IEEE Recommended Practice for Monitoring Electric Power Quality,” *IEEE Std 1159-2019 Revis. IEEE Std 1159-2009*, pp. 1–98, Aug. 2019, doi: 10.1109/IEEESTD.2019.8796486.

[73] J. G. Mayordomo, L. F. Beites, R. Asensi, M. Izzeddine, L. Zabala, and J. Amantegui, “A new frequency domain arc furnace model for iterative harmonic analysis,” *IEEE Trans. Power Deliv.*, vol. 12, no. 4, pp. 1771–1778, Oct. 1997, doi: 10.1109/61.634204.

[74] A. M. Kruchinin, M. Ya. Pogrebisskiy, A. S. Bulgakov, A. Yu. Chursin, and E. S. Ryazanova, “On the Issue of the Arc Steelmaking Furnaces Operating Mode Stability at the Beginning of Melting,” in *2018 19th International Conference of Young Specialists on Micro/Nanotechnologies and Electron Devices (EDM)*, Jun. 2018, pp. 681–685. doi: 10.1109/EDM.2018.8435022.

[75] A. M. Kruchinin, M. Y. Pogrebisskiy, E. S. Ryazanova, and A. Y. Chursin, “Identification of working reactance of industrial arc furnace equivalent scheme based on known specific electric power consumption for melting of charge,” *IOP Conf. Ser. Mater. Sci. Eng.*, vol. 950, no. 1, p. 012012, Oct. 2020, doi: 10.1088/1757-899X/950/1/012012.

[76] “IEEE Standard for Harmonic Control in Electric Power Systems,” *IEEE Std 519-2022 Revis. IEEE Std 519-2014*, pp. 1–31, Aug. 2022, doi: 10.1109/IEEESTD.2022.9848440.

[77] D. Potnuru, A. M. K., and S. Ch., “Design and implementation methodology for rapid control prototyping of closed loop speed control for BLDC motor,” *J. Electr. Syst. Inf. Technol.*, vol. 5, no. 1, pp. 99–111, May 2018, doi: 10.1016/j.jesit.2016.12.005.